The Role of Red Blood Cell Membrane Rigidity on Cellular and Drug Particle Carrier Dynamics in Blood Flow

by

Mario Gutierrez-Ruiz Jr.

A dissertation submitted in partial fulfillment
of the requirements for the degree of
Doctor of Philosophy
(Chemical Engineering)
in the University of Michigan
2021

Doctoral Committee:

Professor Omolola Eniola-Adefeso, Chair
Assistant Professor Netanel Korin, Technion Israel Institute of Technology
Associate Professor Allen Liu
Associate Professor Sunitha Nagrath
Professor Robert M. Ziff

Mario Gutierrez

gutieman@umich.edu

ORCID iD: 0000-0003-2803-5267

Dedication

This dissertation is dedicated to my mother, Beatriz Gutierrez, and godfather, Fernando Ruiz. I am eternally grateful for your unconditional love and support. You mean the world to me.

Acknowledgements

What lies behind you and what lies in front of you, pales in comparison to what lies inside of you.

- Ralph Waldo Emerson

The entirety of this thesis aims to capture a glimpse of the challenging, often frustrating, but always rewarding work that has made me the problem-solver and engineer I am today. Overall, this graduate school experience was unlike anything I had faced before; it broke me down into tiny pieces and made me question my capabilities and motivations. The challenges and struggles ultimately proved to be life-changing lessons for improving myself and bolstering my desire and excitement for improving the lives of others. Despite the challenges, my time in graduate school and at Michigan has been one of the most fulfilling experiences of my life. Specifically, due to the genuine and inspiring folks I met along the way who made this experience irreplaceable.

First and foremost, I want to give the spotlight to my advisor Professor Omolola (Lola) Eniola-Adefeso. Lola, words cannot explain how grateful I am to have met you and worked alongside you. I know I was not the most impressive student, and ultimately, I was not the best student, but you were the best mentor I could have possibly chosen. I truly appreciate your kindness and patience with me. Without you, I could not have navigated this rigorous academic field. I am forever grateful for you believing in me and for motivating me when I needed it the most. Thank you for challenging me, not letting me settle for less, and opening countless doors for me. I am

inspired by your hard work, determination, and excitement for research. I am very excited to see what great things come out of your lab moving forward.

Second, I would like to thank my committee members, Professor Sunitha Nagrath, Professor Robert Ziff, Professor Allen Liu, and Professor Netanel Korin. Thank you all for serving on my defense committee and for providing your insights on my work. Professor Nagrath, I always appreciated your positivity and kind heart. I enjoyed your graduate math class very much in my first year of graduate school. Professor Ziff, I am inspired by your curiosity and excitement for teaching. Professor Liu, I am very excited to see what things will come from your lab in the future. I enjoyed your cellular engineering class and your passion for teaching. Professor Korin, I am beyond thankful for you opening the doors to your lab during my research exchange in Israel. I am deeply grateful for your kindness and hospitality. The experiences I had during the research exchange in your lab were incredible, and I was able to make life-long friendships with your research team.

Thank you to all the former and current lab members of the Eniola Lab. I appreciate the friendship, help, and support I got from all of you. This experience could not have been the same without you. Thank you, Hanieh Safari, Genesis Lopez, William (Billy) Kelley, Alison Banka, Violet Sheffey, Jonathan Lee, Emma Brannon, Logan Piegols, Valentina Guevara, and Rue Felder. We laughed, cried, and complained together. Graduate school was fun because of you guys. It was an absolute pleasure and honor working with every single one of you. Thank you as well to all the undergraduate students who were brave enough to take on my crazy projects. Thank you, Sebastian Ojeda, Tyler Tanski, and Elias Tavarez.

I want to thank all my collaborators who helped this thesis and graduate school experience become multidimensional. Thank you again, Professor Korin, for opening the doors to your lab in

Technion. Special thanks to Maria Khoury and Mark Epshtein of Technion Israel Institute of Technology. Maria, I appreciate your dedication and friendly attitude. Mark, I appreciate your genius and the countless laughs we had together. Thanks to Sharon Singh, M.D., for your collaborative insight on the sickle cell disease projects. I want to give an exceptional thanks to Mark Shamoun, M.D., for your friendship and mentorship. Mark, I am inspired by your genuine kindness and desire to help others. Life is great because of folks like you, never change. Thank you to our computational collaborators at the University of Amsterdam, special thanks to Benjamin Czaja. Ben, thank you so much for your friendship and curiosity, which ultimately led us to work together. Mark Shamoun, Ben, Maria, and Mark Epshtein, I am eternally grateful to have worked with you and hope we can continue our lifelong friendship.

A very special thanks to all the blood donors that supported my research. Literally, my thesis work could not have been completed without your help. Thank you to the sickle cell disease patients who were willing to participate in and donate blood to our studies. Your contributions are very much appreciated. Hopefully, the work presented in this thesis will eventually lead to developing tools for better understanding sickle cell disease and improving the quality of life of folks affected by this terrible disease.

Many thanks to all my great friends I met in graduate school. Graduate school was very challenging, but thanks to your company, it was very manageable. Thanks to Dylan Neale, Abdulla Alqubati, Vyas Ramasubramani, Alison Banka, Eshita Khera, and Steven Chavez. I am honored to have met you all and am looking forward to our continued friendship. I want to thank Maira Gonzalez. Although life took us in different directions, I hold the time we shared together very close to my heart. I appreciate the love and support you gave me in my graduate school journey. I want to give an exceptional thanks to my brothers Eliseo and Eleazar Gutierrez. You guys know

how much your friendship means to me, and I am beyond thankful for the support you guys have given me from day one. Thank you to my childhood friend Zach Peabody for always encouraging me and being my advocate. A very special thanks to the Society of Hispanic Professional Engineers and all the lifelong friends I made in this organization. Thank you, Emily Anne Vargas, Mauro Rodriguez, Hector Perez, Elio Morillo, and Alex Avendaño.

I want to give a very special thank you to Michigan State University. Yes, I am thanking Michigan State University in a thesis coming out of the University of Michigan. In all honesty, I could have never made it to where I am now without first making it through Michigan State University. Thank you to the STARR Charitable foundation and the generous donors for providing me with a life-changing opportunity. If it were not for your generosity, this poor farm boy from Wyoming would have never written this thesis. Thank you to Doug Estry, Korine Wawrzynski, and Janice Hironaka for your mentorship as an undergraduate student and for motivating me and encouraging me to pursue graduate school. Thank you to Patricia Joly for being my Michigan mom when I made the long move to East Lansing. Special thanks to Dennis Guthrie Ph.D. for your mentorship and for encouraging me to pursue a Ph.D. and continued mentorship.

Finally, I would like to thank my family for their unconditional love and support. Thank you to my aunt Dora Gutierrez for helping me with my income taxes and always being my cheerleader. Thank you to my aunt Leticia and uncle Luis Villalpando for encouraging me to maximize my education. Thank you for your unconditional support in making me the best that I can be. A very special thanks to my uncle Demetrio Ruiz for your energizing and friendly soul. Thank you for your enthusiasm to always lend a helping hand. To my father, Mario Senior, I thank you for your courage and desire to give your family a better life and your immense love for my mother. Although you left us too soon, and I never got to grow up with you by my side, I knew

you were still there cheering me on and helping me get back up when I was down. Mama and Nando, I cannot ever find the words to thank you for dedicating your life to my success. The sacrifices you have made and the pain you have endured mean the world to me. I appreciate you beyond what words can explain. I know you beat yourself up for thinking you did not give me enough, but you gave me everything I needed, love. Thank you for teaching me the meaning of loyalty, pride, compassion, kindness, and most of all, love. You are my light; you are my inspiration. My life is beautiful and great because of you. I hope I have made you proud.

Table of Contents

List of Figures

List of Tables

List of Abbreviations

RBCs	Red Blood Cells
SCD	Sickle Cell Disease
HIV	Human Immunodeficiency Virus
VTC	Vascular-Targeted Carriers
WBCs	White Blood Cells
Hct	Hematocrit
RBC-FL/CFL	Red Blood Cell Free Layer
i-sRBCs	Irreversibly Sickled Red Blood Cells
r-sRBCs	Reversibly Sickled Red Blood Cells
Hgb	Hemoglobin
HgS	Hemoglobin SS
HbA	Hemoglobin A1
HbF	Fetal Hemoglobin
HU	Hydroxyurea
EI	Elongation Index
EI_{MAX}	Maximum Elongation Index
AFM	Atomic Force Microscopy
IV	Intravenous
T2D	Type Two Diabetes

IRB-MED	University of Michigan Interval Review Board
ACD	Acid-Sodium Citrate Dextrose
PBS	Phosphate Buffered Saline
K2-EDTA	Tri-Potassium Ethylenediaminetetraacetic Acid
HPLC	High Pressure Liquid Chromatography
TBHP	tert-Butyl Hydroperoxide
MAC-1	Membrane Attack Complex Type 1
PSGL-1	P-Selectin Glycoprotein Ligand 1
LFA-1	Lymphocyte Function-Associated Antigen 1
sLe^a	Sialyl-Lewis A
CLA	Cutaneous Lymphocyte Antigen
FACS	Flow Cytometry Staining Buffer
FSC	Forward Scatter
SSC	Side Scattered Light
FBS	Fetal Bovine Serum
BD	Becton Dickinson and Company
HUVEC	Human Umbilical Vein Endothelial Cells
IL-1β	Interleukin 1β
PPFC	Parallel Plate Flow Chamber
PDMS	Polydimethylsiloxane
WSR	Wall Shear Rate
BSA	Bovine Serum Albumin
WGA	Wheat Germ Agglutinin

PMT	Photo Multiplier Tube
RFP	Red Fluorescent Protein
IQR	Inter-Quartile Range
FITC	Fluorescein Isothiocyanate
UV	Ultraviolet
PEGDA	Polyethylene (Glycol) Diacrylate
CEA	2-Carboxyethyl Acrylate
PI	Photo-initiator
MeOH	Methanol
EDAC	N-(3-Dimethylaminopropyl)-N`-Ethylcarbodiimide Hydrochloride
PS	Polystyrene
MW	Molecular Weight
YG	Yellow/Green
PVA	Polyvinyl Alcohol
EMAL	University of Michigan Electron Microbeam Analysis Lab
SEM	Scanning Electron Microscopy
APC	Allophycocyanin
MFI	Mean Fluorescent Intensity
MESF	Molecules of Equivalent Soluble Fluorochrome
SS	Shear Stress
MCHC	Mean Corpuscular Hemoglobin Concentration
MCV	Mean Corpuscular Volume
VOC	Vaso-Occlusive Crisis

PCA	Patient Controlled Analgesia
EDL	Erythrocyte Diagnostic Lab
CBC	Complete Blood Count
MPs	Micro-particles
NPs	Nano-particles
AR	Aspect Ratio

Abstract

Blood and heart-related diseases remain a significant challenge for modern-day medicine [1]. Blood cell-related diseases have also proven to be challenging to understand and treat, specifically diseases involving the loss of deformability (rigid) in red blood cells (RBCs) [2]. Disease involving rigid RBCs are typically of genetic origin and thus limit treatment options and treatment efficacy [3]. Rigid RBC disorders give rise to many medical complications, including vaso-occlusion, pulmonary hypertension, and cardiac dysfunction [4,5]. Patients inflicted with Sickle Cell Disease (SCD), hereditary spherocytosis, iron-deficient anemia, pyruvate kinase deficiency, human immunodeficiency virus (HIV), malaria, sepsis, and even natural aging all have less deformable (rigid) RBCs than healthy patients [3,6,7]. Rigid RBCs cause major physical damage when traveling through the body by occluding microvasculature, depriving tissues of nutrients, and damaging walls of the spleen, liver, and lungs [5,8].

The core work presented in this dissertation aims to probe how decreases in RBC deformability affect hemodynamics and impact functionality of other blood cells, clarifying the pathology of RBC-related diseases. We initially present a model of artificially rigidified human RBCs which offers an experimental control over extent of membrane stiffness as well as the fractional composition of rigid RBCs in whole blood. Here, we find that the presence of rigid RBCs in blood flow significantly alters the ability of immune cells to adhere to inflammation on the vascular wall of a microfluidic model. In some cases, the presence of highly rigid RBCs reduces leukocyte adhesion to the vascular wall by up to ~80%. Following this initial investigation, we take a pivotal focus on SCD and further quantifying the whole blood characteristics of SCD

pediatric patient blood and its behavior in flow. This thesis presents multiple investigations highlighting the outcome of RBC rigidity in SCD. An interesting clinical case study is highlighted in this work as well as additional *in vitro* work showing how the presence of RBC rigidity alters immune cell adhesion functionality. An artificial model of blood infusion therapy is also developed to test how leukocyte adhesion to inflammation is impacted upon alteration of whole blood composition. This knowledge is essential in understanding why people with diseases related to RBC deformability are susceptible to infection and have irregular immune responses.

In addition, we also investigate how rigid RBCs in blood flow alter the adhesion efficacy of vascular-targeted carriers (VTCs). The field of drug delivery has taken an interest in combating numerous blood and heart diseases such as atherosclerosis via the use of VTCs. Ideally, VTC technology increases drug delivery efficacy and simultaneously reduces cytotoxic effects, precisely localizing drugs only to the disease site through receptor-ligand interactions. Cellular interactions are not yet fully understood. The dynamics of disease-inflicted cells (rigid RBCs) are even less understood, thus compounding the problem of efficient VTC design under diseased blood conditions. We investigate various particle design parameters and assess their vascular wall adhesion performance in the presence of rigid RBCs. We find the vascular adhesion of stiff microparticles is reduced by up to ~50% in the presence of rigid RBCs. Interestingly, deformable hydrogel microparticles can experience an increase in vascular adhesion of up to ~ 80%. This work explores an opportunity to develop new therapeutics with high efficacy in diseased blood.

Chapter 1 : **Introduction**

1.1. Publication Information

The text in this chapter is in part from the publications listed below. Modifications have been made to the published documents to adapt the content to this text. This chapter provides an overview of blood flow dynamics and phenomena. This chapter also touches on common blood disorders characterized by increased red blood cell membrane stiffness and provides a more comprehensive overview of sickle cell disease. Additionally, this chapter provides a background on vascular-targeted carrier therapeutics and design considerations for optimizing performance in variable blood flow conditions.

Mario Gutierrez, Margaret B. Fish, Alexander W. Golinski, and Omolola Eniola-Adefeso. "Presence of rigid red blood cells in blood flow interferes with the vascular wall adhesion of leukocytes." Langmuir 34.6 (2018): 2363-2372. [10]

Mario Gutierrez, Mark Shamoun, Katie Giger Seu, Tyler Tanski, Theodosia A. Kalfa, and Omolola Eniola-Adefeso. "Characterizing bulk rigidity of rigid red blood cell populations in sickle-cell disease patients." Sci Rep 11, 7909 (2021). https://doi.org/10.1038/s41598-021-86582-8 [11]

Mario Gutierrez, Lauro Sebastian Ojeda, and Omolola Eniola-Adefeso. "Vascular-targeted particle efficacy in the presence of rigid red blood cells: Implications for performance in diseased blood." Biomicrofluidics 12.4 (2018): 042217. [12]

1.2. Whole Blood Dynamics and Characteristics

1.2.1. Whole Blood Physiology

Blood is a highly concentrated, non-Newtonian suspension of RBCs, white blood cells (WBCs), platelets, and plasma.[13] Bulk blood flow, as found in most blood vessels, is an anisotropic aqueous suspension, consisting of primarily RBCs in the core while the other blood cells form an outer ring at the wall. [14–16] Healthy RBCs are disc-shaped (6-8 μm diameter) and highly flexible, allowing RBCs to squeeze through capillaries.[13] In healthy humans, RBCs constitute anywhere from 30%-45% v/v of blood, which is defined as hematocrit (Hct).[13] Blood flow properties are influenced by multiple physical factors: cell to cell collisions, the shear rate of flow, RBC deformability, and vessel geometry.[17] The RBC core occupies the center of flow, and the red blood cell-free layer (RBC-FL/CFL) develops near the walls of the vessel, which aids in pushing stiffer objects, e.g., WBCs and platelets, to the vessel wall to sample the endothelium for disease and rupture constantly.[15,16,26,27,18–25] The distribution of blood components in flow, as described, is founded upon hydrodynamic interactions that generate varying levels of lift force.[28] The lift force is a product of the interaction between deformable cells, e.g., RBCs, and the vessel wall in a process deemed wall-induced migration; this specific interaction produces the RBC-FL.[28] Naturally stiffer cells, e.g., WBCs and platelets, are less affected by the lift force and thus do not populate the core of flow as densely as RBCs.[28] Hemodynamic, heterogeneous collisions between the highly deformable RBCs and stiffer WBCs and platelets also promote the distribution of the latter to the vascular wall.[29–31] Specifically, when relatively rigid WBCs collide with deformable RBCs, the RBCs deform, and the stiffer cells are displaced farther towards the wall – a process referred to as margination. This margination phenomenon is illustrated in Figure 1.1. This deformability and shape-driven arrangement of cells in blood flow are essential for maintaining

homeostasis and for providing rapid immune responses in the body.[32] Collagen-activated platelets and inflammatory cytokine-recruited WBCs can quickly reach any site of vascular injury due to their constant proximity to the vascular wall. [32] Interestingly, despite the widely known impact of deformability on cellular margination in blood flow, little experimental work exists explicitly focusing on the effects of RBC rigidity, i.e., loss of deformability, on margination.[29] Work by Passos *et al*. showed that blood containing RBCs with loss of membrane deformability resulted in significant alterations in flow distributions and cellular flow velocity profiles in a microchannel. [33] Mainly, a reduction in velocity bluntness was observed when stiffened RBCs were present in blood flow.[33] Recent computational works have begun to elucidate the transport mechanisms of cell types with different physical properties in blood flow and have underlined the major impact of cell size and rigidity on blood margination.[30,31,34] However, there are many challenges to modeling such highly complex fluid flow as human blood accurately, e.g., selecting appropriate boundary conditions and appropriately modeling the multiphase composition of blood.

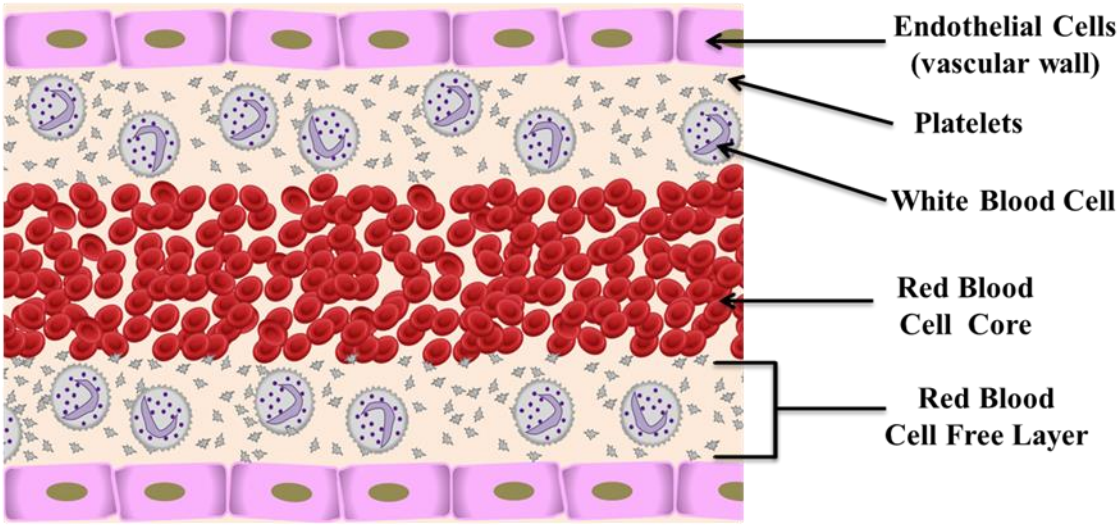

Figure 1.1. Illustration of Blood Flow Margination.

The illustration shows the segregation behavior that can be observed in certain vessels. The more deformable cells, RBC greatly experience a lift force away from the vessel wall forming the RBC core in the center of flow. Other naturally stiffer cellular components localize closer to the vessel wall.

1.2.2. Computational Modeling of Blood Cellular Interactions

Recent work has begun to computationally elucidate the transport mechanisms of cell types with different physical properties in blood flow. [30,31,34–39] Some researchers conclude that the RBC core forms due to high RBC deformability.[29,31] Kumar and Graham cite hydrodynamic, heterogeneous collisions between blood components as a critical reason for blood cell segregation in flow. When relatively rigid platelets or WBCs collide with deformable RBCs, the RBCs deform, and the WBCs displace a farther distance. Additionally, WBCs will encounter more heterogeneous collisions, as they exist in a 1:100 number ratio to RBCs. The work also cites wall-induced migration, also known as lift, as another reason for deformable entities to congregate near the center of flow [30]. Both rigid RBCs and deformable particles can be inserted into these theoretical simulations to predict their behavior. Computational work underlines the importance of heterogeneous collisions, i.e., impacts between rigid and deformable cells, in blood margination, Graham *et al.*[30,31,34] Czaja and coworkers both experimentally and computationally investigate the influence RBC membrane deformability has on platelet margination.[40] Interestingly, in this investigation, it was found that platelet margination to the vessel wall is reduced in the presence of rigid RBCs in blood flow.[40] Additionally, in confirmation with previous work, it was found via cell-resolved simulations that upon heterogeneous cellular collisions, stiffer RBCS experience a greater displacement in comparison to their deformable counterpart.[40] There are a large variety of theoretical models that predict hemodynamic behavior; however, most simulations oversimplify the complexity of blood. For example, some models disregard the blood plasma viscosity ratio; moreover, this parameter has been determined to either tank treading or tumbling behavior for RBCs [30]. There is a sizeable experimental gap in the literature in this area. Thus, there is a critical

need for experimental results that supplement theoretical models to understand bulk blood flow phenomena better and potentially optimize blood-related therapeutics.

1.3. Sickle Cell Disease

1.3.1. Understanding Sickle Cell Disease

SCD is one of the most common and complex genetic blood disorders worldwide. [3,41,42] SCD originates as a mutation of the gene encoding for the oxygen-binding protein hemoglobin. There are multiple genotypes of this hereditary blood disorder, all characterized by mutated hemoglobin S (Hgb S or HbS) production. [42] RBCs with a high content of HbS have a significantly reduced oxygen-binding capability and a high propensity to polymerize under hypoxic conditions. [3,43] The formation of a polymer nucleus and the increased concentration of unbound oxygen inside the RBC then induces oxidative damage on the cellular membrane, leading to a loss in membrane deformability. [2] The oxidative damage to the cell membrane also makes the RBCs prone to lyse, resulting in anemia and the release of hemoglobin into the open bloodstream, which damages the vascular wall, i.e., upregulation of inflammation markers. [5,44–49] Under hypoxic conditions, the mutated hemoglobin can frequently polymerize to cause the trademark sickled-shape of the RBC.[42,50] Historically, the **irreversibly**-sickled RBCs (**i-sRBCs**), i.e., having a permanent sickle shape, were the focus of research in SCD, leading to the understanding that these cells cause significant physical damage to vital organs, including the spleen, liver, and lungs, by occluding microvessels, and depriving the tissues of nutrients and oxygen.[8,51] As such, SCD is characterized by highly detrimental symptoms, including pulmonary hypertension, anemia, and vaso-occlusion that can cause chronic organ damage. [42] These SCD symptoms are also accompanied by severe pain episodes known as “crisis” that represent a significantly reduced quality of life for SCD

patients. [42] Chronic inflammation, vaso-occlusion, and overall negative symptoms in SCD originate from increased rigidity in the RBC membranes. [42,48,52] However, only a small fraction of i-sRBCs are present in the patient's blood at a given time due to their high rate of lysing.[53] Instead, the **reversibly**-sickled RBCs (**r-sRBCs**), i.e., highly rigid but not sickle-shaped, are the main sickled RBCs circulating in SCD, especially under stable, non-crisis conditions. Nevertheless, little attention has been given to how the r-sRBCs, i.e., rigid RBCs, in the bloodstream may impact the dynamics and functionality of other blood cells in SCD, e.g., WBCs, and the potential downstream contribution to disease symptoms beyond the occlusion of the microvasculature.

The current understanding of SCD is mainly focused on the biochemical and genetic components of the disease. Conversely, the increased RBC membrane rigidity – separate from the sickled crescent-shape – is often overlooked as a significant factor in disease severity. Nevertheless, the presence of stiff RBCs (not altered in shape) in blood was recently shown to reduce the vascular wall adhesion of WBCs drastically and increase the vascular wall adhesion of platelet. [10,12,54] This works potentially hints at a more significant role for RBC rigidity in SCD patients' well-being beyond instigating vaso-occlusion. As mentioned in the previous subsections, bulk blood flow is dominated by many flow phenomena. Thus, any alteration in RBC deformability, as present in SCD, likely alters blood cell distribution in ways that contribute to the disease. However, RBC rigidity in SCD is often overlooked as a significant factor in exacerbating disease symptoms associated with the other, non-RBC, blood cells.

The symptoms of SCD present early in life, with the most common initial symptom being dactylitis – inflammation of fingers or toes. As patients progressively age, continued damage to small vessels throughout the body leads to common symptoms such as retinal injury, kidney damage, neurocognitive delay, priapism, and functional asplenia.[55] Late in life, it is common for

patients to suffer from chronic pain disorders, depression, anxiety, pulmonary hypertension, and stroke.[55] Thus, SCD patients have a significantly decreased lifespan by 20-30 years, compared to healthy non-SCD individuals in industrialized countries, and by much shorter in developing nations.[56]

1.3.2. Current treatments in Sickle Cell Disease

To date, the only known curative therapy for SCD is hematopoietic stem cell transplantation, but outcomes depend heavily on the source of cells. Matched, related donors have >90% 5-year event-free survival; however, matched, unrelated donor and cord blood stem cells have a significantly higher mortality rate.[57] Unfortunately, many patients do not have matched related donors and thus are not entrants for transplantation. In addition, it is often overseen that a large proportion of people affected with SCD are located in a developing nation or come from a low social-economic background.[56] Thus, the aforementioned therapy is very likely to be out of reach for many SCD patients as it can be costly.

Other pharmaceutical therapeutic options are aimed at decreasing disease severity by reducing inflammation, such as L-glutamine, or by increasing fetal hemoglobin (%HbF) with agents like hydroxyurea (HU). To date, these mentioned pharmaceuticals are the only US Food and Drug Administration-approved drugs to improve SCD complications.[58] While these treatments prevent some symptoms; breakthrough crises are still observed in most patients.[59,60] Chronic blood transfusion is yet another option. However, it also carries significant risks, e.g., iron overload that is toxic to organs and alloimmunization, the process of forming antibodies against foreign blood products, which can lead to deadly hemolytic crisis.[61] Chronic blood transfusions are often used for SCD patients with recurrent pain crisis or frequent acute chest syndrome.[62]

Previous studies have proposed reducing the %HbS to <30% is beneficial in moderating symptoms versus no transfusion.[63] However, characterization of why this works is lacking.[63] To our knowledge, no widely accepted protocols for targeting post-transfusion Hct or %S have been established. We hypothesize that transfusion in SCD patients directly affects blood cell mechanics, potentially altering WBC adhesion to the endothelium. A better understanding of how transfusion affects WBCs could help clinicians optimize transfusion to reduce infection rates for SCD patients better.

Symptomatic treatment for pain crisis is often with opioids, but long-term use brings consequences, such as central sensitization syndrome and addiction risk.[64] Also, there is concern that the recent attention to a national "opioid crisis" has raised concerns that SCD patients may face reduced access to opioids due to an increased reluctance by clinicians to prescribe, especially with the added difficulty of pain assessment in the absence of a visualizable or measurable cause.[65] During painful episodes, it is clinically typical to treat vaso-occlusive crises with intravenous fluids implementation.[66] Potential alterations to cellular biomechanics due to changes in fluid tonicity are disregarded. However, Carden and coworkers have presented evidence to show that changes in blood tonicity, such as implementing clinical intravenous fluids, alter RBCs deformability and ultimately lead to changes in observed channel occlusion. [66]

1.3.3. Characterizing RBC Stiffness Concerning Pain crisis in Sickle Cell Disease

Common hematological characteristics and clinical observation are the common determinants used to assess SCD complications in a clinical setting. However, this may not be an entirely reliable method for quantifying disease severity as pain is subjective and clinical observations may vary. Thus, using more established and consistent biomarkers for assessing

patients' general condition or response to medication is likely a more suitable option. To date, only a handful of works have focused on elucidating how RBC rigidity directly impacts disease severity in SCD. In two seminal publications, Ballas *et al*. reported that RBC stiffness is predictive for disease severity, where patients with more deformable RBCs, as determined by osmoscans, had a higher rate of crisis.[67,68] However, osmoscans are a measure of RBC deformation in response to changes to osmolality at a fixed shear stress and may not be an accurate measure of deformability in SCD, i.e., RBCs are exposed to a fixed osmolality (~290 mOsm/kg) at varying shear as they transport through different vessels.[69] Also, existing osmoscan data were mainly obtained at a shear stress of 30 Pa, which is larger than values encountered *in vivo*; yet, the characteristic of the osmoscan curve is significantly influenced by shear stress. Thus, recent characterizations of RBC rigidity employ ektacytometry to measure an elongation index (EI), i.e., changes in cell shape, in response to changes in shearing stresses at a fixed, physiological osmolality.[70] However, these primarily measured the average rigidity of all RBCs in the blood sample, which can vary depending on the fraction of normal to sickled RBC (%S; fraction of sickled RBCs), i.e., two patients can register the same bulk blood rigidity but have a significantly different rigidity level in their r-sRBCs due to variation in their %S. Understanding the degree of stiffness in reversibly sickled RBCs is crucial. It would allow for a more accurate characterization of the impact of RBC rigidity on the frequency and, more importantly, the intensity of SCD crisis, vaso-occlusion, and risk of infection. Alternative methods that allow for the characterization of the rigidity of sickled RBCs in isolation, including micropipette, AFM, optical tweezers, and membrane flickering methods, are limited in that they are static techniques, low throughput, labor-intensive, or require specialized manipulation.[70–73] Recent microfluidic approaches offer high throughput but do not quantify RBC stiffness.[72] Interestingly, microfluidic lab-on-a-chip devices have been developed to assess the

RBC condition of donor blood that is to be utilized for infusion therapy purposes, not specific to SCD.[74] A better potential understanding of the scientific basis for pain in SCD can lead to better management, potentially reducing the frequency or need for opioid use.

1.3.4. Impact of Rigid RBCs on WBC Functionality in Sickle Cell Disease

As previously stated in a previous subsection, the unique layout of cells in the blood, RBCs in the core, and other cells in the CFL is, in part, due to the highly deformable RBCs experiencing a lift towards the center of flow while the stiffer cells are pushed to the wall, i.e., margination.[28] With such importance of deformability to cellular distribution in normal blood flow, it is likely that the pronounced rigidity of RBC in SCD changes cell distribution to affect their natural functions. Indeed, the sequestration of RBCs in the capillaries that are said to cause crisis pain is due to the increased margination of sickled RBCs into the CFL and hence their higher concentration in the capillaries.[75] However, the impact of the r-sRBCs on the margination and function of other blood cells is less clear and underexplored. Interestingly, SCD patients are prone to infection that is traditionally linked to the damage to the spleen by i-sRBCs,[44,76], but such increased rate of infection is not often observed in medical conditions where the spleen is deliberately removed in animals.[77] It is plausible that the presence of rigid, r-sRBCs in blood alters WBC margination, which affects vascular adhesion and, thereby, contributes to the reported high infection rate in SCD. Indeed, Boggs *et al*. observed a diminished marginal granulocyte pool in SCD, i.e., the fraction of WBCs present in the tissue space,[78] which they hypothesize is the cause of the abnormally high circulating WBC count typically reported in SCD.

Despite the known role of WBC in the pathogenesis of SCD, there is limited work fully exploring the mechanism of their adhesive interactions under flow conditions with patient blood

or representative models of human blood. The current understanding of the adhesive behavior of WBCs in SCD has been generated with isolated cells and in static adhesion assays, which neglect the biophysical contributions of the rigid RBCs.[79,80] Previously published work using SCD patient blood have focused on elucidating the differences in WBC adhesion molecule expression via flow cytometry,[80] leading to the observation that WBCs are in a pre-activated state and the assumption of their enhanced ability to adhere to the vascular wall in comparison to cells found in the healthy blood. It is known that the expression of P-selectin in an inflamed endothelium significantly contributes to the progression of vaso-occlusive crisis in SCD.[81] Recent work has utilized an *in vitro* microfluidic assay to assess the adhesive interactions between leukocytes and P-selectin in physiological flow conditions.[82] The study mainly focused on assessing whether the drug candidate, Crizanlizumab, could inhibit interactions between leukocytes and P-selectin.[82] The sparse adhesion studies with whole patient blood that exist have focused on the difference in WBC adhesion due to alteration in protein expression with no control for the role of RBC rigidity.[83,84] Though several analyses of WBCs adhesion in mouse models of SCD exist,[84] the differences in RBC geometry and deformability between humans and mice,[85,86] which directly impact margination, would prevent direct extrapolation of mice data to humans.

1.4. Vascular-Targeted Therapeutics Design Considerations

Particle therapeutics have received much attention for use in disease treatment due to their high potential for achieving localized delivery of drugs and imaging agents, and in some cases, for the added benefit of controlled release of therapeutics.[87] The administration of therapeutic particles via intravenous (IV) injection is attractive due to the (1) non-invasive nature and (2) extensive

reach of the vascular system to target tissue throughout the body. Often, disease-specific proteins expressed by the endothelium – the monolayer of cells lining the lumen of most blood vessels – are employed for target recognition by the particle therapeutics, i.e., vascular-targeting. Specifically, in certain diseases, such as atherosclerosis, the endothelium produces an inflammatory response, [88,89], which upregulates inflammatory surface markers not found on the endothelium in healthy tissues and, thus, are attractive for use as targets to disease. [89] To this end, targeted-drug delivery systems employ the conjugation of surface moieties, such as peptides and antibodies, with high affinity for these differentially expressed inflammatory disease markers. In theory, particulate carriers fitted with the disease-specific moieties will be captured to the blood vessel wall expressing the targeted protein in the diseased tissue. However, to target the diseased vascular wall effectively, particularly in mid-to-large arterioles and postcapillary venules, particles must first localize, i.e., marginate, to the vessel walls. [30,90,91] Researchers have shown that particle margination is highly dependent on the biophysical, multicomponent nature of blood. [28,30,31,38,92–96]

RBC deformability is known to drastically alter certain diseases of genetic origin, such as sickle cell disease (SCD) and hereditary spherocytosis, [3,97] and in others that developed upon a viral or parasitic invasion, such as human immunodeficiency virus (HIV) and malaria. [7,97] The RBCs in patients with Type 2 Diabetes (T2D) have also been reported to be significantly less deformable than healthy cells. [98] Metabolic disorders such as obesity and lifestyle habits such as smoking can also reduce the deformability of RBCs. [99–101] Additionally, studies have shown that RBC populations become *stiff*er, less deformable, on average in natural aging. [101,102] Since particle therapeutics aim to treat diseases that are most common in older age groups, such as coronary artery disease, understanding particle dynamics and localization functionality in the presence of

rigid RBCs could hold significant implications for designing particle therapeutics with high efficacy in diseases with altered RBCs. [103–105]

1.5. Dissertation Outline

As mentioned in the previous subsections, the membrane deformability of RBCs can significantly influence blood flow dynamics and alter the functionality of other cell types in the blood. However, there is still a lot to uncover the underlining mechanisms of action that influence the alteration in blood dynamics, specifically in identifying and quantifying the true extent of influence RBC membrane rigidity has on said alterations. Furthermore, there is a lack of *in vitro* models that represent RBC stiffness in whole blood. The characteristic of RBC rigidity is a common attribute in multiple diseases. In this dissertation, we first focus on understanding the fundamental influence of RBC stiffness on flow dynamics and functionality of other blood cells as well as vascular-targeted therapeutics. Secondly, we focus on developing a more robust method for quantifying RBC rigidity in whole blood. Finally, we take a particular interest in investigating RBC rigidity in sickle cell disease and its role in influencing immune functionality and disease outcome.

Chapter 1 provides a background on blood composition and a general overview of blood flow phenomena and methodology for quantifying RBC stiffness. In addition, a brief background on sickle cell disease is provided.

Chapter 2 is a description of the experimental techniques and methodology used to collect data throughout the entire dissertation.

In Chapter 3, we explore how the degree of RBC stiffness and quantity of rigid RBCs in whole blood influence the ability of WBCs to adhere to an inflamed endothelium microfluidic model. Specifically, we identify a non-linear response in WBC adhesion reduction based on the fraction of rigid RBCs present in whole blood. Additionally, we identify alterations in cellular radial distributions in the presence of rigid RBCs.

In Chapter 4, we further develop the methodology presented in Chapter 3. Specifically, we further analyze how ektacytometry measurements are impacted by both the degree of rigid RBCs and fraction of rigid RBCs present in a blood sample using an RBC artificial stiffening model. We make direct comparisons to ektacytometry measurements made on sickle cell patient blood samples.

In Chapter 5, we present an interesting clinical case study. Here we observed and measured via ektacytometry the blood of a group of sickle cell disease patients. Interestingly, the patient diagnosed with the less severe variant of sickle cell disease registered the stiffest RBCs. Additionally, the patient of interest has an irregularly high amount of hospital admissions due to pain crisis.

In Chapter 6, we further analyzed the blood of sickle cell disease patients using the methodology presented in Chapters 3 and 4. We develop an artificial blood model that directly matches the characteristics of sickle cell disease blood samples and test the ability of WBCs to adhere to inflammation. We find that in most cases, RBC rigidity plays a role in reducing the ability for WBCs to adhere to inflammation in blood flow as related to sickle cell disease.

In Chapter 7, we investigate how blood infusion therapy in sickle cell disease alters immune functionality. Specifically, we probe how controlled RBC infusion in sickle cell disease

blood samples alters the ability of WBCs to adhere to an inflamed endothelium in blood flow. We find there is the potential for optimizing infusion therapy by maximizing immune cell adherence.

In Chapter 8, we probe how the presence of rigid RBCs influences the adhesion capability of vascular-targeted carriers. Previous work shows that size, shape, and material characteristics of drug particle carriers greatly influence their targeting capability; here, we see how these effects are compounded by the presence of rigid RBCs in blood flow.

Chapter 9 provides the conclusions for this dissertation and discusses the future directions and outlook for the work presented here.

Chapter 2 **: Materials and Methods**

2.1. Introduction

This chapter provides a detailed list of the experimental protocols and methodology used to generate the experimental data presented in Chapters 3 through 8. Methodology ranging from human blood draw protocols to drug particle model fabrication are provided. Different microfluidic *in vitro* techniques for testing blood and drug particle adhesion capability in blood flow is also described.

2.2. Human Study Approvals and Blood Handling

2.2.1. Human Study Approvals for Non-SCD Blood Donors

For the studies presented in both Chapter 3 and Chapter 8, fresh human blood is obtained on the day of experiments via venipuncture according to a protocol approved by the University of Michigan Internal Review Board (IRB-MED). Informed, written consent was obtained from all subjects before blood collection. Blood was obtained from healthy subjects and drawn into a syringe containing citric acid-sodium citrate- dextrose (ACD) as an anticoagulant and stored at 37 ºC as described in Onyskiw *et al.*[106] For the studies presented in both Chapter 3 and Chapter 8, RBCs were isolated from whole blood by adding 6% dextran to anticoagulated blood in an inverted syringe, which sediments the RBCs from WBCs and plasma. WBC-rich plasma was then stored at

37 °C until recombination with RBCs at specified Hct (% vol/vol). RBCs were washed by suspending in phosphate-buffered saline (PBS) (-/-) and centrifugation. For all other studies, RBCs were isolated strictly via series of centrifugation steps.

2.2.2. Preparation of Human Non-SCD Blood for Ektacytometry Analysis

For the studies presented in Chapters 4, 5, and 6, fresh blood was obtained from healthy, i.e., no SCD donors on the day of ektacytometry measurements via venipuncture. Blood was drawn into standard Vacutainer Lavender K2-EDTA tubes (BD). Multiple tubes were taken from healthy donors. For the work presented in Chapter 4, blood from healthy donors was then separated from WBC-rich plasma via a series of slow-speed centrifugation steps. RBCs from healthy donors were washed thoroughly via suspension in phosphate-buffered saline (PBS -/-) and centrifugation. RBCs and WBC-rich plasma were stored at 4 ºC until artificial rigidification and reconstitution, which was done right before ektacytometry analysis. For the work presented in Chapter 5 and Chapter 6, blood samples in lavender K2-EDTA tubes aimed for ektacytometry analysis are stored and shipped in 4 ºC cold packs overnight.

2.2.3. Study Approvals and Preparation of Human Non-SCD Blood in SCD related Studies

For the work presented in Chapter 6 and Chapter 7, Healthy, i.e., non-SCD donors are informed of the study and give written consent before blood collection. Fresh blood from healthy donors is drawn into standard Green Sodium Heparin Vacutainer tubes (BD). Multiple extra green tubes are taken from non-SCD donors. Blood from healthy donors in green sodium heparin tubes is then separated from WBC-rich plasma via a series of slow-speed centrifugation steps. RBCs from healthy donors are washed thoroughly via suspension in phosphate-buffered saline (PBS -/-)

and centrifugation. RBCs and WBC-rich plasma are stored at 37 ºC until artificial rigidification and reconstitution.

2.2.4. Study Approvals and Preparation of SCD Patient Blood

Blood draw protocols have been approved by the University of Michigan Internal Review Board (IRB-MED). SCD donors and legal guardians are informed of the study and give written consent before blood collection. Fresh blood is obtained on the day of a patient's routine clinical visit via venipuncture. Blood used in perfusion assays is drawn into standard Vacutainer Green Sodium Heparin tubes (BD) and stored at 37 ºC. In addition, three Lavender Vacutainer K2-EDTA tubes are taken from SCD patients for ektacytometry and hemoglobin electrophoresis analysis. Blood sample for ektacytometry analysis, lavender tube, was stored and shipped in 4 ºC cold packs overnight to Erythrocyte Diagnostics Laboratory of the Cancer and Blood Diseases Institute at the Cincinnati Children's Hospital for examination the following day. All SCD patient samples are measured within 24 hours of blood draw. In the scenarios where patients were either not feeling well or had undergone multiple failed needle insertions, additional blood samples were not collected.

2.2.5. SCD Patient Blood Analysis and Characterization

Complete blood counts were run on a Sysmex 9100 XN automated machine. The phlebotomy team collected whole blood (~3 mL) into an EDTA lavender top tube (BD). The sample was then sent to the hematology lab at Michigan Medicine and run according to university protocol and manufacturer's instructions. Results were verified and reported through the electronic

medical records at the University of Michigan. Hemoglobin evaluation was run on a Bio-Rad Variant II cation exchange HPLC system by high-pressure liquid chromatography (HPLC). Whole blood (~3 mL) was similarly collected by the phlebotomy team in an EDTA lavender top tube and run per protocol. HPLC works by separating components of blood through interactions with the absorbent particles. Reports typically consist of five different hemoglobin genotypes, including Hgb S, Hgb A1, Hgb A2, Hgb C, and Hgb F.

2.2.6. Red Blood Cell Rigidification and Sample Preparation

Washed RBCs from healthy donors were suspended in a 2% hematocrit and incubated with a specific concentration of Luperox tert-butyl hydroperoxide (TBHP) (Sigma-Aldrich). RBC deformability was analyzed using ektacytometry. For the work presented in Chapters 3, 4, and 8, four parent concentrations of TBHP were chosen as base RBC rigidities: 1.0, 0.9, 0.75, and 0.5 mM TBHP. Incubation for 30 minutes induced the loss of RBC membrane flexibility. After adequate washing, stiffened RBCs were mixed with healthy RBCs in whole blood in increments of 10% rigid RBC fractions up to a total of 100% while holding the hematocrit constant at ~40%, unless otherwise specified. No RBC lysis was detected for the 30-minute incubation period for any of the TBHP concentrations evaluated. For the work presented in Chapter 6, a specified TBHP concentration is chosen to rigidify healthy RBCs. Stiffened RBCs are then reconstituted into whole blood at specified hematocrit.

2.2.7. Healthy Donor Red Blood Cell Rigidification and Sample Preparation

For the work presented in Chapter 6, two different artificial blood models have been denoted in this study to model/mimic SCD donor blood: the Rigid Model and Non-Rigid Model. More specifically, fresh blood from healthy non-SCD blood donors is separated, compositionally altered, and reconstituted to match unique SCD donor blood characteristics. The Rigid Model uses reconstituted healthy donor blood to match the hematocrit, WBC count, rigid RBC fraction, and approximate rigidity of the rigid population. Alternatively, the Non-Rigid Model matches only the hematocrit and WBC count of the SCD donor blood sample, excepting the rigidity attributes. Washed RBCs from healthy donors are suspended in a 2% hematocrit and incubated with a specific concentration of TBHP to induce loss of RBC membrane flexibility. The approximate TBHP concentration necessary to obtain a desired rigid RBC population stiffness was calculated using methods highlighted by Gutierrez *et al.* [11] Effectively, a TBHP concentration was chosen to achieve a rigid RBC population stiffness like that of the rigid RBC population in a unique SCD patient blood sample. RBCs are incubated for 30 minutes with a specified TBHP concentration to induce the loss of RBC membrane flexibility. Following adequate washing, stiffened RBCs are mixed with healthy flexible RBCs and WBC-rich plasma into specified whole blood conditions matching SCD patient blood characteristics, i.e., hematocrit, rigid-to-healthy RBC fraction, and RBC rigidity conditions.

2.2.8. Ektacytometry Deformability Measurements

All blood samples, both healthy and SCD donors, and artificially reconstructed blood samples, were measured independently using a LoRRca Maxsis Ektacytometer (Mechatronics Instruments BV, Zwaag, The Netherlands) at the Erythrocyte Diagnostics Laboratory of the

Cancer and Blood Diseases Institute at the Cincinnati Children's Hospital. SCD whole blood samples and reconstituted healthy donor samples were diluted ~200x in polyvinylpyrrolidone (MW 360,000) solution. The solution is then transferred into LoRRca automized measuring vessel. Measurements are taken through a range of shear stresses (Pa) up to a maximum of 60 Pa. Cell deformation is expressed as an elongation index calculated by Equation (1), where A represents the major axis and B the minor axis in deformation. Elongation Index (EI) values are plotted versus shear stress (Pa) to obtain the deformability curve.

$$EI = \frac{A - B}{A + B} \quad (1)$$

2.2.9. Adhesion Ligand Density Flow Cytometry Analysis

For the WBC adhesion ligand characterization, isolated whole blood samples were put into a 37 °C incubator. Subsequently, samples were stained and placed on ice for ~30 minutes as follows: MAC-1/CD11b, PSGL-1/CD162, LFA-1/CD11a, sLe^a/CLA, L-selectin/CD62L, (BioLegend). This step is followed by adding a 1-step Lyse/Fix solution (eBiosciences) to eliminate RBCs and fixate WBCs. Samples are washed twice with a FACS buffer solution (PBS -/- +2% FBS, pH ~7.4) before flow cytometry analysis. All flow cytometry analysis was performed on an Attune NxT Acoustic Focusing Cytometer, and results were analyzed using FlowJo software (TreeStar). Neutrophil and monocyte populations were sorted using FSC/SSC. Gating was applied to clarify the signal of interest. Samples analyzed on the same day were compared as a fold difference in intensity of the signal from those of the control group, i.e., Healthy donor samples.

2.3. Preparation of *in vitro* microfluidic studies

2.3.1. Preparation of Endothelial Cell Monolayer

Human umbilical vein endothelial cells (HUVECs) used in all assays were isolated from healthy umbilical cords (Mott Children's Hospital, Ann Arbor, MI) via a collagenase perfusion method, as described by Onyskiw *et al.*[106,107] Briefly, isolated HUVEC were cultured in T75 flasks and seeded onto 30 mm glass coverslips coated with 1% gelatin and cross-linked with 0.5% glutaraldehyde.[108,109] Coverslips were seeded with HUVEC and incubated at 37°C and 5% CO_2 with standard media until confluent density was reached.[108–110] For all studies, HUVECs were only used through the fourth passage. Confluent coverslips were activated with one ng/mL interleukin-1β (IL-1β) to induce inflammation and cell adhesion molecule expression for WBC adhesion assays. Incubation methods between 4-hour and 24-hour inflammation time point only differed in duration of exposure to IL-1β media solution. Previous reports show that E-Selectin receptor expression on HUVECs is maximal (~20 fold increase compared to unactivated HUVEC) 4 to 8 hours after IL-1β initial exposure. [111]

2.3.2. Parallel Plate Flow Chamber Laminar Blood Flow Assays

Laminar blood flow assays were conducted as previously described in Namdee *et al.* to investigate both WBC and drug particle adhesion to inflamed HUVEC monolayer.[106,112] Coverslips with confluent monolayer were held by vacuum to the parallel plate flow chamber (PPFC, Glycotech, Inc.). The PPFC was fitted with a rectangular gasket (0.25 cm x 2 cm, heights: 254 μm, 127 μm). A schematic of the PPFC configuration can be seen in Figure 2.1. Additionally, a microfluidic device was fabricated and employed to achieve a lower channel height of 50 μm.

Briefly, the 50 μm channel was designed using AutoCAD software. A template was fabricated on silicon wafers via a soft photolithography method, as described by Namdee *et al.*[112] Polydimethylsiloxane (PDMS) channels were then made with the use of the silicon wafer template. Individual blood samples containing were perfused through the PPFC in a laminar flow profile for 5 min at physiological WSRs of 200 s^{-1}, 500 s^{-1}, 1,000 s^{-1} by controlling the volumetric flow rate. The volumetric flow rate through the channel (Q) was controlled via a syringe pump (Harvard Apparatus), which dictates the WSR (γ_W), as shown in Equation (2),

$$\gamma_W = \frac{6Q}{h^2 w}; s^{-1} \quad (2)$$

where *h* is the channel height (cm), *w* the channel width (cm), and *Q* the volumetric flow rate (mL/sec). The chamber was flushed with PBS buffer containing 1% BSA at the end of the experiment, and the WBCs adherent to the HUVEC monolayer was quantified using ImageJ. The PPFC was carefully flushed with PBS+/+ buffer (PBS, containing 1% BSA crystals, Ca^{2+}, Mg^{2+} pH ~7.4) prior to the perfusion of the blood to clear out HUVEC surface debris and bubbles. After blood perfusion (5 min), PBS+/+ buffer was continuously added to the PPFC to maintain the fully developed flow profile and to wash out any unbound particles still in flow. Previous publications have shown that E-selectin expression, endothelial cell layer integrity (detachment), and flow profile are maintained within the experimental time frame explored in this work.[113] Fluorescent particle adhesion to HUVEC layer was observed on a Nikon TE2000-S inverted microscope fitted with a Photometrics CoolSNAP EZ digital camera with a Sony CCD sensor. Particle adhesion density was quantified using ImageJ. To avoid potential variation in fluxes along the chamber

length, adhesion data were collected at a constant position of ~1 cm (center) away from the channel entrance and exit. Entrance length estimations predict the flow profile is fully developed ~20 µm from the channel entry, well beyond the center of the channel where most of the data acquisition occurred. Both WBC and particle adhesion to the HUVEC monolayer can be represented as an adhesion density. However, for ease in comparison across blood donor variations, many WBC and particle adhesion experiments were expressed in terms of percent reduction relative to the healthy control of that specific donor, thus normalizing variability across blood donors. All experiments were quantified as the number of bound WBCs or particles/mm^2 HUVEC. Particles were added to whole blood samples at a concentration of ~10^6 particles/mL, or specified concentration, of blood and immediately perfused over the endothelial layer in the PPFC.

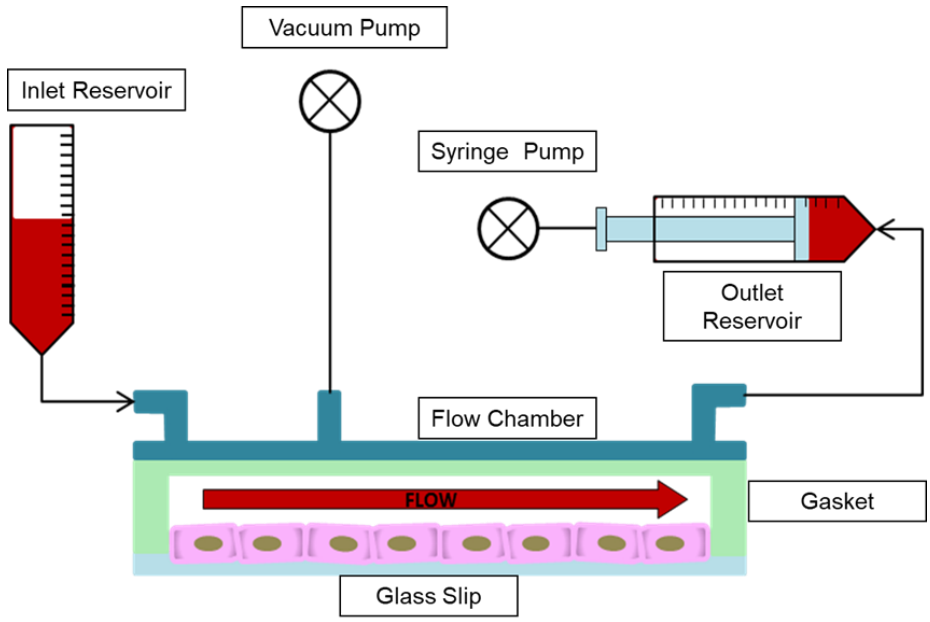

Figure 2.1. Illustration of Parallel Plate Flow Chamber *in vitro* Configuration.

The illustration shows the basic microfluidic set-up used in PPFC assays. HUVEC are cultured onto gelatin coated glass coverslips and subsequently are secured to flow chamber via vacuum adhesion. The inlet reservoir contains the blood under experimental conditions of interest. Flow in the chamber is instigated and adjusted via syringe pump connected to the outlet blood reservoir. The height of the channel is adjusted via interchangeable gaskets.

2.3.3. Red Blood Cell Flow Distribution Studies by Confocal Microscope

Blood samples were perfused through a ~100 µm ibidi channel similar to the PPFC setup as previously described by Namdee and coworkers.[112] Roughly 10% of total rigid RBCs per sample were stained with wheat germ agglutinin (WGA-488) and incubated for 10 minutes before examination; a higher staining percentage of RBC would saturate the fluorescence. For the healthy controls, 10% of total RBCs in the sample were stained with WGA 488. Images were taken using confocal microscopy with a 488-nm laser at 80% power, with the photo-multiplier tube (PMT) voltage set at 700V, 1X gain, and 0% offset. The microscope was run in a round-trip 0.488 ms/line using a 2x digital zoom and a 20x water immersive objective. A total of 52 images were collected per trial by adjusting the focal plane 2 µm height per image. Fluorescently-tagged RBCs were processed and counted using ImageJ by setting a constant threshold and the "Analyze Particle" function. Laser, PMT, and threshold settings were optimized for blank samples (no fluorescent RBCs) to contain less than 1% count of fluorescent RBC positive trials. The shutter speed was set to allow for visualization of individual fluorescent RBCs in the flow. The inside of the channel was marked with a red fluorescent protein (RFP) marker to facilitate the calibration of the starting height (inside-top of the channel) for the scan to begin. Results presented represent the number of detected fluorescent RBCs in each scanned plane, not simply the mean fluorescent intensity, and thus rendered RBC distribution in channel height. RBC distributions of each flow condition were condensed for comparison using Interquartile Range (IQR) analysis. All experiments were normalized to corresponding healthy control, i.e., no rigid RBCs present.

2.3.4. Particle Localization in Blood Flow Studies by Confocal Microscope

Blood samples containing particles were perfused through a ~100 µm ibidi channel, similar to the *in vitro* PPFC setup, as previously described above. Images were taken of the entire height of the channel in increments of 2 µm using a confocal microscope with a 488-nm (to image FITC polystyrene particles) and 543-nm (to image rhodamine hydrogel particles) laser at 80% power. The microscope ran in a round-trip 0.488 ms/line using a 2x digital zoom and a 20x water immersive objective. Fluorescent images of particles were counted using ImageJ by setting a constant threshold and the "Analyze Particle" function and analyzed using the methodology described above.

2.3.5. Sickle Cell Sample Hematocrit Alteration - Artificial Infusion Mimic

For the study presented in Chapter 7, individual SCD patient blood sample from green sodium heparin vacutainer tube is aliquoted at 1 mL volumes into 2 mL Eppendorf tubes. Using a simple mass balance, RBC volume plus plasma volume is equal to total volume; we derive a relationship that determines the RBC volume needed to raise the blood sample to a desired specific hematocrit. This relationship is represented as Equation (3).

$$R_{add} = P_0\left(\frac{1}{1-X_2} - 1\right) - R_0;\ mL \tag{3}$$

Where R_{add} is the volume needed to raise the blood sample to the desired hematocrit. P_0 is the initial plasma volume, X_2 is the desired hematocrit, and R_0 is the initial RBC volume. Both R_0 and P_0 are determined by knowing the initial hematocrit, i.e., X_0. Using RBCs obtained from healthy, non-SCD donors in sodium heparin, we then add controlled volumes of healthy RBCs to the SCD 1 mL Eppendorf aliquots to raise the hematocrit to desired hematocrits. This controlled addition

of healthy RBCs aims to mimic the simple blood infusion therapy process used to treat SCD patients. Once the hematocrit of a specific sample has been fixed to the desired hematocrit, it is ready for PPFC analysis. Of note, the total volume of the aliquots will inevitably change upon the addition of RBCs. Thus, only a fixed 1 mL of blood is taken from each aliquot. The total number of WBCs in each sample is variable. However, the concentration will be equal across all samples.

2.4. Drug Particle Fabrication and Functionalization Process

2.4.1. Deformable Hydrogel Particle Fabrication and Characterization

Deformable hydrogel particles of 2 μm diameter were fabricated by UV-initiated polymerization of polyethylene (glycol) diacrylate (PEGDA), and 2-carboxyethyl acrylate (CEA) as described by Fish *et al*.[114] The PEGDA, CEA, acryloxyethyl thiocarbamoyl Rhodamine B (Rhodamine), and lithium phenyl-2,4,6-trimethylbenzoylphosphinate photoinitiator (PI) were combined into methanol (MeOH) at 20% solids (80% MeOH). The MeOH-PEGDA solution was then emulsified into silicone oil by probe sonication and subsequently exposed to a 365 nm UV light for 10 minutes to initiate polymerization. All materials are obtained commercially, except the PI, which is synthesized internally as previously published.[115,116] Hydrogel particles of a 2 μm diameter were obtained by a series of centrifugation and filtration steps as previously described by Fish *et al*. [114] Centrifugation at low revolution rates helps pellet particle sizes greater than ~8 μm. The supernatant is kept and perfused through 2 μm filter tips (Agilent Technologies). The filtrated suspension is then centrifuged closely to remove small particle sizes outside of the interest size range. The deformability of the particles can easily be controlled by modulating the hydrogel cross-linking density. The Young's moduli (~113 kPa) of the hydrogel particles (20% solids) closely matches a value reported for WBC previously.[114]

2.4.2. Ellipsoidal Shaped Particle Fabrication and Characterization

Polystyrene (PS) rods are produced by using polyvinyl alcohol films to stretch 2 μm Fluoresbrite YG Carboxylate Microspheres (Polysciences, Inc). The spherical 2 μm particles were suspended in 100 mL aqueous solution of 7% w/v, 13,000-23,000 MW polyvinyl alcohol (PVA) (Sigma Aldrich). The vials were placed on a rotator for an hour to be mixed in thoroughly. The solution was then poured onto a single-well OmniTray (ThermoFisher) and placed on a flat shelf in a convection oven at 50°C overnight. The resulting films were cut into 2"x1" strips and attached to a single direction stretching apparatus within a convection oven that holds the strips with two parallel clamps – one stationary and the other moved along a pipe in one linear direction. The oven was preheated to 160°C before a pump pulled the moving clamp down the pipe and stretched the films to produce rod particles. The un-stretched ends of the films were cut off. The remaining films were dissolved with 30% v/v isopropanol (Sigma Aldrich). The rod particles were centrifuged and washed several times to remove the remaining PVA. The recovered particles were imaged using a Philips XL30 FEG scanning electron microscope (courtesy of the University of Michigan EMAL). The particle dimensions were measured using SEM images via Metamorph Software (Molecular Devices, LLC). The rods produced have a ratio of the major axis length to the minor axis length (aspect ratio) of 4 (AR4).

2.4.3. Particle Conjugation with Targeting Ligands

Fluoresbrite™ YG Carboxylated polystyrene rods and spheres were conjugated with NeutrAvidin biotin-binding Protein (Thermo Scientific) via carbodiimide coupling chemistry as previously described. [112] Subsequently, avidin-coated particles were conjugated with biotinylated

sialyl-Lewis A (sLe^a) (Glycotech, Inc.) and stored in PBS (-/-) with 1% wt BSA at 4 °C until ready for use in blood flow experiments. To estimate particle ligand density, particles with NeutrAvidin bonded on their surface are reacted with a range of Sialyl Lewis A (sLe^a) concentrations up to 10 µg/mL. Particles with reacted sLe^a are then stained with fluorescently labeled anti-CLA (allophycocyanin; APC) and subsequently examined via flow cytometry (Attune; Applied Biosystems). The particle populations of interest are gated, and the mean fluorescent intensity (MFI) in the APC regime ~660 nm of each subset of particles is recorded. Using calibration beads (Bangs Laboratories, Inc.), we create a calibration curve to convert MFI values into molecules of equivalent soluble fluorochrome (MESF) values. With the MESF and surface area of a single particle, we can approximate the number of sLe^a sites on a single particle, and the ligand site density is determined by normalizing the sLe^a sites by the particle surface area. In the linear regime, we interpolate in between the range of concentrations tested to determine which sLe^a concentration can achieve the desired number of sites on the different types of particles used. A fixed sLe^a site density of ~1,000 sLe^a site/μm^2 is used in all assays unless otherwise stated.

2.5. Statistics

PPFC *in vitro* flow experiment data is an average of 10 pictures of the HUVEC layer from each trial, with n=3 blood donors for each data point presented. Flow distribution experiments were repeated with n=3 blood donors for each perfusion condition. Trials with SCD donor blood were performed, n=1. Trials using artificially constructed blood models were performed n=3, all with unique healthy blood donors for each data point presented. Particle adhesion data collected from the *in vitro* PPFC model is an average of ten pictures from each trial, with n=3 blood donors

for each data point presented. All data points were included in the analyses and calculations of means or statistical significance for all studies. Data are plotted with standard error bars and analyzed as indicated in figure legends. Specifically, the ten brightfield images obtained for each data point (n =1) were averaged, and the standard error was calculated. The average values obtained for each "n" are averaged over multiple donors (n = 3) and standard error obtained by error propagation calculations. A 2-way ANOVA integrated package on GraphPad Prism was used to analyze any statistical difference between rigid and healthy conditions. Asterisks indicate p values of *<0.05, **<0.01, ***<0.001 and ****<0.0001 and lack of asterisks indicate not significant (n.s.).

Chapter 3 : Presence of Rigid Red Blood Cells in Blood Flow Interferes with Vascular Wall Adhesion of Leukocytes

3.1. Publication Information

The work presented in this chapter is published as: Mario Gutierrez, Margaret B. Fish, Alexander W. Golinski, and Omolola Eniola-Adefeso. "Presence of rigid red blood cells in blood flow interferes with the vascular wall adhesion of leukocytes." Langmuir 34.6 (2018): 2363-2372. [10]

Modifications have been made the published document to adapt the content to this text. This chapter aims to probe how WBC adhesion to inflammation is impacted in the presence of rigid red blood cells in an *in vitro* model of blood flow.

3.2. Abstract

The symptoms of many blood diseases can often be attributed to irregularities in cellular dynamics produced by abnormalities in blood cells, particularly RBCs. Contingent on the disease and its severity, RBCs can be afflicted with increased membrane rigidity as seen in malaria and sickle cell disease. Despite this understanding, little experimental work has been conducted towards understanding the effect of RBC rigidity on cellular dynamics in physiologic blood flow. Though many have computationally modeled complex blood flow to postulate how RBC rigidity may disrupt normal hemodynamics, to date, there lacks a clear understanding of how rigid RBCs

affect the blood cell segregation behavior in blood flow, known as margination, and the resulting change in the adhesion of WBCs. In this work, we utilized an *in vitro* blood flow model to examine how different RBC rigidities and volume fractions of rigid RBCs impact cell margination and the downstream effect on WBC adhesion in blood flow. Healthy RBC membranes were rigidified and reconstituted into whole blood and then perfused over activated endothelial cells under physiologically relevant shear conditions. Rigid RBCs were shown to reduce WBC adhesion by up to 80%, contingent on the RBC rigidity and the fraction of treated RBCs present in blood flow. Furthermore, the RBC core was found to be slightly expanded with the presence of rigid RBCs, by up to ~30% in size entirely comprised of rigid RBCs. Overall, the obtained results demonstrate an impact of RBC rigidity on cellular dynamics and WBC adhesion, which possibly contributes to the pathological understanding of diseases characterized with significant RBC rigidity.

3.3. Introduction

Blood related diseases remain common today and are difficult to manage due to their complex nature.[1] Blood cell diseases, in particular, have proven challenging to understand and treat, despite decades of research, specifically those diseases involving the loss of RBC deformability.[2] Diseases involving rigid RBCs are typically of genetic origin and have been studied mainly from this biological perspective, with their genetic nature limiting treatment options and efficacy.[3] Patients inflicted with SCD, hereditary spherocytosis, iron-deficient anemia, pyruvate kinase deficiency, HIV, malaria, sepsis, and even natural aging have less deformable (rigid) RBCs than healthy patients.[3,6,7,101] It is well known that rigid RBCs cause major physical damage when traveling through the body by occluding microvasculature, depriving tissues of

nutrients, and damaging the spleen, liver, and lungs walls.[5,8] This damage produces further complications such as pulmonary hypertension, and cardiac dysfunction.[4,5] However, to date, there is little understanding of the direct impact of RBC rigidity on the functionality of other blood cells and the downstream contribution to disease manifestation beyond the occlusion of microvasculature.[9]

The ability to fully elucidate the effects of cellular rigidity and shape on hemodynamic blood margination can offer useful insight into the pathology of the many diseases in which RBC rigidity has been implicated,[3,6,7,101] including in SCD that is the most described disease associated with altered RBC deformability. SCD is a hereditary multisystem disease,[3] which affects millions worldwide; estimates suggest that ~100,000 Americans are affected.[3] The polymerization of HbS produces long chains, which results in the sickling shape of the RBC, loss of membrane flexibility, reduced cell lifespan, and impaired blood flow to limbs.[3,50] Treatments for SCD are limited and highly invasive, e.g., use of narcotics, blood transfusions, and bone-marrow transplants.[3,117] However, little is known about the potential direct impact of the altered RBCs on the margination functionality of other blood cells, particularly WBCs. Indeed, SCD patients are known to have compromised immune responses to infections, which is attributed mainly to splenic dysfunctions.[45] However, it is possible that RBCs significantly alter cellular distribution in blood flow, and hence WBC margination, which would affect the natural immune response.

To address the research gaps highlighted, we experimentally probe the direct effects of rigidified RBCs on the resulting margination of WBCs from bulk blood flow to the vessel wall via a PPFC and human blood flow with the presence of rigidified RBCs in this chapter. Our results show that rigid RBCs in flow produced varying effects contingent on the level of RBC rigidity, the concentration of rigid RBC, and the magnitude of the blood flow shear rate. Overall, the work

presented in this chapter experimentally bypasses challenges including difficulty in accurately modeling hemodynamics, translating computational work into realistic *in vitro* models, and obtaining blood from disease inflicted patients. Ultimately, findings gained from a comprehensive investigation of cellular dynamics in blood flow can lead to profound advances in the understanding the pathology of many diseases.

3.4. Results

3.4.1. Effect of Tert-Butyl Hydroperoxide on RBC Membrane Deformability

It was key to first quantitatively characterize RBC membrane rigidities to determine the effects on hemodynamics. To produce a range of RBC deformability, as encountered across diseases,[118] we utilized four concentrations of TBHP to treat RBCs, 1.0 mM, 0.75 mM, 0.5 mM and 0.25 mM, and measured their ability to elongate under shear stress via ektacytometry, as described in the *Materials and Methods* chapter. Deformability is characterized by the change in axis ratio, known as EI – Equation 1. Figure 3.1.A. shows the EI curves obtained from the four TBHP treatments. There was no statistical difference between healthy RBCs and RBCs treated with 0.25 mM TBHP; therefore, we excluded 0.25 mM from the remainder of this work. Treatments of 0.5 mM, 0.75 mM, and 1.0 mM TBHP yielded significantly different EI curves versus the healthy control, translating to 2, 8 and 40 times less deformable (more rigid), respectively, than healthy RBCs at the highest applied shear. Furthermore, at low shear stress (≤2 Pa), RBCs treated with 0.5 and 0.75 mM TBHP behave similarly to healthy RBCs. A WSR of 1,000 s^{-1} in flow is equivalent to a shear stress of ~5 Pa, which is typically seen in vessels such as arterioles and capillary networks.[119,120] WSRs of 500 s^{-1} (~ 2.5 Pa) is seen in venules, and WSRs

of 200 s^{-1} (~1 Pa) are typical in large veins.[119,120] Comparing the results to previous work, the deformability of the RBCs treated with 0.5 mM TBHP are similar to those taken from a patient inflicted with sickle cell disease, while the deformability of RBCs treated with 0.75 mM TBHP mirrored those taken from a patient with sickle cell disease during a severe painful crisis.[121] From brightfield images of RBCs, there is little detectable change in shape of the healthy cells (Figure 3.1.B.) as compared to ones treated with 1.0 mM TBHP (Figure 3.1.C.). Indeed, previous works have shown that RBCs exposed to lower concentrations (0.5 and 1.0 mM) of TBHP exhibit negligible membrane protein degradation and morphological changes. [122]

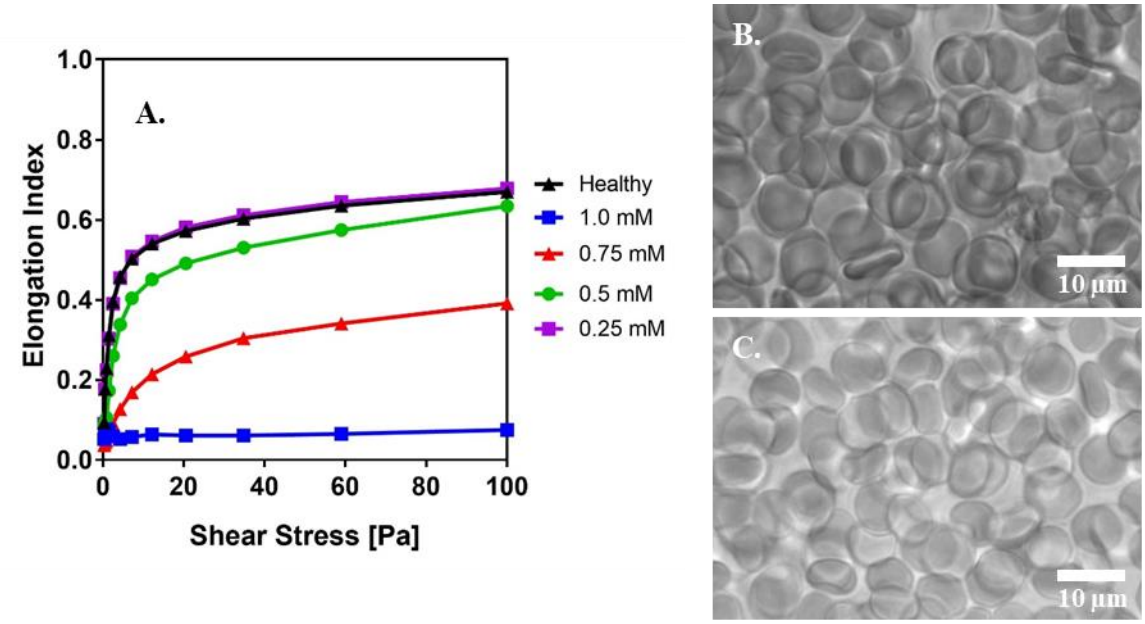

Figure 3.1. Red Blood Cell Characterization via Ektacytometry.

(A) Elongation indices of RBCs after treatment with 1.0, 0.75, 0.5, and 0.25 mM tert-butyl hydroperoxide and upon controlled applied shears. Representative image (60x) of (B) healthy (no TBHP) and (C) 1.0 mM TBHP treated RBCs in buffer at 2% Hct.

3.4.2. Effect of Rigid RBCs on Leukocyte Adhesion as a Function of RBC Rigidity and WSR

Once we quantitatively characterized the physical properties of the RBCs, we investigated how the presence of rigid RBCs in the whole blood affects leukocyte adhesion to the endothelium.

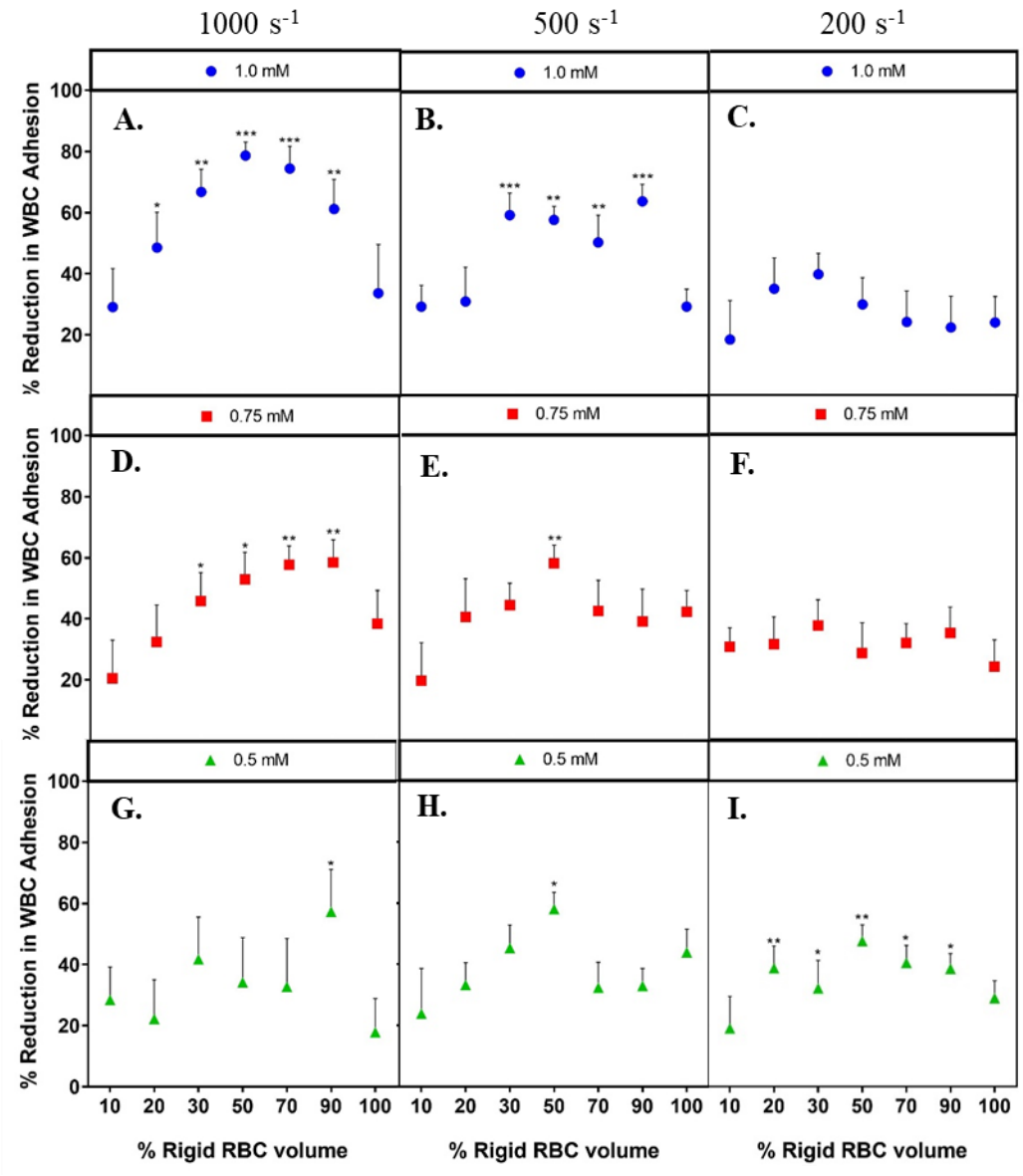

Figure 3.2. White blood cell binding to inflamed endothelium *in vitro* by Red Blood Cell Rigidity and Wall Shear Rate.

Quantified WBC binding to an IL-1β inflamed endothelial layer as a function of rigid RBCs present, i.e., % volume rigid RBC, for the different WSRs of (A, D, G) 1,000 s^{-1}, (B, E, H) 500 s^{-1}, and (C, F, I) 200 s^{-1}. All blood samples were reconstituted to a hematocrit of 40%. Trials plotted as reduction compared to healthy controls, i.e., no rigid RBCs present. Each figure represents one of three rigid RBCs treatments of 1.0 mM TBHP treated RBCs (most rigid), 0.75 mM TBHP treated RBCs, or 0.5 mM TBHP treated RBCs (least rigid). Statistical analysis of adherent density was performed using two-way ANOVA to test all WBC adhesion versus healthy WBC adhesion control. (*) indicates $p<0.05$, (**) indicates $p<0.01$, (***) indicates $p<0.001$, and (****) indicates $p<0.0001$. Error bars represent standard error.

We used an *in vitro* PPFC model and prepared blood as described in the *Materials and Methods* chapter. RBCs were reconstituted into a whole blood sample at a hematocrit (Hct) of 40%, and the sample is perfused through the PPFC at different physiologically relevant WSRs (1,000 s^{-1}, 500 s^{-}

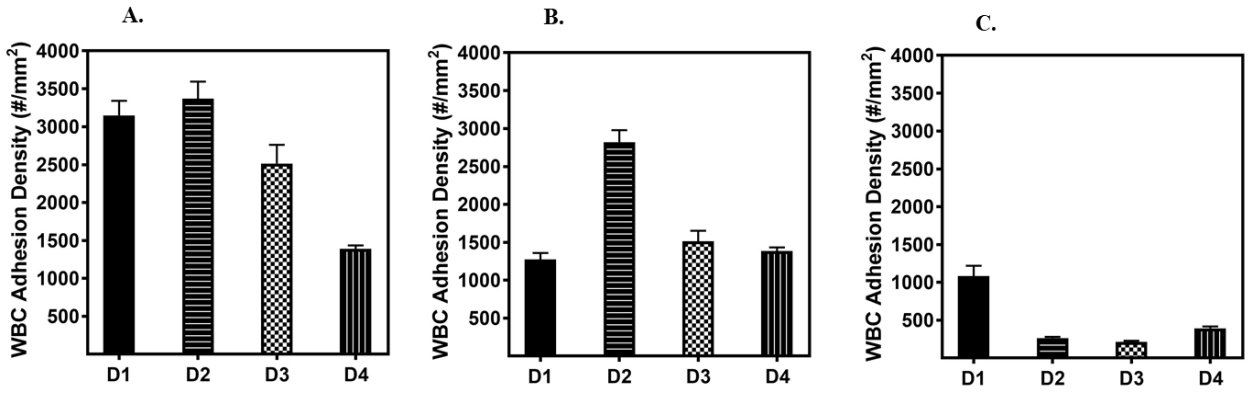

Figure 3.3. Donor Variation in White Blood Cell Binding.

Quantified WBC binding to an inflamed endothelial layer after 5 mins of laminar whole blood flow as a function of healthy blood donor. Error bars represent standard error for each donor. WBC binding at (A) 200 s^{-1}, (B) 500 s^{-1}, (C) 1,000 s^{-1}.

^{1}, and 200 s^{-1}). We tested a range of RBC rigidities and percentage of rigid RBCs in blood to gain a general insight on the impact of these cells on hemodynamics and WBC margination. Figure 3.2. shows the impact of RBC rigidity on WBC adhesion relative to WBC adhesion in whole blood flow of a healthy control, as a function of RBC stiffness and WSR in a ~250 µm height channel. We chose to represent the data in this way, i.e., percent change, owing to the natural variation in donor WBC adhesion. Figure 3.3. shows the absolute cell adhesion density at three distinct WSRs – 1,000 s^{-1}, 500 s^{-1}, and 200 s^{-1} for reference. The data in Figure 3.3. also indicates WBC adhesion is reduced as WSRs increases in alignment with previous reports in the literature[24,123,124]. For all TBHP treatments, we observe that the addition of rigid RBCs results in WBC adhesion reduction across all examined WSRs. Interestingly, a linear increase in the ratio of rigid to healthy RBCs did not translate to a linear decrease in WBC adhesion across the different treatments. The most substantial reduction in WBC adhesion, ~80%, was observed for the most rigid RBCs (1.0 mM TBHP treatment) at the *highest* WSR of 1000 s^{-1} evaluated for the condition in which 50% of the RBCs were healthy, and the other 50% were rigid (Figure 3.2.A.). A visual representation of this high WBC adhesion knockdown to the endothelial layer is presented in Figure 3.4. A slight recovery in WBC adhesion is observed when the fraction of rigid RBCs present is increased to

100% for the 1000 s^{-1} and nearly all WSRs. As the RBC rigidity decreased from *high* (1.0 mM TBHP) to *moderate* (0.75 nM TBHP) to *low* (0.50 nM TBHP), at the 1000 s^{-1} shear, we see a decrease in the magnitude of the WBC adhesion reduction to ~60 - 70%. Moreover, the location of the peak adhesion shifted to between 70 and 90% rigid RBCs in blood for the *moderate* and *low* rigidity RBCs, respectively, compared to high rigidity where the maximum reduction was observed at 50%. The importance of the level of RBC rigidity on the impact of rigid RBCs on WBC adhesion was diminished at the intermediate WSR of 500 s^{-1} evaluated. The maximum reduction in WBC adhesion observed for the 500 s^{-1} assays was ~60% for all degrees of rigidity examined and occurred for the condition in which 50% of the RBCs were healthy, and the other 50% were the rigid (Figure 3.2.B., 3.2.E., and 3.2.H.). Interestingly, the level of WBC adhesion reduction at 500 s^{-1} was not significantly different when compared to 1,000 s^{-1} despite a more substantial number of cells normally adherent at the former WSR, suggesting the impact of RBCs on WBC adhesion occurs at the point of WBC capture to the wall and not after adhesion. Of note, most WBC adhesion occurs in venules, which experience WSRs close to 500 s^{-1}. [119,125–127] At 200 s^{-1}, a reduction in WBC adhesion of ~45-50% was observed when 50% of the RBCs had a *low* level of rigidity. However, the reductions in WBC adhesion observed for most conditions at the 200 s^{-1} WSR were not significant relative to the control (Figures 3.2.C., 3.2.F., and 3.2.I.); thus, no peak reduction observable for any concentration of rigid RBCs present.

3.4.3. Effect of Rigid RBCs on Leukocyte Adhesion as a Function of Hematocrit

We utilized an *in vitro* PPFC model to examine the effect of different Hct on WBC adhesion to an activated endothelial monolayer. Since the amount of total whole blood per trial was held constant, lowering Hct required an increase in the plasma volume and decrease in total RBC volume. We began by reconstituting our blood samples with WBC rich plasma to Hcts of 40%, 30%, and 20%. Afterwards, we examined healthy, i.e., no rigid RBCs present, WBC adhesion onto an inflamed endothelial monolayer. All three examined Hcts were reconstituted back-to-back with WBC rich plasma from the same donor (eliminating donor variation across different Hct), thus the concentration of WBCs/mL of plasma was the same for Hcts evaluated.

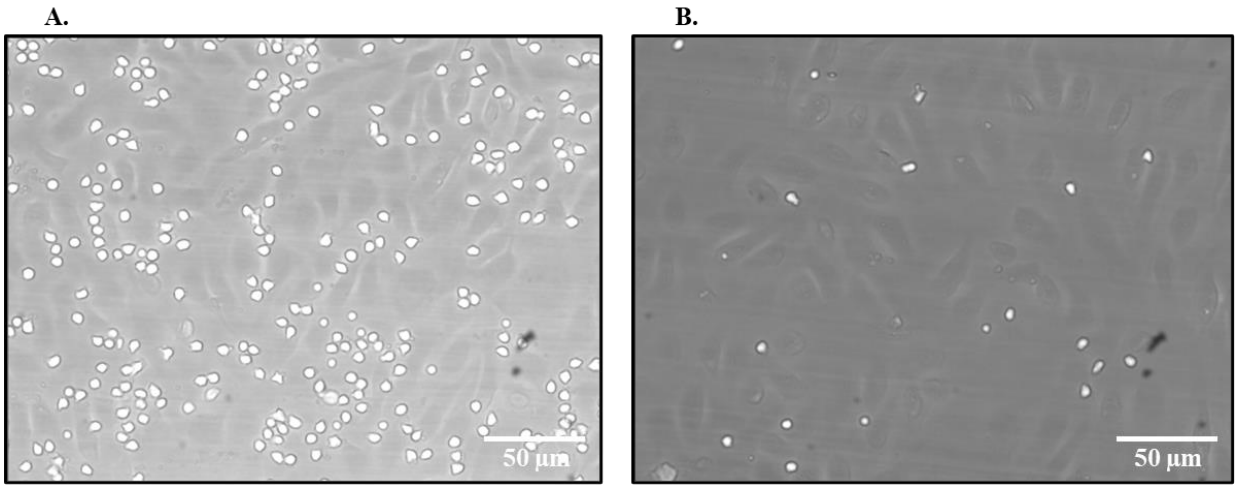

Figure 3.4. White Blood Cell Binding on Confluent Monolayer of HUVEC.

Brightfield images of WBCs adhered to HUVEC while blood is perfused at a WSR of 1,000 s^{-1}. (A) shows condition with healthy blood, i.e., no rigid RBCs present. (B) shows condition with 50% rigid RBCs treated with 1.0 mM TBHP present.

Furthermore, since the volume of WBC rich plasma increased as the Hct decreased, the total number of WBCs in the whole blood sample increased as the Hct decreased. The WBC adhesion density at different Hcts at a WSR of 1,000 s^{-1} is shown in Figure 3.5.A. We observe that WBC adhesion is significantly lower at Hcts of 30% and 20% respectively, and there was no significant difference in WBC adhesion between Hct of 30% and 20%. Given that the channel height was fixed at 254 µm in this work, the decrease in the Hct from 40% to 30% likely significantly alter

the RBC core and CFL dynamics, thus reducing WBC adhesion to the vessel wall. The difference in the size of the RBC core when the Hct decreases from 30% to 20% is likely not significant enough to observe a notable decrease in WBC adhesion.

Subsequently, we investigated how the addition of rigid RBCs effected WBC adhesion at lower Hcts. We compared the WBC adhesion trends at the lower Hcts of 30% and 20% to the adhesion trend for the condition utilized in Figure 3.2.A., i.e., 40% Hct with 1.0 mM TBHP. We again compared normalized WBC adhesion data to eliminate WBC adhesion variation between donors and at different Hcts. Figure 3.6.A. shows the impact of RBC rigidity on WBC adhesion relative to WBC adhesion observed with no rigid RBCs present for low Hcts. The degree of rigidity and WSR were constant at 1.0 mM TBHP and 1,000 s^{-1}, respectively. Figure 3.6.B. compares the normalized (relative to 40% Hct) reductions in WBC adhesion with the 30 and 20% Hct flows.

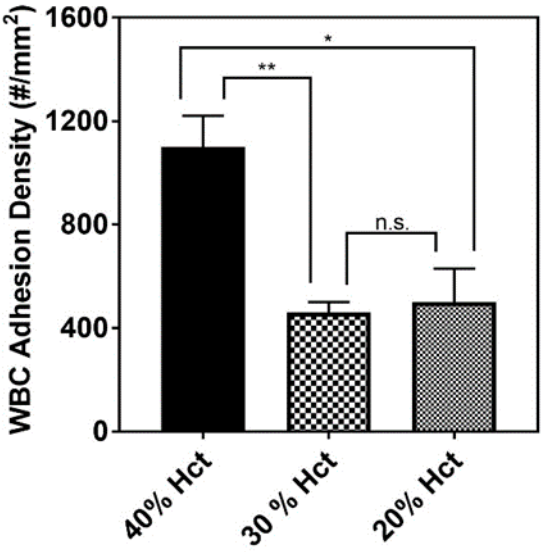

Figure 3.5. Blood Margination and White Blood Cell Adhesion Density at Different Hcts.

Quantified WBC binding to an inflamed endothelial layer after 5 mins of laminar whole blood flow as a function of healthy blood hematocrit (Hct) at 1,000 s^{-1}. Error bars represent standard error for each donor. Concentration of WBCs (~$6x10^6$ WBCs/mL of plasma) is kept the same for all conditions. (*) indicates $p<0.05$, (**) indicates $p<0.01$, and (n.s.) indicates no statistical difference is found. Error bars represent standard error.

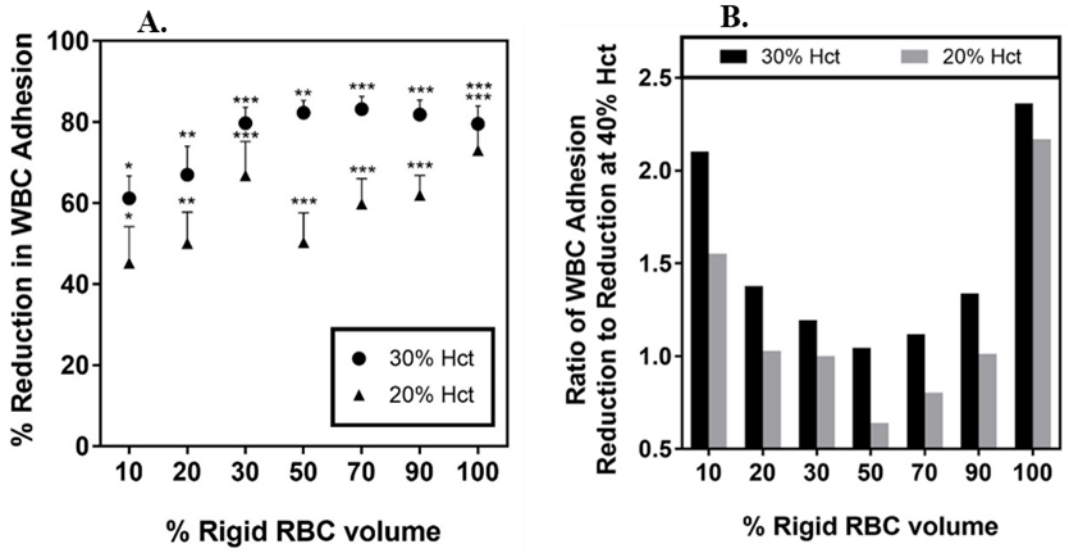

Figure 3.6. White Blood Cell Binding at Low Hematocrit.

(A) Quantified WBC binding to an IL-1β inflamed endothelial layer as a function of rigid RBCs present, i.e., % volume rigid RBC. All results are WBC adhesion after 5 mins of laminar whole blood flow with a constant TBHP treatment of 1.0 mM and WSR of 1,000 s^{-1}. All trials plotted as reduction compared to respective healthy controls RBC, i.e., no rigid RBCs present, same Hct, thus eliminating donor variation in WBC adhesion levels. (B) Relative difference in normalized WBC binding reduction between WBCs in 30% Hct and 20% Hct as compared to WBC binding at 40% Hct. WBC concentration (~$6x10^6$ WBCs/mL of plasma) kept constant upon Hct change. Error bars represent standard error. Statistical analysis of adherent density was performed using two-way ANOVA to test all WBC adhesion versus healthy WBC adhesion control. (*) indicates $p<0.05$, (**) indicates $p<0.01$, (***) indicates $p<0.001$, and (****) indicates $p<0.0001$.

For the 30% Hct case, WBC adhesion reduction was higher at most concentrations of rigid RBCs relative to the reduction levels observed with 40% Hct, as indicated by the ratio of WBC adhesion reduction at 30% to reduction at 40% Hct being greater than 1 for all concentration of rigid RBCs in flow. This observed enhanced reduction in WBCs at 30% Hct may be due to the higher ratio of WBCs-to-RBCs present in the blood sample at lower Hcts, i.e., increased probability of heterogeneous collision, for the conditions presented in Figure 3.6.[30,31] Interestingly, for the 20% Hct case, a significantly smaller ($p<0.01$) reduction in WBC adhesion is observed as compared to the 40% Hct case when 50 – 70% of the RBCs present were rigid, pointing to a different RBC core-CFL dynamics at such a low hematocrit in a large channel. Here, since the WBC concentration in plasma is kept constant, an even lower Hct of 20% would imply a much higher

plasma volume and hence a higher ratio of WBCs-to-RBCs in flow, which likely translates to a reduced probability of mismatch collisions. However, the rigid RBCs at the 50 – 70% concentration in blood may expand the core in a manner that positively benefits WBC adhesion. Indeed, numerous computational and theoretical models have highlighted the complex and, in some cases, non-linear relationship between RBCs and the CFL. [15,16,26,27,18–25] In the absence of the capacity to directly visualize the interactions between normal RBC, rigid RBCs and WBCs as was the case in our systems, such models would likely be needed to understand better the non-linear relationship highlighted in Figure 3.6.

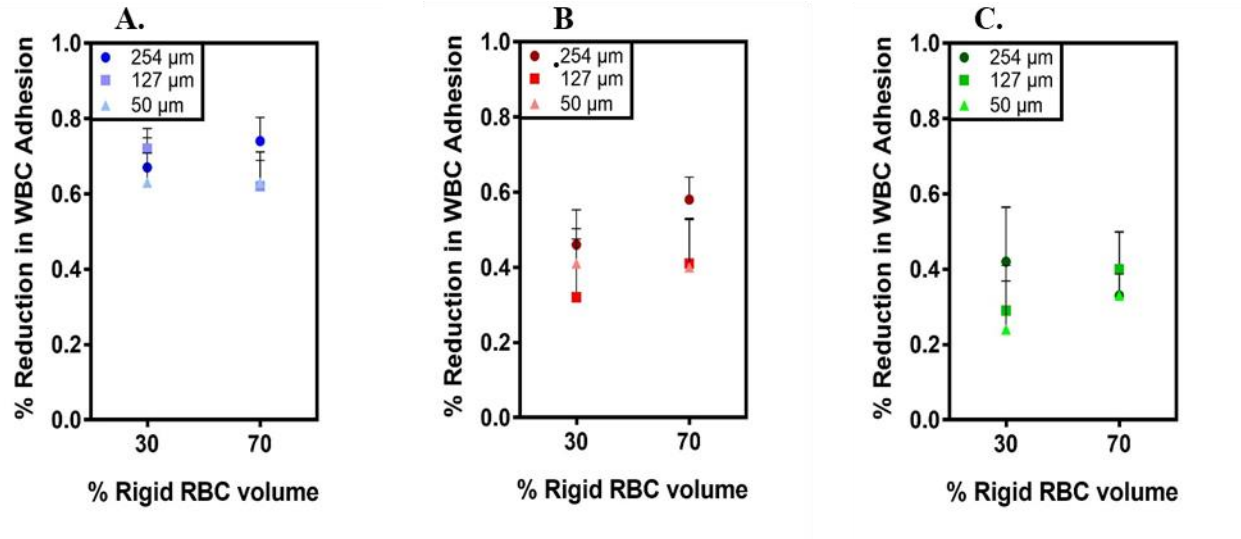

Figure 3.7. White Blood Cell Binding Impact by Changing Channel Height.

Quantified WBC binding to an inflamed endothelial layer as a function of channel height. Channel heights utilized consisted of 254 µm, 127 µm, and microchannel 50 µm. These results keep a constant wall shear rate of 1,000 s^{-1}. All trials normalized and plotted in reduction as compared to respective healthy controls, i.e., no rigid RBCs present, thus eliminating donor variation in WBC counts. (A) 1.0 mM TBHP treated RBCs (most rigid), (B) 0.75 mM TBHP treated RBCs, (C) 0.5 mM TBHP treated RBCs (least rigid). Statistical analysis of adherent density was performed using two-way ANOVA to test all WBC adhesion versus healthy WBC adhesion control. All conditions are non-significant versus the healthy WBC control. Error bars represent standard error and include error propagation for multiple donors.

3.4.4. Effect of Rigid RBCs on Leukocyte Adhesion as a Function of Channel Height.

Once we understood how Hct could affect how severely rigid RBCs alter their WBC adhesion patterns, we then investigated different flow channel heights to see how these trends

would hold in various vessels throughout the body. WBC adhesion data was collected using channel heights of 127 µm and 50 µm, and compared to the normalized results from the 254 µm channel. We utilized a setup similar to the PPFC previously described above for the 127 µm height and an additional PDMS microchamber for the 50 µm height. We down selected to 30% and 70% rigid RBCs conditions to compare to healthy RBCs in 127 µm and 50 µm channels. As discussed in the Discussion section of this chapter, the work by Dobbe *et al*. shows that sickle cell disease patients blood typically consists of ~30% disease inflicted (*rigid*) RBCs under stable conditions and ~70% when experiencing a severe crisis.[121] All blood samples were reconstituted to a 40% Hct. Figure 3.7. illustrates that no significant difference in WBC adhesion patterns, i.e., normalized WBC adhesion, is found between channel heights in the presence of the highly rigid (1.0 mM TBHP-treated) RBCs. The WBC adhesion for both channels trends are nearly identical and yield no statistically significant difference; baseline adhesion is shown in Figure 3.8. Examination of

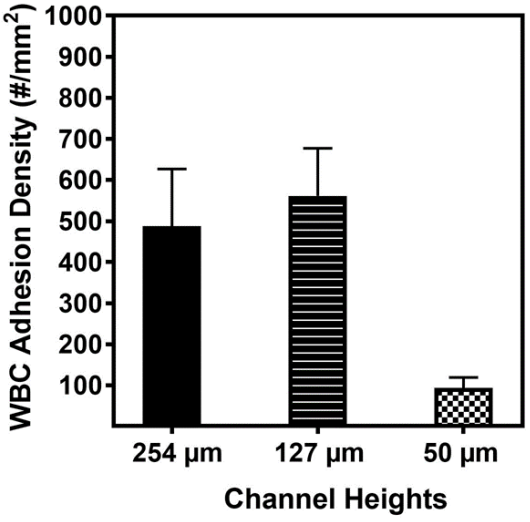

Figure 3.8. White Blood Cell Binding Variation with Channel Height.

Quantified WBC binding to an inflamed endothelial layer after 5 mins of laminar whole blood flow as a function of WSR with no TBHP treatment. All points were taken at a WSR of 1,000 s^{-1}. Error bars represent standard error for each donor.

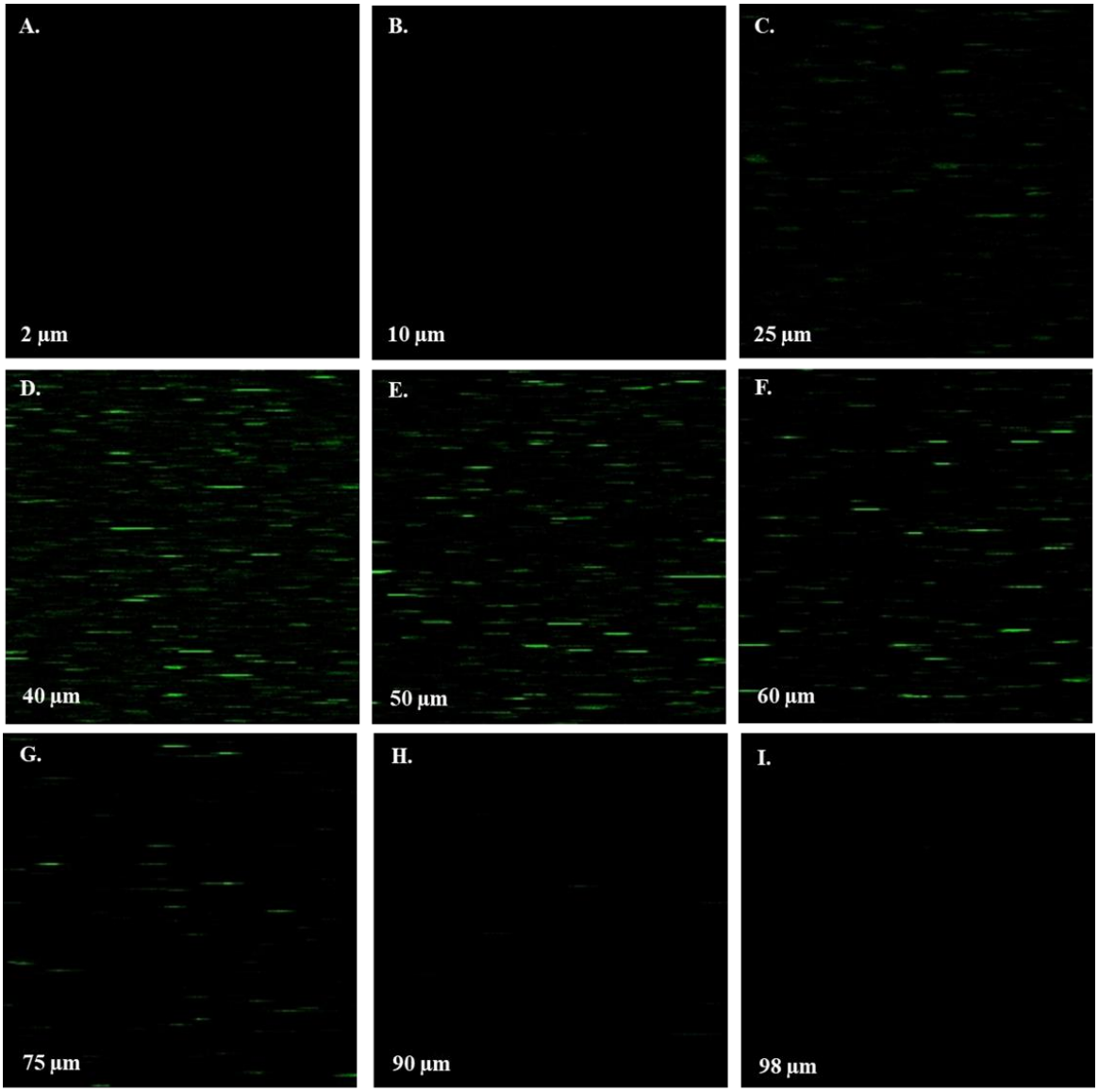

Figure 3.9. Confocal Images of Fluorescent Red Blood Cells in Blood Flow at Different Height Increments.

Whole blood with fluorescently tagged with WGA-488 healthy RBCs flowing in a channel of height 100 µm at 1,000 s^{-1}. The blood sample is reconstituted to a hematocrit of 40%. The direction of flow is from left to right. Images show RBC density at different heights within the channel while in flow. Cross-sectional image is ~164 µm by ~164 µm.

0.75 mM and 0.5 mM TBHP treated RBCs under the 127 µm and 50 µm channels yielded similar results when compared to WBC adhesion data for the 254 µm channel (Figures 3.7.B. and 3.7.C.). Given that no significant difference in WBC adhesion patterns is observed across all channel heights examined, we can speculate that disruption in WBC adhesion patterns scales in the different vessel sizes similar to the ones tested here.

3.4.5. Rigid Red Blood Cell Distributions in Blood Flow.

To better understand how these trends in WBC adhesion by percent rigid RBCs, RBC deformability, channel size, WSR, and hematocrit developed, we investigated the hemodynamic distribution of the cells types of interest under flow conditions. By leveraging confocal microscopy to generate Z-stack images, we investigated the distribution of rigid RBCs within a channel height. To determine how rigid RBC distributions are altered in blood flow, a proportion of rigidified RBCs were stained with wheat grain agglutinin (WGA) 488, reconstituted into whole blood at 40% Hct, perfused through a 100 µm channel, and imaged via confocal microscopy as described in the *Materials and Methods* chapter. The generated images depicted fluorescently tagged RBCs at different planes of the channel height and allowed rigid RBC distributions to be compiled across the channel height. Figure 3.9. shows a subset of Z-stack images depicting fluorescently tagged RBCs in flow at different heights within the 100 µm channel under a healthy condition, i.e., no rigid RBCs present; a subset of healthy RBCs is fluorescently tagged. We probed whole blood samples containing RBCs treated with either 1.0 mM, 0.75 mM, or 0.5 mM and examined their distribution under flow with the confocal microscope at a WSR of 1,000 s^{-1}. The results are presented as the IQR of the rigid RBCs. Figure 3.10.A. shows the normalized IQRs, and Figures 3.10.B., 3.10.C., and 3.10.C. show the raw distributions for the 30%, 70%, and 100% rigid RBCs in flow, respectively. All rigid RBC distribution IQRs were normalized to the respective healthy RBC control IQR from the same donor. High percentages of rigid RBCs present significantly ($p<0.05$) increase the IQR of the rigid cells, and thus the number of interactions between rigid cells and WBCs in the RBC-FL. The result presented in Figure 3.10.A. show changes RBC core size due to rigid RBC distribution do not directly explain the non-linear reduction in WBC adhesion

observed under different rigid RBC concentrations in the flow. We find that for flow consisting of 100% of rigidified RBCs at the *high* and *moderate* degree of rigidity, i.e., 1.0 mM and 0.75 mM TBHP, the rigid RBC core is expanded by nearly 30% and 20%, respectively. Meanwhile, rigid RBCs do not significantly modify the RBC core size while in combination with healthy cells (30

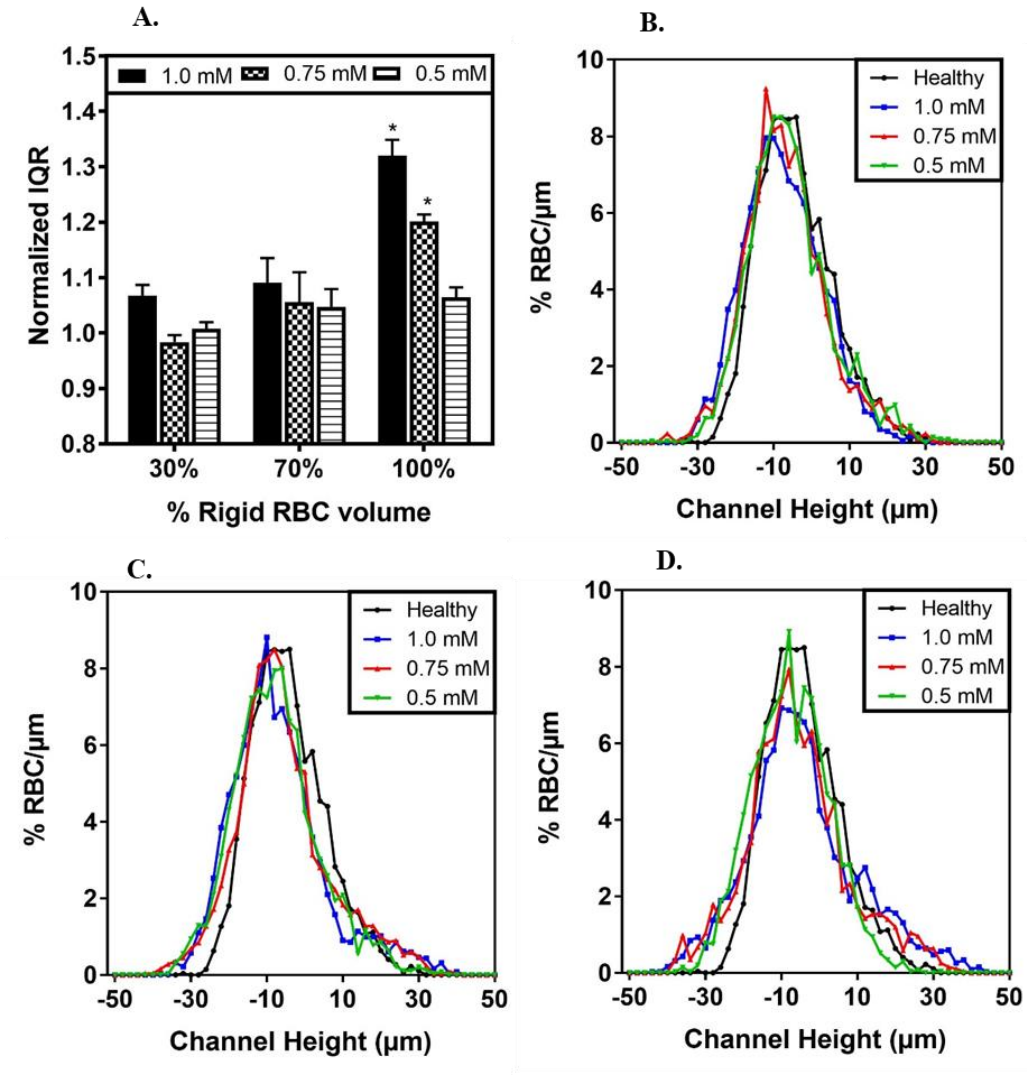

Figure 3.10. Normalized Interquartile Ranges (IQR) of Rigid Red Blood Cell Confocal Distribution.

Quantified rigid cell distribution, normalized and presented as IQRs in a channel of height 100 µm at 1,000 s^{-1} with varying TBHP treatments and rigid RBC % vol. Statistical comparisons are to healthy IQR at unity. Quantified rigid red cell distributions within the channel height at three different degrees of rigidity at (B) 30%, (C) 70%, and (D) 100% rigid RBCs present in flow. Statistical analysis of IQR magnitude was performed using two-way ANOVA determine the effect of the prevalence and degree of RBC rigidity. (*) indicates $p<0.05$. Error bars represent standard error and include error propagation for multiple donors.

and 70% rigid RBCs). As shown in Figure 3.2. (A, D, G), maximum WBC adhesion reduction was

observed when both soft and rigid RBCs are present in near equal amount (50% rigid RBCs for the 1.0 mM TBHP treated RBCs).

3.5. Discussion

Change in membrane rigidity can be attributed to lipid peroxidation. [122,128] Thus, this work decouples the changes in RBC shape and rigidity often found together in diseases to evaluate the impact of rigidity only. Looking at the results in the context of SCD, RBCs treated with 0.75 mM TBHP represent the level of rigidity observed in SCD RBCs during a severe painful crisis. For these *moderately* rigid RBCs, the maximum negative impact on WBC adhesion (~60% reduction, $p<0.01$) was seen when 70% of the RBCs present in flow were rigid (Figure 3.2.D.) for the 1000 s^{-1} WSR. Interestingly, a pervious report by Dobbe *et al.* suggests that roughly 70% of total RBCs are rigid in patients when undergoing a painful crisis in SCD, indicating that the ability of WBCs to marginate may be severely impacted in these patients depending on the blood flow characteristics of the affected vessels.[121] In general, roughly 30% of the total RBCs are abnormally rigid, with rigidity analogous to the *0.50 mM TBHP* treatment, in a patient with SCD under stable health, i.e., no crisis present. Here, we show that even the low presence of rigid RBCs in blood significantly reduced WBC adhesion (Figure 3.2.G.). Thus, the poor immune response of patients inflicted with SCD, or another disease relating to RBC deformability may, in part, be due to the physical presence of rigid RBCs altering WBC function.

The pattern of maximum WBC reduction observed in Figure 3.2. may arise due to the combined effect of (1) an expanded RBC core due to stiffer RBCs being less affected by the lift force, and thus do not populate the core of flow as densely as normal RBCs, and (2) heterogeneous collisions, i.e., collisions between a rigid and a deformable cells, as described by Graham and coworkers. [30,31] Specifically, the mismatched resulting trajectories upon heterogeneous collisions

are a contributing factor for the formation of the RBC core and successful margination of the considerably stiffer WBCs and platelets to the vessel walls. We speculate that upon rigidification, RBCs also begin to marginate outside the RBC core where they more frequently collide with WBCs, preventing WBCs from the normal rolling and, hence, firm adhesion to endothelium. Overall, Figure 3.2. shows higher degrees of rigidity and higher WSRs contribute to a more significant reduction in WBC adhesion with rigid RBCs, which is consistent with maximum impact and cell displacement with collisions in blood flow. Interestingly, the negative impact of rigid RBCs on WBC adhesion is maximum when near equal amount healthy (*soft*) and rigidified (stiff) RBCs are present, which represents maximum occurrence of heterogonous collisions. We speculate that the recovery seen when the concentration of rigid RBCs increases beyond 50 – 60% is attributed to the decrease in heterogeneous collisions due to the increasing presence of rigid RBCs and depletion of healthy RBCs. However, the 100% rigid RBCs are likely not able to tightly pack in the core as healthy RBCs, explaining the persistence of the reduction in WBC adhesion even with the elimination of soft-stiff RBC heterogeneous collisions.

From literature, we know that the RBC core aids in pushing stiffer objects, e.g., WBCs, to the vessel wall where they can probe the endothelial layer.[18–20] The formation of the RBC core and CFL is inevitable regardless of the blood Hct; However, at lower Hcts, the RBC core becomes thinner due to the smaller number of RBCs present since RBC tend to migrate to the center of the flow vessel while WBCs and platelets are pushed to the wall. [16,21] Consequently, the CFL increases in width if the channel size is kept constant. It is known that the RBC core supplies a cushion that forces WBCs towards the vessel wall, enhancing their margination. [16,21] Indeed, computational analysis of WBC margination under varying Hcts by Fedosov *et al*. [25] and Marth *et al*. [26] confirmed that WBC margination is much weaker at low concentrations of RBCs in the flow. Additionally,

the lower RBC concentration likely allow better motion of rigid cells to the wall and hence maximum disruption of WBC adhesion. These results suggest that the presence of rigid RBCs may be more detrimental in anemic patients, especially if WBC count is high. Lower Hcts and high WBC counts are typically seen in diseases such as SCD. [129]

WBCs experience a slight recovery in their adhesion as the concentration of rigid RBCs increased to 100% for the high WSR assays, e.g., Figure 3.2.A. We previously speculated that this adhesion improvement is due to the decrease in heterogeneous collisions between healthy RBCs and stiff RBCs as the concentration of rigid RBCs increases despite the expanded core with the 100% rigid RBCs in the flow. Taken together, data in Figures 3.2. and 3.10. suggest a combination of the mismatch in RBC rigidity between the healthy (*soft*) RBCs and rigid (*stiff)* RBCs, and the resulting heterogeneous collision, and enlarged RBC core inhibit the ability of WBCs to marginate and firmly adhere to the vessel properly. However, the former appears to be more impactful than the latter.

3.6. Conclusion

In this study, we show that the presence of rigid RBCs has a negative effect on the adhesion of WBCs to an inflamed human endothelium in blood flow. We utilize TBHP to artificially decrease RBC membrane flexibility and generate rigid RBCs simulating various hematologic disorders. Rigid RBCs are reconstituted into whole blood and perfused through microchannel model at physiologically relevant wall shear rates (WSRs). We find that higher degrees of rigidity in RBCs and higher WSRs produce the most significant WBC adhesion reduction. We observed a decrease in WBC adhesion as high as 80% when rigid RBCs are present in blood flow.

Interestingly, these results show that WBC adhesion reduction is maximized when a combination of both healthy *soft* RBCs and *stiff* RBCs are present, thus increasing rigid RBC concentration does not translate to worse WBC adhesion. This work offers experimental evidence that heterogeneous collisions (*soft* and *stiff*) between blood cells (RBC-to-RBC and RBC-to-WBC) hinder WBC adhesion to endothelial wall. We also show that RBC core is expanded, up to ~30%, when rigid RBCs are present, meaning rigid RBCs are abnormally positioned closer to the vessel wall. The presented results may offer insight in understanding why people with disease relating to RBC deformability are susceptible to infection and have a poor immune response as we observed a significant reduction in WBC adhesion in blood conditions analogous to blood conditions of RBC-diseased patients. The need for further research of the impact RBC rigidity has on hemodynamics is paramount towards gaining a better understanding of disease manifestation and for the design of treatment methods with high efficacy.

Chapter 4 : Characterizing Bulk Rigidity of Rigid Red Blood Cell Populations in Sickle-Cell Disease Patients

4.1. Publication Information

The work presented in this chapter is published as: Mario Gutierrez, Mark Shamoun, Katie Giger Seu, Tyler Tanski, Theodosia A. Kalfa, and Omolola Eniola-Adefeso. "Characterizing bulk rigidity of rigid red blood cell populations in sickle-cell disease patients." Sci Rep 11, 7909 (2021). https://doi.org/10.1038/s41598-021-86582-8 [11]

Modifications have been made to the published document to adapt the content to this text. The goal of this chapter is to explore an improvement to the ektacytometry technique that allows for the more accurate estimation of average rigidity in rigid red blood cell populations in blood samples.

4.2. Abstract

In this work, we utilized a parameterization model of ektacytometry to quantify the bulk rigidity of the rigid RBC population in SCD patients. Current ektacytometry techniques implement laser diffraction viscometry to estimate the RBC deformability in a whole blood sample. However, the diffraction measurement is an average of all cells present in the measured sample. By coupling an existing parameterization model of ektacytometry to an artificially rigid RBC model, we

formulated an innovative system for estimating the average rigidity of the rigid RBC population in SCD blood. We demonstrated that this method could more accurately determine the bulk stiffness of the rigid RBC populations. This information could potentially help develop the ektacytometry technique as a tool for assessing disease severity in SCD patients, offering novel insights into the disease pathology and treatment.

4.3. Introduction

The rigidity and hemoglobin (Hgb) composition of RBCs in SCD patients varies highly, and a high HbS content does not necessarily correlate to an increased cellular membrane stiffness. [130] For example, there can be a scenario with a large population of HbS concentrated RBCs (%S fraction) with moderate to low cellular membrane stiffness or another situation with a small %S fraction with RBCs with high membrane stiffness. Thus, a complete understanding of the impact of RBC rigidity in SCD symptom presentation would require the ability to characterize this property in individual patient blood. Therefore, several methods have been explored to characterize the mechanical properties of RBCs, including micropipette aspiration, atomic force microscopy, microfluidic devices, and optical tweezers. However, these methods are limited since they require single RBC isolation and are static techniques. [73] For one, the design and fabrication of robust microfluidic devices can be highly labor-intensive. [71,95,131] Conversely, traditional ektacytometry, or laser diffractometry, is more convenient and precise than other methods and thus has been adopted as a promising technique for testing RBC deformability.[73] Ektacytometry was initially developed and successfully used to screen for RBC membrane disorders such as hereditary spherocytosis. [132] This method in recent decades has been repurposed for the investigation of SCD. [70]

Ektacytometry principally works by inducing controlled shear stress on a suspension of RBCs in diluted blood. The resulting deformation from the applied shear stress is captured by shining a laser onto the sample, which creates a single diffraction pattern. The general technique can make three different types of measurements: (1) an Osmoscan which holds cells at constant shear stress while varying osmolality, (2) a deformability scan which keeps cells at a fixed osmolality while changing the shear stress, (3) an Oxygenscan which varies both the shear and oxygen gradient. [133–135] Cellular deformability, i.e., elongation, is then reported as an Elongation Index – a ratio of the difference between the major and minor axes in the cellular diffraction patterns over their sum. However, most works using ektacytometry to evaluate how RBC rigidity impact disease severity in SCD have focused on osmoscans, [67,68] which may not entirely recreate the *in vivo* setting. RBCs in blood flow are exposed to a relatively fixed *in vivo* osmolality (~290 mOsmol/kg) and varying shear as they transport through different blood vessels. Alternatively, measurements that employ analysis of RBC elongation in response to changes in shearing stresses at a fixed osmolality may offer a better description of RBC stiffness in SCD. [70] Oxygenscans, the other form of shear-based analysis, are a robust method recently developed, which can measure the maximum RBC elongation at normal oxygen conditions and minimum RBC elongation under hypoxic conditions and point of sickling. [135] However, regardless of the shear-based method employed, ektacytometry is critically limited. It renders average deformability for all RBCs in the sample, [70,133,134], i.e., across both stiff and healthy RBCs. This average measurement of deformability may underestimate the rigidity of HbS-rich (%S fraction) or sickle RBC population in the blood, which could be a critical complication when it comes to assessing a patient's well-being or treatment response. A sample with a small overall fraction of extremely rigid RBCs could render a similar elongation curve as a sample with a high fraction of moderately stiff RBCs.

Previous studies have investigated how laser diffractions in ektacytometry differ based on non-homogeneous mixtures of RBC deformability. [136] However, to date, there is no established method for isolating and directly characterizing the rigidity of the HbS RBC population in patient blood.

Here, we present an approach to estimate the average rigidity of the HbS-rich (rigid) red cell population in SCD via a method that implements artificially rigidified RBCs mixed into whole blood at different rigid-to-healthy ratios. Said samples are measured via traditional shear-based ektacytometry deformability analysis. We then parameterize the measurements to develop a numerical model that predicts the rigid RBC population's bulk rigidity in SCD blood samples. This method can estimate the stiffness of sickled RBC populations with greater certainty, potentially serving as a platform for understanding disease severity in SCD patients and monitoring the efficacy of novel and established treatment options.

4.4. Results

4.4.1. Measurement of Artificially Rigid RBC Populations in Whole Blood Samples

In an ektacytometry scan, a collection of EI values plotted as a function of shear stress renders deformability curves. Previous work has determined that the critical factor in characterizing alterations in cell deformability is the maximum achievable EI, i.e., EI_{max}. [137] Accordingly, measurements from healthy donors registered the highest EI_{max} values (~0.62). In contrast, SCD donors tended to have lower EI_{max} values. Next, we built an artificially rigid RBC approach, where the RBC membrane stiffness is easily altered to test how changing the fraction of rigid RBCs affects the EI_{max} of the whole blood. We artificially rigidified healthy donor RBCs via treatment with TBHP in varying concentrations to obtain RBCs with a range of stiffness from

slightly to *highly* rigid. Short interactions (<60 minutes) with relatively low concentrations of TBHP (<3.0 mM) induces lipid peroxidation and membrane protein crosslinking in RBCs.

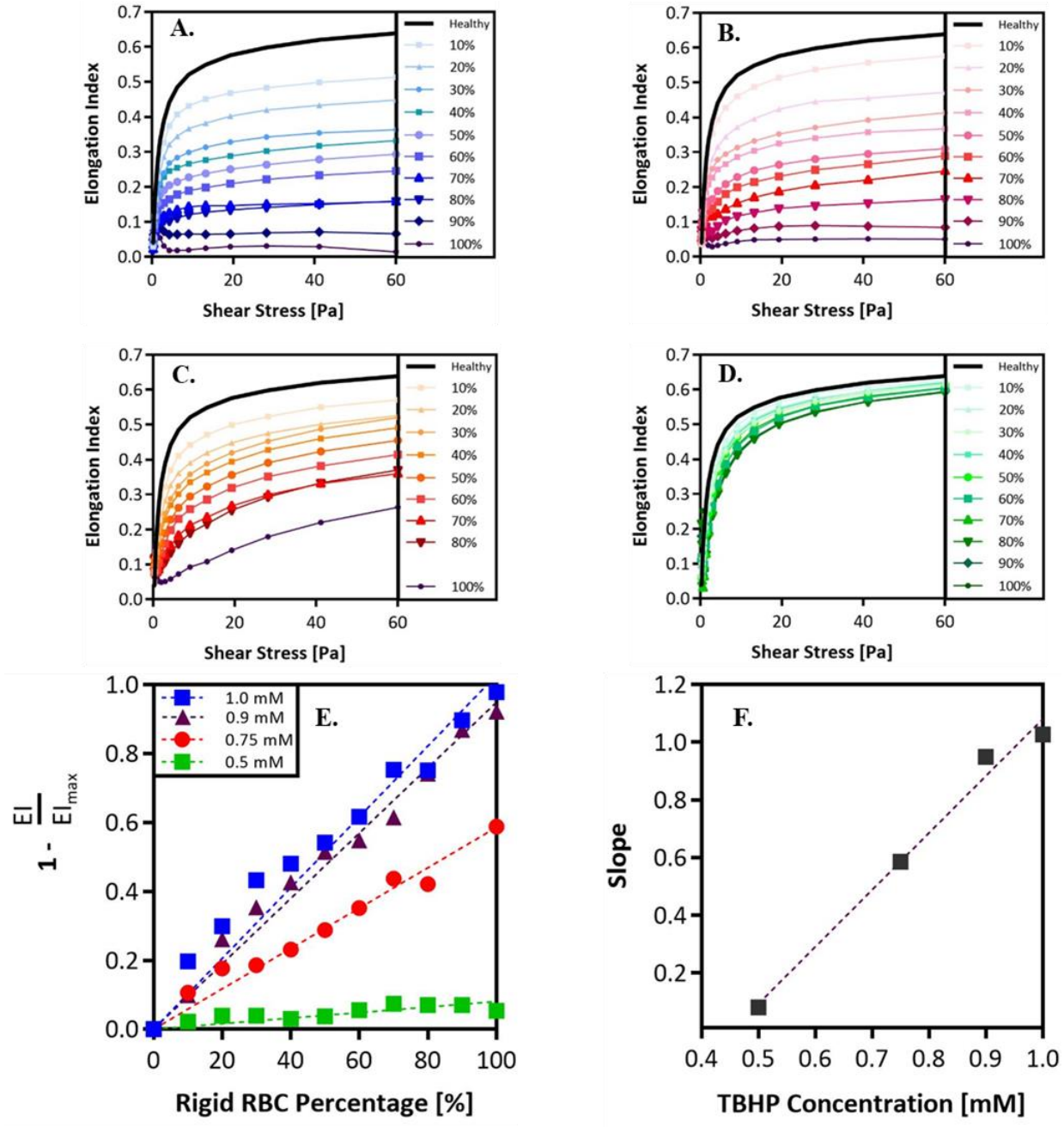

Figure 4.1. Ektacytometry Analysis of Various Rigid Red Blood Cell Populations with Varying Red Blood Cell Membrane Stiffnesses.

Ektacytometry curves for various rigid-to-healthy fractions ranging from 0% to 100% in increments of 10% rigid RBCs present. Rigid RBCs have been treated with: (A) 1.0 mM. (B) 0.9 mM. (C) 0.75 mM. (D) 0.5 mM TBHP. (E) Maximum EI recorded at 60 Pa for each rigid fraction condition is compared to EImax of the healthy condition, these ratios are plotted as a function of rigid RBC fraction present. Linear regression is used to determine the slope of these rigid-to-healthy ratio trends. (F) Slopes of rigid-to-healthy ratio trends are plotted as a function of TBHP concentration.

Prolonged exposure will result in structural alteration in protein networks and eventual RBC lysis. [138] We combined the stiffened RBCs with healthy (non-treated) RBCs in whole blood at different stiff-to-healthy ratios and measured the changes to the EI values. [10] The resulting deformability curves plotted along with the curve for the 100% healthy RBCs sample are shown in Figure 4.1. As expected, ektacytometry measurements yielded smaller EIs as higher fractions of rigid RBCs were present in the blood. Thus, the samples with 100% treated RBCs registered the lowest EI_{max} for all TBHP concentrations evaluated. However, the spread between the curves became less pronounced with lower TBHP concentrations. Based on the 100% rigid fraction conditions, we observed that the *highly* stiff RBCs were the ones treated with 1.0 mM TBHP. The RBCs treated with 0.9 and 0.75 mM RBC treatments yielded *intermediate* stiffnesses while the 0.5 mM TBHP treatment yielded only *slightly* rigid RBCs.

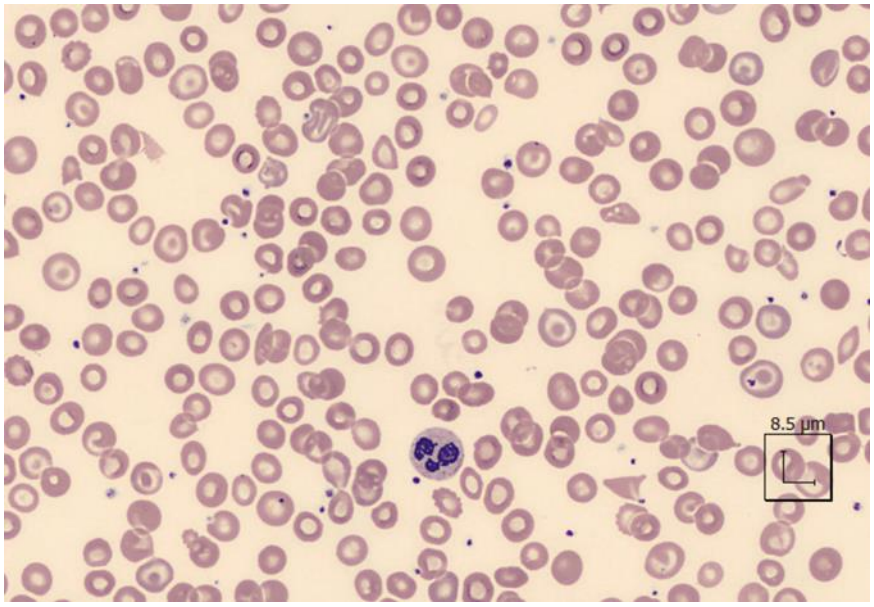

Figure 4.2. Blood Smear Image of SCD Patient.

Standard blood smear image of SCD patient 10, genotype SS. Patient 10, 15-year-old male on hydroxyurea therapy. Patient 10 has a %S fraction of 79.3% as determined by standard electrophoresis analysis. Only ~7.3% of RBCs in visible smear show shape deformation from regular RBC discocyte shape.

4.4.2. Building a Predictive Algorithm for Estimating Bulk Stiffness of the Rigid RBC Population in Sickle Cell Disease Blood

To understand how the spectrum of rigid RBC fractions affects EI curves and EI_{max}, we parameterized the curves in Figure 4.1.A-D. The EI_{max} recorded in every blood sample was divided by the average maximum EIs of healthy blood to produce a ratio of relative stiffness. Subsequently, we plotted these EI ratios as a function of rigid RBC fractions, as shown in Figure 4.1.E. We found

Table 4.1. Sickle Cell Disease Patient General Information and Ektacytometry Maximum Elongation Index Values.

Information includes SCD genotype, age in years, gender (male or female), current patient therapy chronic transfusions (CT) or Hydroxyurea (HU), %S fraction as determined by blood electrophoresis, and maximum EI measured via ektacytometry in the actual SCD patient blood sample. The table also includes the predicted EImax of rigid population, i.e., %S Fraction. Missing therapies indicate the patient is not under any type of treatment at the time of the measurement.

Patient	SCD Genotype	Age	Gender	Therapy	%S Fraction	Measured Bulk EI_{max}	Predicted Rigid RBC Pop. EI_{max}
#	-	years	(M/F)	-	%	-	-
1	SS	13	M	CT	20.7	0.465	~ 0.01
2	SS	6	F	CT	48.7	0.421	0.198
3	SC	18	M	HU	50.3	0.465	0.299
4	SS	9	M	CT	75.2	0.266	0.145
5	SS	19	F	CT	21.1	0.539	0.188
6	SS	18	M	CT	34.4	0.462	0.136
7	SS	13	M	HU	89.9	0.297	0.259
8	SS	16	M	CT	43.1	0.401	0.095
9	SS	1.5	F	-	89.9	0.548	0.539
10	SS	15	M	HU	79.3	0.454	0.407
11	SC	17	M	HU	47.6	0.301	~ 0.01
12	SS	15	M	CT	55.8	0.482	0.362
13	SS	2	F	CT	37.4	0.606	0.561
14	SS	21	F	-	90.6	0.512	0.499
15	SS	15	M	HU	86.6	0.437	0.407

a linear relationship between the EI_{max} achieved and the rigid RBC fractions in a blood sample. As expected, the *highly* rigid RBCs in blood had a more substantial impact on reducing the EI_{max} than *intermediate* and *slightly* rigid RBCs, as shown by the slopes of the linear trends in Figure 4.1.E. plotted as a function of TBHP concentration in Figure 4.1.F. Parameterization of the relationship between the slope of rigid EI-to-healthy EI ratios versus TBHP concentration implies that we can interpolate between TBHP concentrations that were not experimentally tested. The correlations obtained by the parameterization of the EI measurements in Figure 4.1. were imported into a MATLAB code to construct a predictive algorithm that can estimate the TBHP concentration. Thus, the rigid RBC population's relative stiffness in a patient blood sample can be determined via two input variables: 1) EI_{max} recorded in the standard deformability measurement and 2) fraction of rigid or sickle RBCs in the patient's blood sample.

Given the linearity of the relationships between the stiffness and fraction of the rigid RBC population in a blood sample, we hypothesized that our predictive algorithm could be used in combination with electrophoresis and hemoglobin analysis of patient blood to map the relative stiffness of the rigid (HbS) RBC populations in SCD. To this end, we measured the EIs for fifteen unique SCD patient blood samples. Table 4.1. lists the SCD genotype, age, gender, current medical intervention/therapies, %S fraction, and measured maximum bulk EI for all patient blood evaluated. A standard blood smear image was collected for patient 10, shown in Figure 4.2. The maximum EI of each measured patient blood sample (measured bulk EI_{max} in Table 4.1.) combined with the corresponding %S fraction is used as initial inputs to estimate the *maximum* stiffness, i.e., EI_{max}, of the HbS only RBC population for each patient. Meaning, we match each patient's actual EI curve to an EI curve generated for an artificially rigid RBC blood that matches the measured bulk EI_{max} and %S (i.e., rigid RBC) fraction of the patient's blood. The matched artificial EI curve,

generated with the MATLAB algorithm, can then be backtracked to estimate what TBHP concentration can produce a curve that matches the actual raw patient deformability curve. Hence, the rigid RBC population's apparent stiffness in the patient sample can be represented as a TBHP

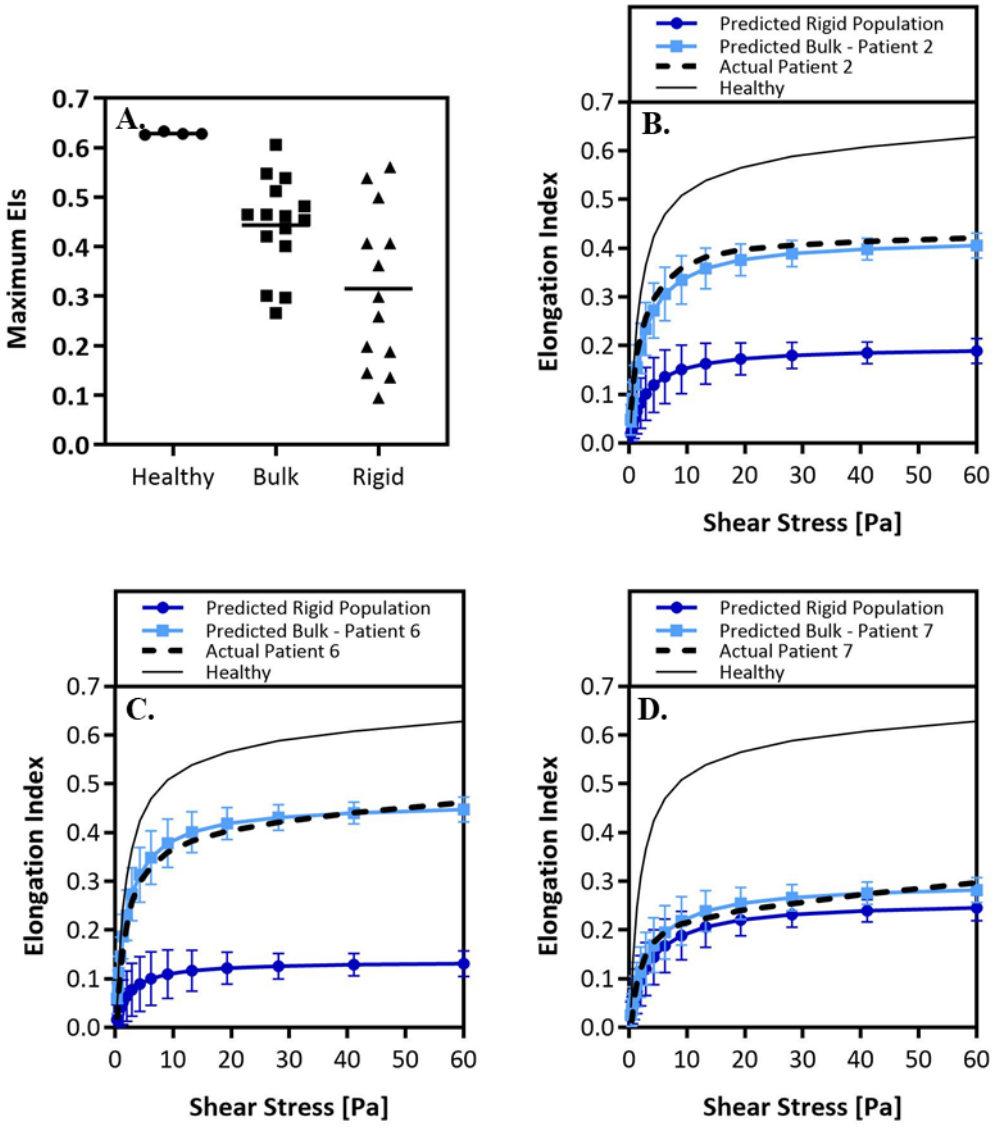

Figure 4.3. Predicting the Rigidity of the Rigid Red Blood Cell Populations in Sickle Cell Disease Patients.

(A) Average maximum EIs of healthy donors, actual bulk patient measured maximum EIs, and predicted maximum EIs of rigid population. Actual healthy and patient ektacytometry curves compared with predicted patient bulk ektacytometry curve and predicted curve of the rigid RBC population: (B) patient 2. (C) patient 6. (D) patient 7. Error analysis of the predicted EIs as a function of shear was performed using least square difference analysis. Error bars are plotted as standard deviation of the predicted elongation values. Student's t-tests are performed to determine significance between Actual Patient curves and Predicted Bulk Curves, no significant difference is found for any patient using an α=0.05, p-values > 0.05.

concentration. That is, the rigid RBC population in the SCD patient blood has a rigidity similar to the rigidity of healthy RBCs that had been artificially stiffened with a specified concentration of TBHP. Once we knew the representative TBHP concentration for a given patient blood sample, we extrapolated the % rigid fraction to a 100% to predict the maximum EI for 100% rigid RBCs, i.e., the maximum stiffness of only the rigid population or %S fraction.

The values of the maximum EIs of measured patient bulk blood (bulk) are plotted in Figure 4.3.A. next to maximum EIs obtained for healthy blood samples and the predicted maximum EIs of only the HbS (rigid) fraction for each patient's blood. We observed a very narrow range in maximum EI of healthy blood measurements, while a wide range of maximum EIs is shown for SCD patient bulk blood measurements. Importantly, we saw a broader distribution in the maximum EI values of only the HbS populations with an average lower than the average maximum EIs of the raw SCD patient and healthy blood. From this data, we calculated ratios that compare the estimated maximum EIs of the sickle population in the patient blood samples to 1) the maximum EI in a healthy blood sample and 2) the maximum EI of the bulk SCD patient blood sample. A ratio value higher than unity suggests that the maximum EI of the rigid RBC population is much lower than what is measured by bulk blood measurement, thus underestimating the stiffness of the HbS population, i.e., sickled RBC, in an SCD patient.

$$EI(SS) = EI_{Max}\frac{\left(\frac{SS}{SS_{1/2}}\right)^{m}}{\left(\frac{SS}{SS_{1/2}}\right)^{m}+1} \quad (4)$$

Subsequently, we used the predicted maximum EI of the rigid RBC population (shown as "rigid" in Figure 4.3.A.) for each patient's blood to create a deformability curve for the patient's HbS only population, labeled as "Predicted Rigid Population" in Figure 4.3.B-D., according to an

approach previously described by Baskurt *et al*. [139]. This simplified Skreestra-Bronkhorst model, Equation (4), also takes into account parameters, such as the shear stress associated with half the EI_{max} ($SS_{1/2}$, also estimated in our parameterization model) and the range of shear stresses (SS) evaluated in the ektacytometry measurement. The variable "m" was a parameterization slope that was simply left at a value of 1. To confirm the validity of our approach to creating HbS, i.e., rigid population, only elongation curve, we again utilized the Skreestra-Bronkhorst plotting model, Equation (4) to see if the deformability curves of the SCD patient bulk measurements can be replicated accurately, as well as a healthy deformability curve. We found an acceptable precision of the parameterization model when we compared the elongation curve derived from the actual measurement of a patient's bulk blood to the predicted representative curve for the patient's blood. The precision is visually represented in Figure 4.3.B-D. for patients 2, 6, and 7, which shows combined plots of the (i) predicted HbS only RBC elongation curve alongside the (ii) predicted patient bulk deformability curve, (iii) actual patient bulk deformability curve, and finally, the (iv) a healthy deformability curve for reference. Figure 4.4. shows similar plots for all patients evaluated in this study.

Interestingly, Figures 4.3.B. and 4.3.C. show drastic differences in the *bulk* blood's and the "sickle RBC" population's deformability curves. In some cases, the rigid population yielded a maximum EI that was ~2 times smaller than what a bulk measurement yielded. However, in other cases, as shown in Figure 4.3.D., we observed very little difference between the actual raw bulk measurement and the predicted curve of the sickle.

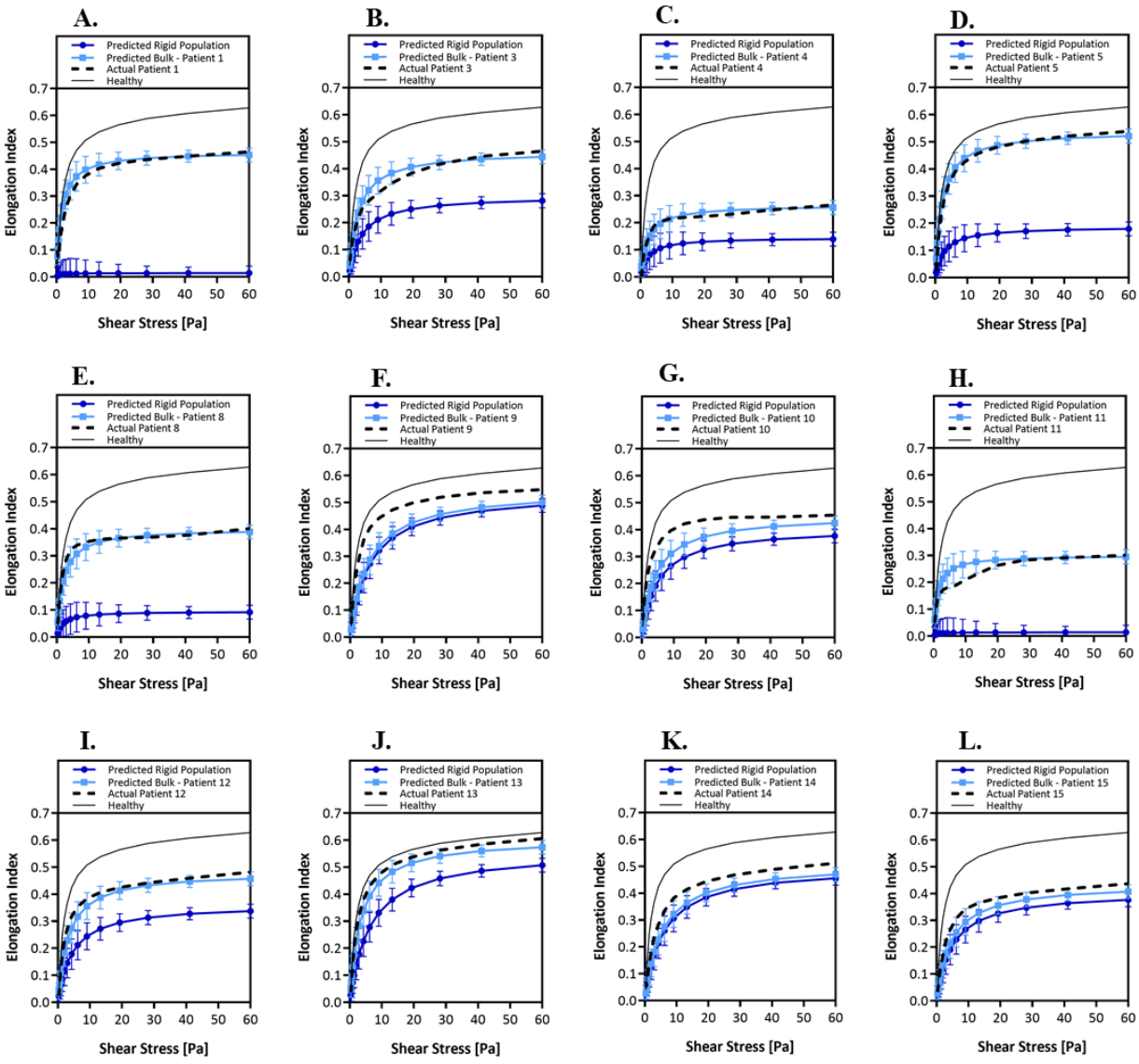

Figure 4.4. Predicting the Rigidity of the Rigid Red Blood Cell Populations in Sickle Cell Disease Patients.

Actual healthy and patient ektacytometry curves compared with predicted patient bulk ektacytometry curve and predicted curve of the rigid RBC population: (A) patient 1. (B) patient 3. (C) patient 4. (D) patient 5. (E) patient 8. (F) patient 9. (G) patient 10. (H) patient 11. (I) patient 12. (J) patient 13. (K) patient 14. (L) patient 15. Error analysis of the predicted EIs as a function of shear was performed using least square difference analysis. Error bars are plotted as standard deviation of the predicted elongation values. Student's t-tests are performed to determine significance between Actual Patient curves and Predicted Bulk Curves, no significant difference is found for any patient using an α=0.05, p-values > 0.05.

4.5. Discussion

One of the critical characteristics of SCD is the increased rigidity of the RBC membrane. [42,48,52] While there is evidence of its crucial role in the evolution of symptoms in SCD, [140] RBC rigidity is often disregarded as a minor side-effect of SCD rather than a critical biomarker. More than a mere inconvenience, RBC rigidity has the potential to be utilized as an indicator of a patient's condition or response to new medications or therapies. For example, Gutierrez *et al*. showed that the presence of rigid RBCs in blood flow significantly reduced white blood cells (WBCs)' adhesion to an inflamed vascular wall. [10] Interestingly, the results found a non-linear correlation between the fraction of rigid RBCs present in whole blood flow and the level of reduction in WBC adhesion across a range of RBC stiffness levels as explored in this work. [10] Additional work by Qiu *et al*. investigates the impact of rigid RBCs in blood flow on the functionality of the endothelium in a microvasculature-on-a-chip device. [140,141] Results from this work showed that even in the absence of vaso-occlusion and complications relating to hemolysis, endothelial dysfunction and increased permeability was detectable after only mechanical interactions with stiffened RBCs. Although these studies have begun to unravel the critical associations between RBCs stiffness and the complications seen in SCD, e.g., endothelial dysfunction and vaso-occlusion, there is still a need for further sophisticated models for investigating the effect of RBC stiffness in SCD. More intricate models also offer the potential to be used as analytical tests for novel therapeutics and understanding patient response to medication.

In this work, we presented an estimation method that can more precisely characterize the rigid RBC population's stiffness in SCD based on the general shear-based ektacytometry measurement of patient blood. Originally developed as a screening tool for RBC membrane

disorders, [132] and repurposed for the investigation of SCD, ektacytometry has yet to reached widespread clinical use. While ektacytometry has been proven to be a robust method for investigating RBC deformability, it is not perfect. The bulk blood measurement achieved via Ektacytometry deformability scans can register similar EI values for two different patients with vastly different stiffness in the rigid RBC populations due to variation in the HbS fraction population. Here, we implemented artificially rigid RBCs to evaluate rigid RBC fraction's impact on bulk blood stiffness. Our results showed that ektacytometry deformability measurements are highly influenced by the degree of RBC rigidity in the sample and the fraction of rigid RBCs present (Figure 4.1.A-D.). Samples containing rigid RBCs with a higher degree of stiffness showed the highest variability in deformability analysis upon change of the rigid fraction. These deformability measurements for artificially rigidified RBCs in blood allowed us to understand better how ektacytometry curves are altered by the amount of the stiff (i.e., sickled) RBC population in SCD blood. This understanding formed the base of our predictive model. Using the maximum EI measured and knowledge of the fraction of rigid RBCs in a mixed sample, we can estimate the rigid population's stiffness in a patient's blood.

The rigid conditions in SCD patient blood can vary depending on the medication, age, and genotype. We collected fifteen unique SCD whole blood samples from a diverse pool of donors ranging in SCD genotype, age, gender, and current therapy (Table 4.1.). We determined the fraction of HbS RBCs, i.e., what we denote as the rigid population, in the patient sample via electrophoresis and HPLC hemoglobin analysis. Using what we learned from the artificially stiffened RBCs in the blood combined with a raw ektacytometry measurement of an SCD whole blood sample and hemoglobin data, we estimated the stiffness of the %S fraction, i.e., the rigid population in an SCD patient.

Our results showed that the rigid population's stiffness in an SCD patient sample is often underestimated (Table 4.1.). For patient 2, we see that the EI_{max} of the stiff RBCs, 48.7%, is 3.2 folds lower than the maximum EI given by the bulk raw measurement. Similarly, the EI_{max} of the stiff RBCs was 4.4, 4.7, and 6.7 folds smaller than the bulk blood value for patients 4, 6, and 8, respectively. This result implies that the HbS RBCs, i.e., rigid population, in these SCD patients have a high degree of rigidity, which was similar to rigidity obtained for artificially rigidified RBCs incubated in 1.0 mM TBHP. Of note, the estimated stiffness of the rigid RBC population of patients 1 and 11 were predicted to be higher than the rigidity of our most stiff conditions measured and used to generate the numeric algorithm, i.e., RBCs treated with 1.0 mM TBHP. For these samples, the interpolative model cannot predict the rigid populations' max EI since it is out of range of our most stiff conditions measured (100% stiff fraction, 1.0 mM TBHP). Still, the max EI of the rigid population is many folds greater than the maximum EI in a healthy condition and the bulk raw standard measurement of the SCD sample. It is important to note that this analysis does not suggest that the maximum EI is consistently overestimated in every patient sample, but rather that it is a possibility. For example, for patients 9, 10, 13, 14, and 15, the maximum EI for the HbS RBCs was only ~1.1 times fold lower than the bulk raw measurement maximum EI. The estimated maximum EI of the rigid RBC population is compared to the maximum EI measured in the standard bulk deformability measurement, as shown in Figure 4.3.A. We observe that the average maximum EI for the rigid populations in the SCD patients is notably lower, ~0.32, compared to the standard bulk measurements, ~0.45. However, given the wide range of EIs constituting the averages, a statistically significant average was not calculated.

We did not observe any specific correlation between the current therapy, i.e., chronic transfusion or hydroxyurea, and the rigid population's stiffness in an SCD patient sample.

Hydroxyurea works by raising the levels of fetal hemoglobin in the patient's RBCs, which increases the oxygen binding capability and is expected to improve deformability in SCD RBCs. [142–144] However, one of the stiffest patient conditions we measured was that of patient 11, who was being treated with hydroxyurea at the time of the sample collection. One potential explanation for this discrepancy might be the shorter length of time the patient was on hydroxyurea medication than other patients on the same treatment. Also, we did not find a correlation between the stiffness of the rigid population and the patient genotype. Due to the availability of donors, thirteen of fifteen donors were genotype SS, and two donors were genotype SC. Again, one of the stiffest patient conditions measured was that of patient 11 with genotype SC. This observation is interesting since the genotype SC is typically regarded to be clinically less severe compared to genotype SS in regards to symptoms and occurrences of painful crises. [42,145]

For patients 2 and 6, we predicted the maximum EI of the rigid RBC populations to be 3.2 and 4.7 folds smaller than what was recorded in the measurement of their whole blood. That is, the predicted ektacytometry curves are shown to be considerably different from the bulk, raw measurements (Figure 4.3.B. and 4.3.C.). On the contrary, we see there is not a considerable difference between the rigid population's predicted curve and the actual bulk measurement in patient 7, with only a 1.2 times fold difference in maximum EIs, Figure 4.3.D. This visualization of the deformability curves shows that our predictive model can estimate the rigid population's stiffness in an SCD patient sample with greater precision.

Although the method presented here can predict with greater precision the stiffness of the rigid RBC population in an SCD patient blood sample, it is deficient in some areas. First, like traditional ektacytometry, our model cannot distinguish which RBCs have undergone irreversible shape change, i.e., configuration to a sickled crescent shape. Often a misunderstood disease, blood

from SCD affected individuals is thought to be entirely composed of sickle-shaped RBCs, i.e., crescent-shaped. [50] However, the reality is that irreversibly sickle-shaped RBCs (ISCs) are highly fragile and short-lived. [146] Therefore, the majority of HbS-rich RBCs in circulation retain their discocyte-shape and yet remain rigid. [146,147] An example of this is shown in Figure 4.2., wherein a standard blood smear of patient 10, genotype SS with a comparatively high %S fraction of 79.3%, only ~7.3% of RBCs in the smear show shape deformation from regular RBC discocyte shape. Second, others have reported that the presence of ISCs in a blood sample alters the elongation diffraction patterns imaged by ektacytometry. [148] That is, higher amounts of ISCs lead to more considerable differences in apparent bulk elongation indices, similar to results shown by Parrow *et al*. However, these studies focused on using Osmoscan analysis. [70,148]

Thirdly, our predictive model was built using the deformability measurements of artificially stiffened RBCs; Thus, the degree of stiffness in this model system was uniform regardless of the %rigid fraction. This assumption is carried over when using the model to predict the stiffness of the %S fraction in an SCD patient blood sample. However, it is essential to note that there is likely a range of stiffnesses in a patient's %S RBC population, i.e., not all rigid RBCs have the same degree of rigidity. The novelty of our model is the capability to neglect the contribution of the healthy, i.e., HbA, RBCs in a standard ektacytometry measurement. Another point of interest is that the measurements performed in this study were standard deformability elongation analysis without any alteration in the blood's oxygen conditions. A recent development in ektacytometry technology is the Oxygenscan feature, [135], which determines the point of sickling of HbS-rich cells in a blood sample by alternating oxygen conditions. However, in terms of measuring a maximum elongation index at maximum shear stress, the end result is still the same

regardless of oxygen conditions. Given that our model is built using only information from maximum elongation, our approach is complementary to the Oxygenscan.

Finally, improvements to the ektacytometry method, as demonstrated here, could increase its prevalence as a reliable tool for measuring RBC rigidity. This approach can also lead to the utilization of ektacytometry as a tool for understanding patient response to therapies. For example, blood transfusions are a standard treatment for SCD patients.[62] A previous work has proposed that reducing the %S population to less than 30% is beneficial for moderating symptoms in SCD patients. [63] However, the reasons why this is the case remain unexplored, and it is unclear what role the stiffness of the %S population plays in altering symptoms. [63] The prior work by Gutierrez *et al*. showing the presence of artificially rigid RBCs in blood flow reduces WBC adhesion to inflamed endothelium drastically, depending on the RBC rigidity level and fraction in blood. [10] Given the wide variability in the stiffness of HbS-rich RBCs from patient to patient demonstrated in Figure 4.3.A., the arbitrary prescription of reducing the %S population to less than 30% with transfusion may not be ideal for every patient. Specifically, some patients could have increase infection risk, depending on the amount and stiffness level of the HbS-rich RBCs present in the blood. Thus, the insight into the stiffness of the HbS-rich RBC populations offered by our presented method may be helpful in optimizing transfusion therapies. In another example, as previously mentioned, Qiu *et al*. show that rigid RBCs' mechanical impact alone was sufficient to create endothelial injury. [140] This damage to the endothelium led to inflammation, which causes endothelial dysfunction in SCD, contributing to crises. [140] Given that stiffened, HBS-rich RBCs have a higher propensity to marginate, i.e., migrate near the blood vessel wall, [40] we anticipate these altered cells are likely well-positioned to cause endothelial damage regardless of their composition in blood. Thus, understanding the rigidity level of the HbS population can offer

insight into crisis risk. However, more clinical studies are necessary to probe this possibility thoroughly.

4.6. Conclusions

Overall, this work presents an innovative approach for a more thorough examination of the ektacytometry-based assessment of RBC stiffness in SCD patients. We utilize information from an RBC deformability measurement combined with standard electrophoresis and hemoglobin analysis to build a parameterization model to predict the rigid RBC population's bulk rigidity in a patient's blood with greater precision. Although extensive future work is needed to prove ektacytometry as a robust clinical tool, knowledge from the presented model offers a better understanding of the bulk stiffness in a rigid or sickle population of a patient blood sample. This information could help diagnose disease severity in SCD, understand the variation of infection susceptibility in different SCD patients, and assess how patients respond to blood transfusions or novel medication.

Chapter 5 **: Red Blood Cell Stiffness Driving Patient Symptoms: A Study of Red Blood Cell Population Rigidity in Sickle Cell Patient Genotype SC Relation to Overlooked Clinical Symptoms**

5.1. Publication Information

The work presented in this chapter is not yet published. This work will be submitted as a clinical case study article as: Mario Gutierrez, Mark Shamoun, and Omolola Eniola-Adefeso. "Red Blood Cell Stiffness Driving Patient Symptoms: A Study of Red Blood Cell Population Rigidity in Sickle Cell Patient Genotype SC Relation to Overlooked Clinical Symptoms."

This chapter aims to present an interesting clinical case study that suggests that red blood cell rigidity could play a more prominent role in sickle cell disease patient outcomes than initially believed. The data presented in this chapter is limited data that are unable to draw definitive conclusions but rather highlight an interesting clinical observation.

5.2. Abstract

Sickle cell disease is a systemic hematological disease. Various genotypes of the disease exist; however, the two most common include hemoglobin SS (Hgb SS) and hemoglobin SC (Hgb SC) disease. Hgb SC is typically considered a less severe genotype; however, some patients with SC disease still have significant complications. Ektacytometry is utilized to measure red blood cell deformability in sickle cell patients and may help identify patients at risk for severe disease. We

describe a patient with genotype hemoglobin SC with a more severe phenotype, which we show having very rigid red blood cells via ektacytometry. The patient of interest is oddly hospitalized at a higher frequency, ~4x, in comparison to other SCD pediatric patients and has an irregularly high amount of hospital days per year, 85 days.

5.3. Introduction

Sickle cell disease, a hereditary multisystem illness, is one of the most prevalent blood cell diseases, affecting over 100,000 Americans and millions worldwide.[3,52] Previous studies have shown many biochemical mechanisms of SCD pathology, including activation of the vascular endothelium, leukocytosis, oxidative stress from tissue reperfusion, and intravascular and extravascular hemolysis.[3] The symptoms of SCD are dependent on the genotype of SCD – two of the most common being Hgb SS and Hgb SC. The Hgb SS is the most prevalent and severe genotype. At the same time, the Hgb SC is clinically accepted as milder due to fewer hemolysis markers and fewer associations with severe complications, including stroke, early mortality, and vaso-occlusive pain episodes.[145] However, for both of these subtypes, the RBCs are often afflicted with increased membrane rigidity due to the high concentration of mutated or abnormal Hgb S inside the RBC. Furthermore, the mutated hemoglobin's polymerization under hypoxic conditions can alter the RBC shape to an irreversibly-sickled form.

Due to natural aging, the RBC hemoglobin density or mean corpuscular hemoglobin concentration (MCHC) increases moderately; however, this is severely accelerated in SCD.[51,149,150] During deoxygenation, sickle cells experience a loss of potassium that causes an ion imbalance and the loss of water from the cell, resulting in a higher MCHC.[149,150] Past studies have reported that this loss of potassium from Hgb SC RBCs is higher compared to SS due to the presence of Hgb C.[149] This unique pathophysiology of SC cells results in cells that, although they contain

approximately half Hgb S compared to SS cells, have a high MCHC. Interestingly, this implies that, depending on their hydration conditions, the SC RBCs can lose membrane deformability as much as, or more, SS cells. [151] However, while they have similar sickling rates to SS cells, the Hgb SC have a reduced capacity to irreversibly sickle – i.e., they are less likely to change shape permanently.[150]

Unsurprisingly, the irreversibly-sickled RBCs have been a primary focus of research in SCD, leading to the understanding that these cells cause significant physical damage when traveling through the body by occluding microvasculature, depriving tissues of nutrients and oxygen, and damaging vital organs such as the spleen, liver, and lungs.[8,152] The combination of vessel occlusion and tissue deprivation of oxygen results in a vaso-occlusive pain crisis experienced by SCD patients. Shape alteration in RBCs is dependent on a variety of factors, including oxygen conditions and hemoglobin contents of individual RBCs. Under stress, Hgb S will spontaneously polymerize and result in RBC shape alteration.[153] Although the staple crescent-like shape is the most frequent shape deformation; it is not always guaranteed.[39,153,154] However, alterations to the membrane flexibility are assured.[39] Importantly, rigidified, non-deformed RBCs have a longer lifespan than RBCs that have undergone shape deformation to the sickled confirmation.[155,156] Thus, SCD patients live more with the consequence of rigid, normal-shaped, i.e., discocyte, RBCs than the sickle-shaped, which may prove to be more critical in maintaining their general well-being. Herein, we describe a patient with Hgb SC disease with a more severe clinical course, found to have very rigid red blood cells.

5.4. Results

Our patient is an 18-year-old African American male (Patient 1) with a history of Hgb SC first diagnosed at age 7. His father is heterozygous for hemoglobin S, and his mother is heterozygous for hemoglobin C. He has one unaffected sibling and a sister who also has Hgb SC

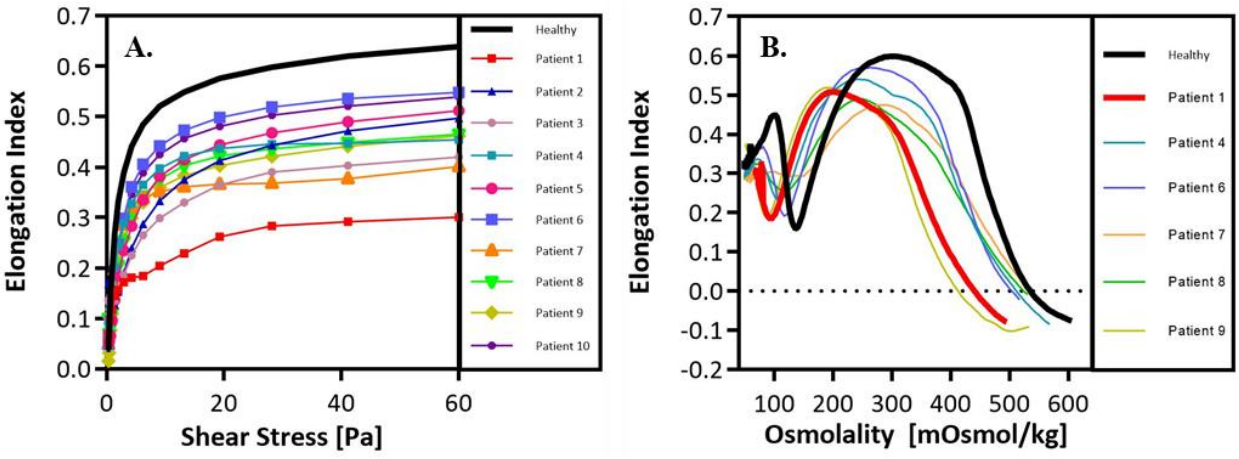

Figure 5.1. Sickle Cell Patient Red Blood Cell Deformability Analysis Via Ektacytometry.

(A) Standard ektacytometry deformability analysis at constant osmolality (~290 mOsmol/kg) and variable shear stress. (B) Osmoscan ektacytometry analysis at constant shear stress (~30 Pa) and variable osmolality.

(Patient 2). Over the last few years, Patient 1 has struggled significantly with vaso-occlusive crises (VOC) that seemed exaggerated for his genotype. In 2017, he was admitted 12 times for VOC, and in 2018 he had 8 admissions. In 2018, he was admitted for 85 days with an average length of stay of 10.6 days.

In contrast, patients with Hgb SS studied (n=7) had an average of 1.3 admissions per year and an average length of 5.4 days per stay. During most admissions, Patient 1 was started on an opioid-based, patient-controlled analgesia (PCA) pump at the time of admission and often required additional ketamine continuous infusion or other pain modalities to help control his pain. His care was managed by the acute pain service, palliative care, and pediatric hematology, and he had a patient-specific pain plan in place to expedite care. He was controlled at home with

ibuprofen/acetaminophen and opioids. He was also enrolled in our pain clinic with psychology for coping mechanisms, including music therapy, exercise, and heating pads. His frequency of pain crisis and sensitivity to dehydration and weather change seemed abnormal for a patient with Hgb SC genotype, and thus his blood was collected for further investigation.

We measured the deformability of blood from several SCD patients in the Erythrocyte Diagnostic Lab (EDL) at Cincinnati Children's Hospital using an ektacytometer (Lorrca), which quantifies the elongation of RBCs as a function of shear stress at a constant physiologic osmolality as described in the Materials and Methods chapter. Blood samples were obtained via venipuncture according to a protocol approved by the University of Michigan IRB and following the declaration of Helsinki. Informed consent was obtained for each patient before the blood draw, and samples were collected into a syringe containing EDTA as the anticoagulant as described in the Materials and Methods chapter. Table 5.1. lists all the patients evaluated, including the SCD genotype, general demographics, RBC stiffness measurement, hospitalization, and pain frequency. Except for Patient 1, ektacytometry deformability and Osmoscan analysis were performed once for each patient. The ektacytometry analysis was performed three different times, each ~16 weeks apart, for Patient 1. All patient samples were collected during routine clinical visits, i.e., collected in a stable state of health. Figure 5.1. shows the deformability curve obtained for all patient blood evaluated with Figure 5.1.A. showing RBC elongation analysis at constant osmolality and variable shear stress. Figure 5.1.B. shows elongation analysis with constant shear and variable osmolality, i.e., osmoscan. From these curves, a maximum Elongation Index (EI_{MAX}) can be defined as the maximum deformability of RBCs at high shear stress, which is accepted as a measure of the rigidity in blood. A lower EI_{MAX} value relative to healthy blood is indicative of the presence of

Table 5.1. Sickle Cell Disease Patient Demographics and Hospitalization Information.

Table with patient information including SCD genotype, age in years, gender (male or female), maximum Elongation Index recorded via ektacytometry of the patient blood sample, and current patient therapy chronic transfusions (CT) or Hydroxyurea (HU). Missing therapies indicate the patient is not under any type of treatment at the time of the measurement. The table also includes Information regarding the patient hospitalization frequencies and medical complications.

Patient	SCD Genotype	Age	Gender	Therapy	Maximum Elongation Index	Admissions in 2018 for Pain	Hospital Days for Pain	Other Complications
#	-	years	(M/F)	-	-	-	-	-
1	SC	17	M	HU	0.301	8	85	N/A
2	SC	10	F	HU	0.497	8	54	N/A
3	SC	12	F	-	0.420	1	4	N/A
4	SS	15	M	HU	0.454	2	10	Acute Chest x 1, AVN x1
5	SS	21	F	-	0.512	0	0	N/A
6	SS	1.5	F	-	0.548	0	0	N/A
7	SS	16	M	CT	0.401	2	7	N/A
8	SS	13	M	CT	0.465	0	0	N/A
9	SS	18	M	CT	0.462	2	9	N/A
10	SS	19	F	CT	0.539	3	12	Acute Chest x 1

stiff RBCs. As with previous reports, the estimated EI_{MAX} for healthy blood is ~0.63.[10] The EI_{MAX} obtained for Patient 1 was 0.30, while the blood from other patients ranged from 0.40 to 0.55.

We find that there is a moderate negative Pearson correlation between the EI_{MAX} values measured and the number of hospital days for pain. There is a very significant difference between the EI_{MAX} values measured from Patient 1 (μ_{pat1}=0.332, n=3) and the EI_{MAX} values of the other nine patients (μ_{ops}=0.478, n=9), yielding a p-value of 0.003 as determined by a Student's t-test 1-tail analysis. Indeed, the mean elongation of Patient 1 blood is classified as an outlier when grouped into the elongations of the other nine patients. By excluding Patient 2 from this analysis, we find there is a very significant difference (p=0.009) for the number of hospital days for pain per

admission between Patient 1 and Patients 3-10. In fact, for Patients 3-10, there is an average of 4.2 hospital days with pain for every admission, compared to the 10.6 hospital days with pain per admission for Patient 1. Figure 5.2. shows elongation curves for Patient 1 during different time periods, as well as comparison to other notable SCD patients.

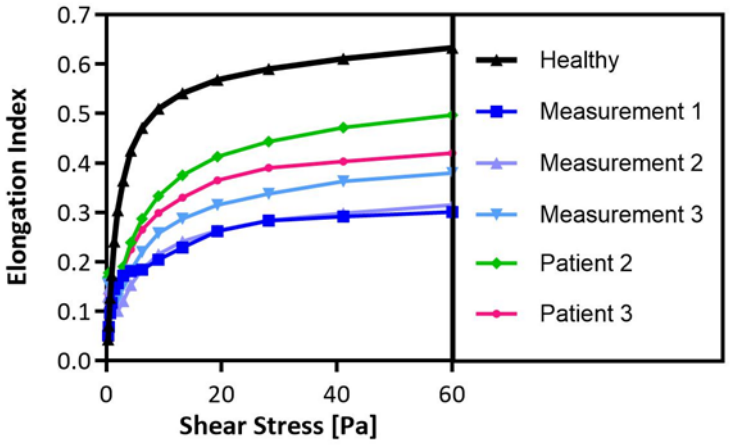

Figure 5.2. Deformability Analysis Via Ektacytometry of Focus Patient in Comparison to other SC Patients.

Standard ektacytometry deformability analysis at constant osmolality (~290 mOsmol/kg) and variable shear stress. Ektacytometry analysis of focus patient taken at three different time periods, compared to deformability analysis of other SC patients.

5.5. Discussion

Previous studies have used ektacytometry to measure rigidity as a function of changing osmolality at constant shear stress.[157] Figure 5.1.A. shows a comparison of our deformability data at constant osmolality with varying shear stress and vice-versa in Figure 5.1.B. We opted to interpret our EI_{MAX} with a deformability analysis based on data collected at constant osmolality and varied shear stress rather than with osmoscan since the former mimics the physiologic environment where RBCs experience changing shear stress as they flow through the various blood

vessels at a fixed, physiologic osmolality. As shown, patient 1, which is our patient described above, showed the lowest EI_{MAX} (~0.301) indicative of the presence of an ultra-rigid RBC population, which is interesting given his SC genotype but fits with the high VOC experienced by this patient. Similar to observations seen by Ballas *et al*., we observe from Figure 5.1.B. that the RBCs in the blood sample from Patient 1 are highly dehydrated, as expected to be seen in an SC sample.[151] This dehydration is likely one of the factors driving the extreme rigidity of the RBCs in the patient.

Our patient, as well as his sibling (Patient 2), were on hydroxyurea treatment in 2017 through 2019, which is known to increase RBC deformability and a resulting higher EI_{MAX} value.[157] However, despite hydroxyurea treatment, our patient still had a reduced EI compared to other patients. In 2019, our patient was started on chronic transfusions with a partial exchange, given his severe phenotype, and after initiating chronic transfusions, his EI_{MAX} increased (~0.37) and frequency of pain crisis subsequently decreased, as shown in Figure 5.2., Measurement 3. Patients 5 and 6 show similar curves to our healthy control, and neither required hospitalization for any complications of sickle cell disease. Patient 10 did have multiple hospitalizations; however, this patient did have difficulty with transportation, and although they were on chronic transfusions, appointments were missed. Patient 10's rigidity was obtained while the patient was on every 3 to 4-week transfusions, and the missed appointments likely contributed to the hospitalizations.

The patient's younger sister was also analyzed (Patient 2); however, her EI_{MAX} was higher and closer to other SCD patients' values. Clinically, his sister still required multiple admissions, but had 54 hospital days in 2018 and required significantly less intervention per stay. During many of her admissions, she did not require a PCA and instead could be managed on intermittent intravenous morphine or oral pain medications. Previous studies focusing on the psychological

impact of SCD and on children and their siblings suggest that little attention is given to family members or siblings who are not chronically ill or are healthy.[158–160] These siblings often are subject to anxiety, feelings of rejection, and even jealousy.[158–160] Given the context of this complex social situation, it is likely that the number of hospital days and admissions of Patient 2 are skewed and do not actually represent an independent patient clinical outcome. For these reasons, we opted to remove Patient 2 from a statistical analysis comparing the hospital days with pain per admission between all the patients (Patients 3-10) and Patient 1.

Additionally, we compare Patient 1 to Patient 3, Figure 5.2. Patient 3 is also an SC genotype and expresses a phenotype, which is much more typically seen in SC patients. The EI_{MAX} observed for Patient 3 is 0.42, closer to values observed in stable patients. In comparison, Patient 3 was admitted only once in 2018 for a duration of four days with pain. Certainly, Patient 3's clinical stability is something regularly observed in SC patients.

5.6. Conclusions

In conclusion, our patient is observed to have abnormally highly rigid RBCs despite treatment and presents an abnormally high occurrence of pain for an SCD patient with what is regarded as a clinically less severe genotype, SC. Previous studies show SC patients tend to receive a late diagnosis, often not until the occurrence of a severe or fatal health complication.[161] Utilizing RBC deformability analysis may allow for the identification of patients with a high risk for complications in the absence of a significant level of hemolysis or irreversible sickling. Although it is difficult to determine the entire and exact contribution RBC rigidity has on the development of VOC in our patient, it is likely a contributing factor to the variation in patient disease phenotypes in SCD and warrants further exploration in how one could use RBC deformability analysis for

predictive outcomes in patients, especially for those not on chronic transfusions or hydroxyurea therapies.

Chapter 6 **: Mechanical Impact of Rigid Red Blood Cells in Sickle Cell Disease and on Leukocyte Adhesion Performance**

6.1. Publication Information

The work presented in this chapter is not yet published. This work will be submitted as a research article to *Annals of Biomedical Engineering* as: Mario Gutierrez, Mark Shamoun, Tyler Tanski, and Omolola Eniola-Adefeso. "Mechanical Impact of Rigid Red Blood Cells in Sickle Cell Disease and on Leukocyte Adhesion Performance."

This chapter aims to probe how WBC adhesion to inflammation is impacted in the presence of rigid red blood cells in an *in vitro* model of blood flow, which has been closely tailored to match the blood characteristics of sickle cell disease patients. Overall, we aim to understand better the extent of impact red blood cell rigidity has on immune cell adhesion functionality.

6.2. Abstract

One of the significant outcomes of SCD is the alteration of RBC membrane rigidity. Although duly noted as a remarkable characteristic of the hematological disease, knowledge of the extent to which rigid RBCs influences leukocyte adhesion capability to inflammation in SCD is limited. Despite the known role of white blood cells in SCD pathogenesis, there is limited work fully exploring the mechanism of their adhesive interactions under flow conditions with patient blood

or representative models of human blood. This study seeks to probe further the impact RBC rigidity has on immune response, specifically adhesion to inflammation, related to SCD. We analyze differences between SCD and healthy non-SCD blood donor leukocyte adhesion ligand profiles. Furthermore, we describe a series of artificially constructed blood models which match key characteristics of SCD patient blood, including hematocrit, total leukocyte counts, fraction of rigid RBCs, and average degree of stiffness in the rigid RBC population. We couple the actual SCD patient blood samples with our artificially constructed blood models with a microfluidic blood flow model to test how leukocytes adhere to inflammation in flow. We find that the presence of rigid RBCs in the blood flow reduces leukocyte adhesion capability to inflammation. When specifically focusing on the artificially constructed blood model, and the RBC rigidity factor is removed, we find that leukocyte adhesion to the inflamed vessel was improved. The findings from this study highlight the role rigid RBCs have on leukocyte adhesion tendencies in SCD.

6.3. Introduction

Sickle cell disease is a complex genetic blood disorder affecting millions across the world. [3,42] SCD is defined by the mutation in the gene directing the production of the oxygen-binding protein hemoglobin. [55] Although multiple Hgb variants exist, by far, the most common one is HbS. Two defining qualities of HbS are its reduced capacity to bind oxygen as opposed to healthy Hgb and its propensity to polymerize with other HbS molecules. Individuals who have inherited HbS alleles from both parents suffer sickle cell anemia, the most acute type of SCD. [55,130] Red blood cells (RBCs), or erythrocytes, serve as the vehicle for Hgb transport across the body. [13] Under stressful circumstances in SCD, RBCs with high concentrations of HbS are likely to experience mild to severe shape alteration, resulting in the classic ‘sickle’ shape. [55] Additionally, RBCs will

experience a reduction in membrane flexibility and an increase in cell fragility. Outcomes include hemolysis, reduced gas exchange capacity, anemia, and an increased risk for a vaso-occlusive crisis. [5,44,55] At first, seeming like minor alterations, these changes to RBCs result in a cascade of detrimental outcomes that contribute to an overall reduced quality of life and high mortality rates in SCD patients. [55]

The higher deformability of RBCs compared to that of the other major cellular components, i.e., WBCs and platelets, resulting in a smaller displacement upon a heterogeneous cellular collision, essentially reducing the likelihood of RBC motion towards the vessel wall. [31,34] This higher distribution of RBCs in the center of flow is critical to maintaining hemostasis as it allows WBCs and platelets to interact and rapidly adhere to the wall in response to infection or vessel injury. Gutierrez *et al*. previously showed that in the presence of artificially rigidified RBCs in blood flow, WBC adhesion and platelet localization to an inflamed vascular wall model is reduced drastically. [10,40] Thus, any alteration in RBC deformability, as present in SCD, likely alters blood cell distribution in ways that contribute to the disease. However, RBC rigidity in SCD is often overlooked as a significant factor in exacerbating disease symptoms associated with the other, non-RBC, blood cells, i.e., WBC, and is poorly investigated as a contributing factor in immune challenges of SCD patients.

In SCD, the combination of i-sRBCs, WBC, and platelet adhesion to an activated endothelium lead to episodes of vaso-occlusive crisis. [46,55] Abnormally higher baseline WBC counts are associated with SCD. [53,55] Interestingly, the higher number of immune cells in this condition correlates with increased morbidity and mortality. [55,163,164] A higher absolute number of neutrophils in SCD have been correlated as a predictive biomarker for clinical complications, including vaso-occlusive crises and clotting issues.[163] Despite an increased number of WBCs, SCD

patients are prone to infection that is traditionally linked to the damage to the spleen by i-sRBCs.[44,165] However, it is plausible that rigid RBCs present in blood alters WBC margination, which affects vascular adhesion and, thereby, contributes to the reported high infection rate in SCD. Boggs *et al*. observed a diminished marginal granulocyte pool in SCD, i.e., the fraction of WBCs present in the tissue space, which they hypothesize is the cause of the abnormally high circulating WBC count typically reported in SCD. [78]

In this chapter, we present a series of artificially stiffened RBC blood models that have been tailored to match the blood conditions of actual SCD patients closely. We use these blood models and SCD patient blood to probe the extent to which RBC membrane rigidity is a contributing factor in altering WBC adhesion performance related to vascular inflammation in SCD. We find that when the RBC membrane rigidity factor has been removed from blood flow, WBC adhesion to inflammation is improved. The findings reported here present an opportunity to understand further the impact of the biophysical interactions of the rigid RBCs on WBC adhesion and the contribution to disease symptoms in SCD.

6.4. Results

6.4.1. SCD Patient Blood Collection and RBC Stiffness Characterization

We begin this study with the collection of blood samples from SCD patients during routine visits. General information is collected from the SCD patients, including the specific SCD genotype, age, gender, and current therapy plan. The blood sample includes hematocrit, WBC count, percent hemoglobin S (HbS or %S Fraction), and ektacytometry RBC elongation analysis. Using the approximation method described by Gutierrez *et al*., the %S fraction population's stiffness is estimated, and an analogous rigidity for this population is also estimated.[11] This

information can be found in Table 6.1. The majority of the SCD patients in this study are of the homozygous SS genotype, twelve out of fifteen. The remaining three patients express the milder

Table 6.1. Sickle Cell Disease Patient Demographics and Blood Profile Information.

Table with patient information including SCD genotype, age in years, gender (male or female), current patient therapy chronic transfusions (CT) or Hydroxyurea (HU). Missing therapies indicate the patient is not under any type of treatment at the time of the measurement. Blood characteristics include hematocrit, total WBC count, HbS %S Fraction, maximum Elongation Index recorded via ektacytometry of the patient blood sample, estimated maximum Elongation Index of %S Fraction, and analogous rigidity of %S Fraction represented as a concentration of tert-butyl peroxide (TBHP, mM). Incubation of healthy RBCs with TBHP induces loss of membrane deformability.

Patient	SCD Genotype	Age	Gender	Therapy	Hct	WBC Count	%S Fraction	Measured Bulk EI_{max}	Estimated Rigid Pop. EI_{max}	Analogous Rigidity
#	-	years	(M/F)	-	%	$x10^6$	%	-	-	mM
1	SS	2	F	CT	24.7	6.7	37.4	0.606	0.561	0.51
2	SC	17	M	HU	32.7	8.7	47.6	0.301	EI_{min} >	1.03
3	SS	15	M	CT	20.5	14.4	55.8	0.482	0.362	0.67
4	SS	9	M	CT	17	15.3	75.2	0.266	0.145	0.86
5	SS	19	F	CT	23.6	19.9	21.1	0.539	0.188	0.82
6	SS	18	M	CT	23.1	18.9	34.4	0.462	0.136	0.87
7	SC	18	M	HU	31.1	7.8	50.3	0.465	0.299	0.73
8	SS	6	F	CT	25.8	10.5	48.7	0.421	0.198	0.81
9	SS	13	M	CT	29.3	13.4	20.7	0.465	EI_{min} >	1.13
10	SS	16	M	CT	27.6	15.1	43.1	0.401	0.095	0.9
11	SS	1.5	F	-	25.5	7.6	89.9	0.548	0.539	0.53
12	SS	15	M	HU	21.4	18.5	79.3	0.454	0.407	0.64
13	SS	13	M	HU	19.3	17.2	89.9	0.297	0.259	0.76
14	SS	20	F	HU	24.8	9.9	68.9	-	-	-
15	SC	10	F	HU	32.1	5	42.4	-	-	-

genotype SC. Our study's patients ranged from eighteen months to twenty years of age with a median age of fifteen years. Eight of the patients are administered regular blood infusion therapy, and six patients are being treated with Hydroxyurea therapy. Patient 11, the youngest donor, was not on either therapy at the blood collection time. The average hematocrit across all fifteen patients was around 25% and an average WBC count of 12.6 million per milliliter of blood. The average %S Fraction across all fifteen patients was ~54%. We obtained ektacytometry elongation analysis for thirteen out of the fifteen SCD patients who took part in this study. Two patients opted out of the ektacytometry analysis. The average maximum elongation index for the thirteen patients measured was ~0.439.

6.4.2. Leukocyte Adhesion Ligand Profile Characterization of SCD Donor Blood

To determine critical differences between a non-SCD and SCD patient WBC adhesion capabilities, we tested the adhesion ligand composition of both blood donor types. The five adhesion ligands chosen for examination were macrophage-1 antigen (MAC-1), P-selectin glycoprotein ligand-1 (PSGL-1), lymphocyte function-associated antigen 1 (LFA-1), sialyl lewis a (sLe^a), and L-selectin. The cell surface density of these five key adhesion ligands was examined via flow cytometry analysis in both neutrophils and monocytes of both non-SCD and SCD blood donors, Figure 6.1.A. Comparing fold differences in the density of each adhesion ligand between healthy non-SCD and SCD blood donors, we see that MAC-1 is overexpressed nearly 4x times in SCD donor neutrophils. All four other key adhesion ligands are under-expressed in SCD donors. Specifically, L-selectin, which is underexpressed ~3.5x less in SCD donor blood. We then take a closer look at the configuration in which the expressed MAC-1 is found on both healthy non-SCD

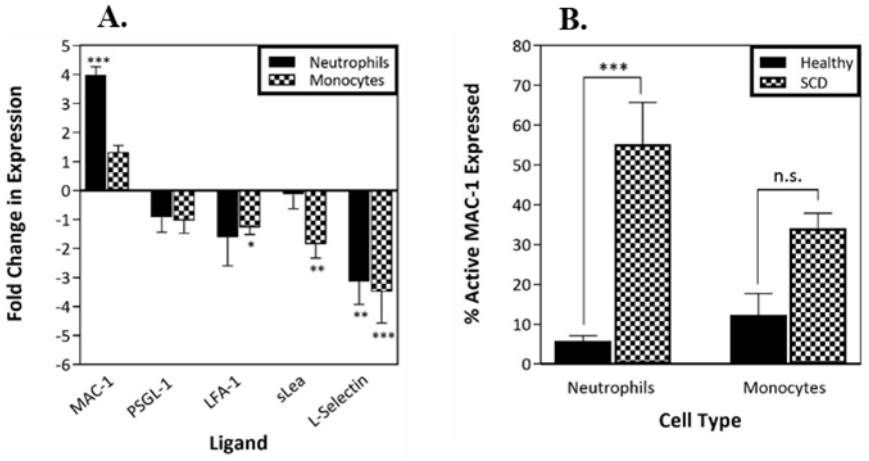

Figure 6.1. White Blood Cell Adhesion Ligand Expression Difference Between Sickle Cell Patients and Healthy non-SCD Controls.

Leukocytes of interest are neutrophils and monocytes. (A) MAC-1/CD11b, PSGL-1/CD162, LFA-1/CD11a, sLe^a/CLA, L-Selectin/CD62L ligand expression fold difference in SCD patients compared to expression in healthy controls. (B) Difference in active MAC-1 ligand expression in SCD patient WBCs compared to healthy control. Statistical analysis was performed using two-way ANOVA to test of fold change in ligand density expression between SCD donor and non-SCD donor WBCs. (*) indicates $p<0.05$, (**) indicates $p<0.01$, (***) indicates $p<0.001$, and no asterisks represent no significant difference found. Error bars represent standard error.

and SCD blood donors' neutrophils and monocytes. More specifically, we aim to find what percentage of the expressed MAC-1 is in an open or active configuration. We find that the active MAC-1 configuration is present in a much higher percentage in SCD neutrophils and monocytes than in non-SCD cells, Figure 6.1.B. All examined blood was processed and analyzed within two hours of being drawn from blood donors.

6.4.3. SCD Patient Leukocyte Adhesion to Time-Varied Inflammation

Next, we aimed to examine if WBC adhesion in SCD patients was variable with varying inflammation timing to an endothelium. Specifically, we wanted to see if WBC adhesion density to an endothelium would differ after four hours and after twenty-four hours of inducing inflammation via exposure to inflammatory cytokine, IL-1β. The blood of seven unique SCD patients was examined, all blood being perfused at three different shear rates, 1,000, 500, and 200

s^{-1}, Figure 6.2. We see that for seven out of the seven patients examined, WBC adhesion density significantly reduced when examined at the second inflammation time point. These results

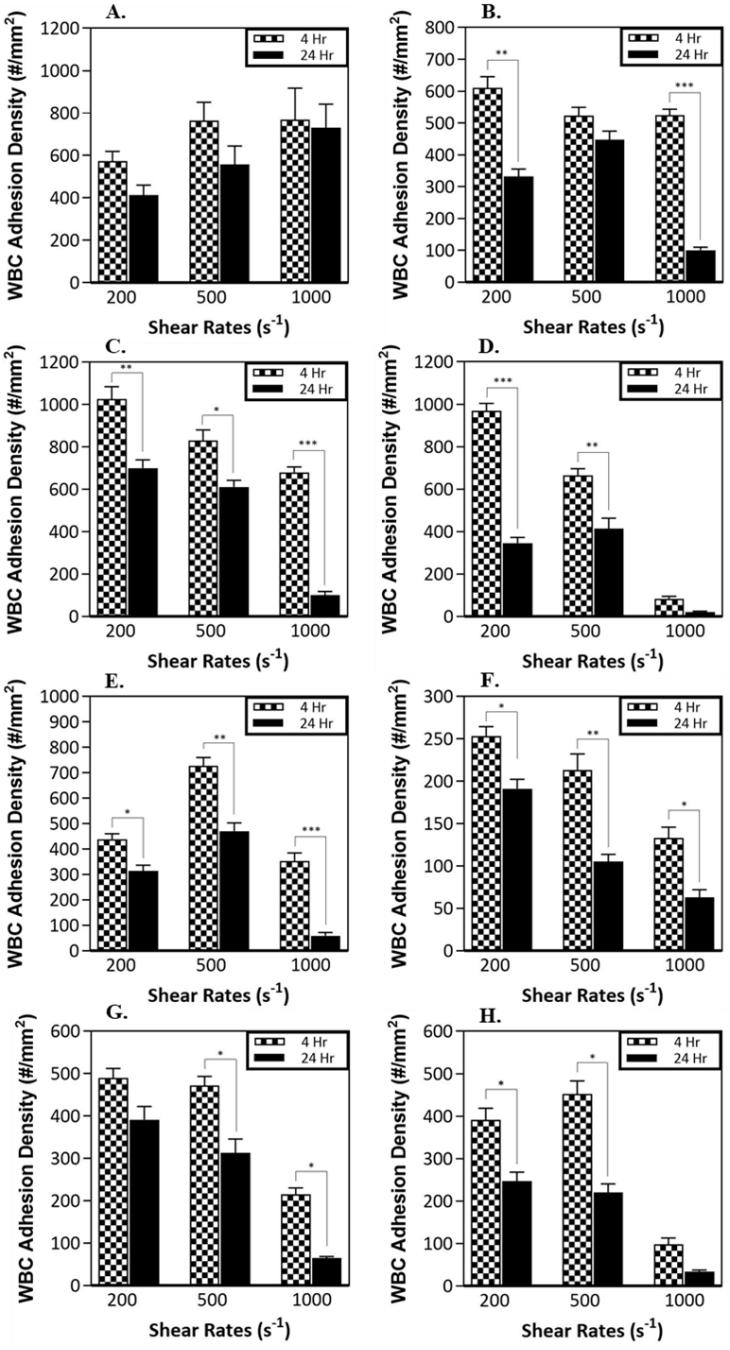

Figure 6.2. Sickle Cell Patient White Blood Cell Adhesion Density to Inflamed Endothelium.

Quantified WBC binding to an inflamed endothelial layer as a function of WSR and time of HUVEC exposure to inflammatory cytokine IL-1β, i.e., 4- or 24-hour inflammation activation. (A) Average WBC adhesion in healthy non-SCD donors. WBC adhesion for SCD Patient (B) 3, (C) 4, (D) 5, (E) 6, (F) 7, (G) 8, (H) 14. Statistical analysis of adherent density was performed using two-way ANOVA to test all WBC adhesion at 4-hour activation versus adhesion at 24 activation. (*) indicates $p<0.05$, (**) indicates $p<0.01$, (***) indicates $p<0.001$, (****) indicates $p<0.0001$, and no asterisks represent no significant difference found. Error bars represent standard error.

suggested that for this study, WBC adhesion in SCD patients is maximized at 4 hours after inflammation to endothelium as opposed to twenty-four hours later. This pattern is something that is also typically observed in WBC adhesion patterns in non-SCD blood.

6.4.4. SCD Patient versus Artificially Constructed Blood Model Leukocyte Adhesion

Using the microfluidic PPFC experimental approach, we aimed to examine the adhesion capability of WBCs to an inflamed endothelium under different blood conditions. More specifically, we wanted to control the presence of rigid RBCs to observe whether RBC membrane stiffness in SCD is a factor influencing the adhesion WBCs in blood flow. The microfluidic channel height was kept constant at ~127 μm, and blood was perfused at three different shear rates, 1,000, 500, and 200 s^{-1}, chosen due to their relevance in venules. Three separate blood models were used to isolate the rigidity factor. First, we examined the actual blood taken from SCD donors, denoted as Actual condition. Secondly, we utilized healthy non-SCD donor blood, where we reconstituted this blood to match all conditions of the specified SCD donor blood, specifically the hematocrit, WBC count, approximate stiffness of the HbS population, and the fraction of stiff RBCs in the blood. This second blood model was denoted as the Rigid Model. Thirdly, we again used healthy non-SCD donor blood to reconstitute all SCD donor blood conditions except RBC stiffness, denoted as Non-Rigid Model. This modeling process is repeated for eight unique SCD blood donors, Figure 6.3. The WBC adhesion is examined using each unique model for all eight measured SCD donors. We observe that WBC adhesion tends to be higher in the blood models originating from healthy non-SCD donors. Furthermore, the best performer in higher WBC adhesion density was the Non-Rigid blood model in all eight unique cases, hinting that the absence of rigid RBCs in the whole blood translated to a higher WBC adhesion capability.

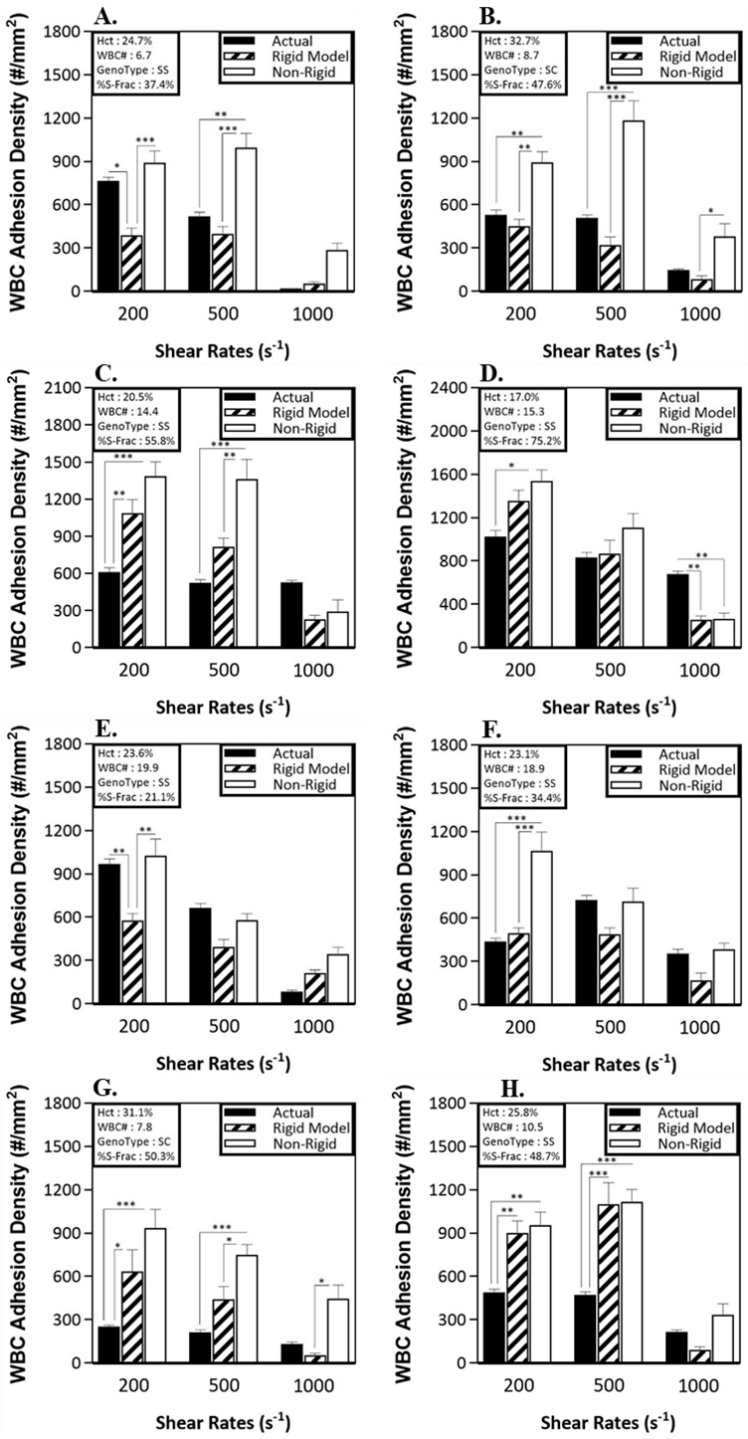

Figure 6.3. White Blood Cell Adhesion to Inflamed Endothelium in the Presence of Artificially Rigidified Red Blood Cells.

Healthy non-SCD donor whole blood was obtained and altered through a series of centrifugation steps to match SCD patient blood conditions including hematocrit, WBC count, %S fraction or rigid RBC fraction, and bulk rigidity of the rigid RBC population in the SCD patient blood sample. RBC membrane rigidity was achieved via incubation of healthy non-SCD RBCs at appropriate concentrations of tert-butyl hydroperoxide that would allow to best match the bulk rigidity of the rigid population in the SCD patient blood sample. Inflammation of the endothelium is induced by exposure to inflammatory cytokine IL-1β for four hours prior to blood perfusion. Quantified WBC binding to an inflamed endothelial layer as a function of WSR for SCD Patients (A) 1, (B) 2, (C) 3, (D) 4, (E) 5, (F) 6, (G) 7, (H) 8. Statistical analysis of adherent density was performed using two-way ANOVA to test all WBC adhesion at 4-hour activation versus adhesion at 24 activation. (*) indicates $p<0.05$, (**) indicates $p<0.01$, (***) indicates $p<0.001$, (****) indicates $p<0.0001$, and no asterisks represent no significant difference found. Error bars represent standard error.

6.4.5. Leukocyte Adhesion Ligand Profile Characterization of Rigid Blood Model

Upon observing the overexpression of MAC-1 and under-expression of L-selectin adhesion ligands in SCD neutrophils and monocytes, we aimed to test whether typical processing and handling of WBCs in healthy non-SCD donors would alter the expression of these key adhesion ligands. Healthy non-SCD donor neutrophils exposed to centrifugation (denoted as Neutro-Spin) increased their expression of MAC-1 up to 150% instead of a slight ~10% increase in neutrophils that were not centrifuged. Both conditions were measured approximately three hours post draw. A subsequent analysis was taken ~3.5 hours after the first test, ~6.5 hours after the initial blood draw. A slight increase in MAC-1 expression is observed at the second time point. A similar pattern is observed for MAC-1 expression in monocytes, Figure 6.4.A. The adhesion ligand L-selectin was also examined in a similar process to the one seen in Figure 6.4.A.; alternatively, the reduction or shedding percentage of L-selectin was tracked, Figure 6.4.B. Overall, Figure 6.4.A. and 6.4.B.

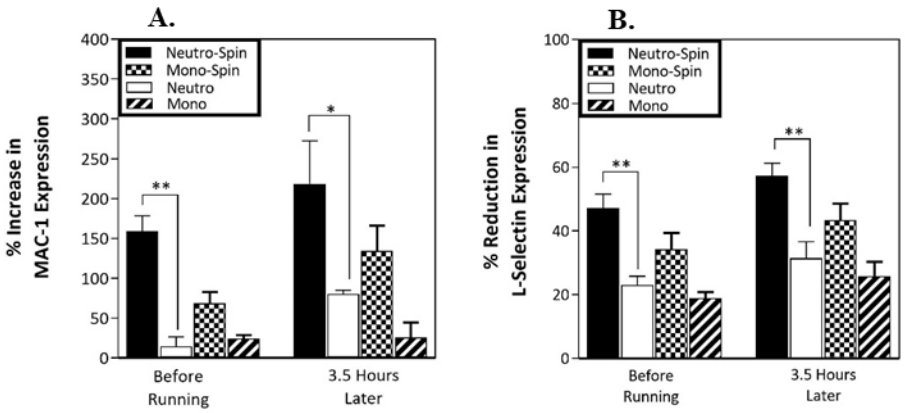

Figure 6.4. White Blood Cell Adhesion Ligand Expression After Recomposition Process.

Examined leukocytes ligand density percent change on neutrophils and monocytes. Time periods denote 1) right before running perfusion assay (~3 hours after initial blood draw) and 2) ~3.5 hours after start of perfusion assays (~6.5 hours after initial blood draw). Spin notation denotes having undergone centrifugation. (A) Increase in MAC-1 ligand expression of non-SCD donor WBCs. (B) Decrease in L-Selectin ligand expression of non-SCD donor WBCs. Statistical analysis was performed using two-way ANOVA to test of percent change in ligand density expression in non-SCD donor WBCs that have been idled vs. centrifuged. (*) indicates $p<0.05$, (**) indicates $p<0.01$, and no asterisks represent no significant difference found. Error bars represent standard error.

show that neutrophils and monocytes processed via centrifugation will result in the cells' activation.

6.5. Discussion

The loss of RBC membrane deformability is a significant outcome of SCD manifestation. [42,55] Increased RBC stiffness is linked to the frequency and severity of pain crisis and the cause of altered WBC adhesive interactions that lead to a high rate of infection in SCD. [46,55,78] More specifically, these complications are common when SCD patients are in a crisis state, which exhibits the formation of i-sRBCs in the blood population. [42,55] Substantial work has investigated in detail the systemic and cellular complications that arise in a vaso-occlusive pain crisis and specifically on the impact of i-sRBCs. Evidence presented by Qiu *et al.* suggests endothelial damage is a possibility only in the presence of rigid RBCs. [140,141] They investigate in a microvasculature-on-a-chip device how the single factor of rigid RBCs present in flow will alter endothelial integrity, with complications such as vaso-occlusion absent from the experimental setting. [140,141] However, there exists a disparity in understanding the rigid RBCs role, not i-sRBCs, play in influencing immune challenges in SCD patients under stable conditions. To our knowledge, no present work has focused on investigating the impact of RBC rigidity has on WBC adhesion functionality at steady, non-crisis conditions in SCD. Despite the known role of WBC in the pathogenesis of SCD, there is little work fully exploring the mechanism of their adhesive interactions under flow conditions with patient blood or representative models of human blood.[46] The current understanding of the adhesive behavior of WBCs in SCD has been generated with isolated cells and in static adhesion assays, which neglect the biophysical contributions of the rigid RBCs. [79,80]

In this work, we present a blood flow model that probes how RBC membrane rigidity impacts the ability of WBCs to adhere to inflammation in a vascular wall. More specifically, we utilize an artificial stiffening process to alter healthy RBCs to modulate the membrane stiffness. Along with this capability, we alter the whole blood composition of a healthy non-SCD blood donor sample to match a blood sample's characteristics from an SCD patient, e.g., hematocrit, WBC count, the fraction of stiff non-i-sRBCs, and degree of stiffness in the rigid RBC population. This study begins with the collection of SCD patient blood samples. Details from our SCD donor pool are shown in Table 6.1.

Work by Benkerrou *et al.* using SCD patient blood has focused on elucidating the differences in WBC adhesion molecule expression via flow cytometry, leading to the observation that WBCs are in a pre-activated state and the assumption of their enhanced ability to adhere to the vascular wall in comparison to cells found in the healthy non-SCD blood. [80] In line with prior work on characterizing SCD WBC molecule expression, our results show SCD donor WBCs are in a pre-activated state, Figure 6.1. We specifically examine the density of five adhesion molecules that play a vital role in the adhesion interactions of leukocytes and inflamed endothelial cells, MAC-1, PSGL-1, LFA-1, sLe^a, and E-Selectin. We find that MAC-1 is over-expressed (~3.8x), and L-selectin is under-expressed (~3.5x) in SCD neutrophils and monocytes compared to those of healthy non-SCD donors, Figure 6.1.A. Also, we see that a higher fraction of the MAC-1 expressed on both neutrophils and monocytes is in the active configuration. These results are not out of the norm and led us to hypothesize that WBCs of SCD patients are more likely to adhere to inflammation due to their pre-activation state.

Subsequently, we aim to understand if there are any differences in the optimal adhesion patterns of WBCs between SCD patients and non-SCD donors. Specifically, we study how the

varied time expression of inflammation surface receptors bind WBCs in a vascular wall microfluidic model. Our receptors of interest are E-selectin and iCAM-1, a common leukocyte adhesion molecule. Previous studies have quantified the maximal expression of E-selectin and iCAM-1 after inducing inflammation onto HUVEC via exposure to interleukin-1β. [110,111,166,167] E-selectin expression on HUVEC is maximized approximately four to six hours after exposure to iL-1β and returns to basal levels after twenty-four hours. However, iCAM-1 expression is maximal after twenty-four to forty-eight hours of initial exposure to the inflammatory cytokine. [110,111,166,167] Given the adhesion ligand profiles of our SCD patient pool, Figure 6.1., we wanted to test if there was any significant difference in the ability for WBCs to adhere to an inflamed endothelium four and twenty-four hours after exposure to inflammatory cytokine. We were able to examine the WBC adhesion with varied HUVEC inflammation time for seven of our SCD blood donors, Patients 3, 4, 5, 6, 7, 8, and 14, Figure 6.2. Our healthy, non-SCD blood donor control, Figure 6.2.A., does not show any significant difference in the WBC adhesion density to endothelium after four and twenty-four hours after inflammation at any of the three examined shear rates, 1,000, 500, and 200 s^{-1}.

Interestingly, all seven examined SCD donors displayed a significantly reduced capacity to adhere WBCs to inflammation after twenty-four hours of inflammation to the vessel wall. It is possible that the activated profile of the SCD donor WBCs, reduced L-selectin, is the cause of the reduced WBC adhesion density at twenty-four hours. E-selectin plays a crucial role in the initial capture and weak adherence of WBCs to the vessel wall. [166,167] After twenty-four hours of initial inflammation, E-selectin expression is minimal. It is possible that reduced weak interactions led to an inability for WBCs to form tight binding between integrins and iCAM-1, despite MAC-1 being over-expressed in WBCs of SCD patients.

The sparse adhesion studies with whole patient blood that exist have focused on the difference in WBC adhesion due to alteration in protein expression with no control for the role of RBC rigidity. [83,84] Though several analyses of WBCs adhesion in mouse models of SCD exist, [84] the differences in RBC geometry and deformability between humans and mice, which directly impact margination, would prevent direct extrapolation of mice data to humans. [86] For this reason, we aim to build an artificial human blood model to probe the RBC rigidity factor. Previous work by Gutierrez *et al.* utilized an artificial stiffening process to rigidify healthy non-SCD donor RBCs and reconstitute these rigidified RBCs into whole blood. [10] We take the blood information collected from our SCD patients, Table 6.1., and aim to match not only the hematocrit and WBC count but also the fraction of rigidified RBCs and the average stiffness of the rigid RBC population. We were able to do this for eight of our SCD donors, Patients 1-8. In parallel with actual SCD patient blood, the modeled blood is perfused through a microfluidic chamber modeling a vessel wall that has been inflamed to observe WBC adhesion density, Figure 6.3. When comparing the WBC adhesion performance of our modeled blood to that of actual SCD patient blood, variability is observed. Significant differences at 200 s^{-1} shear rates between the modeled rigid blood and SCD blood are found for Patients 1, 3, 5, 7, and 8. At the shear rate of 500 s^{-1}, differences were only found for Patients 7 & 8, and for 1,000 s^{-1} shear rate, the only difference was in Patient 4. Interestingly, most of the significant differences in WBC adhesion density are observed between the actual SCD patient blood and the modeled blood that excludes rigid RBCs, i.e., the Non-Rigid model. All these mentioned differences occurred at the low and intermediate shear rates of 200 s^{-1} and 500 s^{-1}. Possible causes for the differences seen in the WBC adhesion density between the actual SCD blood and the Rigid Model blood are possible inconsistencies in matching the RBC stiffness. The RBC stiffness matching method presented by Gutierrez *et al.* is not perfect.[11] First,

there is a distribution of RBC stiffness within the rigid fraction of an SCD blood sample, and the matching model oversees this by modeling the %S fraction stiffness uniformly and not a distribution. Although these assumptions might approximate and match an ektacytometry measurement, these differences might not perfectly translate into a blood flow model.

In addition, a considerable shortcoming of the modeled blood is any possible inconsistencies in the adhesion ligand profile of the WBCs of the SCD donors and modeled blood. Consequently, we aimed to probe if the healthy non-SCD donor blood's recombination process to match the SCD patient blood altered the adhesion ligand profile of the WBCs in any way. We find that the whole blood's centrifugation pre-activated the WBCs as an increase in MAC-1 expression, ~150% increase, and shedding of L-selectin expression, ~45% decrease, is observed in both neutrophils and monocytes opposed to idled blood, Figure 6.4. Interestingly, although not a perfect match in density magnitude, this pattern is in line with leukocytes' activation state in SCD.

Overall, the results from this study are interesting when placed into the context of vaso-occlusion in SCD. There is substantial evidence that shows the contribution of WBCs in SCD complications, including thrombosis and infection.[76,163,164,168] It is also well documented that SCD patients tend to have abnormally higher total WBC counts than healthy non-SCD people.[55,163,164] The most widely accepted description of mechanisms contributing to SCD pathophysiology suggests contributing factors include sickled RBCs, platelets, plasma proteins, vascular wall conditions, blood flow conditions, and even WBCs.[75,163] Previous work has shown that microvascular vaso-occlusion occurs most commonly in post-capillary venules.[169] This is to be noted, given that the physiological adhesion of WBCs is most common in venules.[119,125–127] Certainly, this implies that WBC adhesion to the vascular wall is correlated to higher incidences of vaso-occlusion in SCD.[75]

Generally, the results presented in this study suggest that WBC adhesion efficiency is higher in the absence of rigid RBCs in blood flow. Comparing across all flow conditions examined in this study, SCD donor blood and the artificially constructed Rigid Blood Model had lower WBC adhesion efficiency compared to the Non-Rigid Model, i.e., no rigid RBCs present. The instinctive conclusion would be that rigid RBCs present in blood flow will lead to lower WBC adhesion densities, resulting in less risk of microvascular occlusion. However, this narrative is simplistic and does not encapsulate the entire complexity of factors leading up to vaso-occlusion. One considerable observation from this investigation was that we never observed any RBC adhesion to the inflamed endothelial layer for all blood conditions, neither in the SCD donor blood in the artificially constructed blood models. It is known that in SCD, RBC adhesion to the vascular wall is a significant contributor to inflammation cascades and ultimately vaso-occlusion.[170] It is likely that this observation is due to the lack of i-sRBCs present in the artificial blood models and low abundance in the SCD donor blood. Considering SCD donor blood was collected from patients in stable condition. It is known that i-sRBCs are highly adhesive.[146,147,169] It is also possible that the time-scale of the blood flow experiments performed in this study, there was no major endothelial dysfunction that would induce RBC adhesion. One major shortcoming of this study was that we did not explore how factors such as blood plasma and platelets contribute to WBC adhesion to inflammation but instead focused entirely on isolating the factor of RBC stiffness. Such factors could also cause further endothelial dysfunction. In the absence of considerable endothelial dysfunction, i.e., heme-activation, the inflammation model presented here likely more closely resembles a rapid inflammation occurrence in an otherwise steady-state condition. Certainly, there are many pieces to a complicated puzzle, and the factor of RBC rigidity is just one piece. It may be difficult to make any definitive conclusion regarding vaso-occlusion. However, we can

conclude that the presence of rigid RBCs in blood flow certainly influences WBC adhesion in a microfluidic vascular wall model. More specifically, WBC adhesion to inflammation, in the absence of RBC adhesion to the vascular wall, is decreased when rigid RBCs are present in blood flow.

6.6. Conclusions

The knowledge uncovered from this work highlights the intricate impact RBC membrane rigidity has on reducing the capacity for WBC to properly adhere to an inflammatory challenge in a vessel wall model. Also, further evidence is shown that highlights the interactions between immune cells and RBCs in blood flow. Having a high count of WBCs does not necessarily translate to high adhesion to inflammation. Undoubtedly, the presence of rigid RBCs alters the ability of WBCs to adhere to an inflamed vessel wall. The insights gained from this study could have a profound impact on better understanding the pathophysiology of SCD. [171,172] This newfound understanding can lead to novel approaches to disease management, ultimately reducing infections, hospitalizations, and opiate use in the large patient population unable to receive a hematopoietic stem cell transplant. [173]

Chapter 7 : Alteration in Leukocyte Adhesion Patterns to Inflammation Upon Administration of Infusion Therapy in Sickle Cell Disease

7.1. Publication Information

The work presented in this chapter is not yet published. This work will be submitted as a research article to *the Journal of Biomedical Science* as: Mario Gutierrez, Mark Shamoun, Logan Piegols, and Omolola Eniola-Adefeso. "Alteration in Leukocyte Adhesion Patterns to Inflammation Upon Administration of Infusion Therapy in Sickle Cell Disease". This work is largely preliminary work and substantial subsequent investigations will be performed before submission for publication as a journal research article.

The goal of this chapter is to probe how WBC adhesion patterns to inflammation are altered with the controlled addition of healthy RBCs to SCD blood. We mimic the infusion process by adding controlled volumes of non-SCD RBCs to pre-infusion SCD blood samples. Subsequently, we utilize an *in vitro* blood flow PPFC model to quantify WBC adhesion to an inflamed endothelial layer. Overall, we aim to understand how infusion therapy administration influences WBC adhesion patterns in SCD.

7.2. Abstract

One of the major outcomes of SCD is the increased rate of hemolysis. Among many other detrimental side effects, an increased hemolysis rate leads to an overall reduced capacity for

oxygen transport in the blood. One of the most common therapeutic options for SCD patients is that of blood transfusions. Understandably, the main focus of blood transfusions in SCD is to directly address the reduced oxygen transport capability problem and reduce the risk for vaso-occlusive pain crisis. However, little is known about how blood infusions can alter cellular biophysical interactions, specifically those of immune cells. Vascular inflammation and infection are common in SCD, as well as high immune cell counts. Evidently, one of the common characteristics of SCD is an increased propensity for loss of RBC deformability. Evidence has shown that loss of RBC deformability can drastically impact cellular distributions in blood flow and the adhesion capability of immune cells. In this study, we aim to understand how immune cell adhesion to an inflamed *in vitro* vascular wall model is impacted upon the controlled addition of healthy non-SCD red blood cells to mimic the blood infusion process. We find that leukocyte adhesion density to the vascular wall is highly variable upon addition to RBCs to SCD patient samples. Of all the SCD infusion patients we examined, each registered a notable change in leukocyte adhesion patterns upon infusion. These results serve as an essential consideration when implementing infusion therapy, and there is a desired target for immune cell adhesion.

7.3. Introduction

To date, the two most prevalent therapies for managing SCD are the use of pharmaceuticals, typically Hydroxyurea, and the use of chronic blood transfusions.[174] Over the past decades, the popularity of chronic transfusions as an intervention method for treating SCD has grown in popularity. The rate of blood transfusions in children in the US has more than doubled over the past decade.[175,176] The growing popularity of blood transfusions can be accounted for due

to the higher availability of quality blood supply and increased safety. Multiple studies have shown evidence of the efficacy of blood transfusions towards preventing stroke in young SCD patients.[63]

The current standard practice employs the use of three variations of transfusion, simple infusion, manual exchange infusions, and automated RBC exchange.[175] One of the outcomes of all the transfusion interventions is lowering the HbS percentage and increasing hemoglobin A (HbA). One of the advantages of simple transfusions is their overall simplicity and minimal use of specialized equipment. However, this method offers less control over the %HbS and an increased risk for infusing to a hyperviscosity point and high iron accumulation. Although simple, this methodology is time-consuming and interventions are spaced out in short time periods. Manual exchange transfusions are typically implemented using an apheresis machine. In this methodology, there is the added step where the infusions patients' blood is also drained, phlebotomized, during the infusion of healthy donor blood. This added process results in less risk for reaching blood hyperviscosity and iron accumulation and increased control over the %HbS.[175] Although not a widespread method due to the need for highly specialized equipment and staff, automated RBC exchanges offer the best control over %HbS and reduction of adverse transfusion side effects. When implementing blood transfusions, a general rule of thumb is to aim for ~10 g/dL hemoglobin in SS genotype SCD patients.[175] Indeed, one of the outcomes of blood transfusion interventions is the reduction of %HbS or fraction of RBCs with a high propensity to have increased membrane rigidity. Clinically this is the desired outcome in terms of reducing blood hyperviscosity risk and increasing oxygen transport capability. Previous work has shown that leukocyte adhesion to inflammation in a vascular wall can be variable based on the fraction of rigid RBCs present in whole blood flow.[10] Thus, there exists the need to further study how leukocyte adhesion to inflammation behaves under varying %HbS content upon transfusion administration.

One of the unfortunate results of increased hemolysis in SCD is increased heme-activated inflammation in endothelial cells.[170] Increased chronic inflammation often leads to vaso-occlusive problems and can also lead to other vascular complications. [76,170,177] Studies have shown that SCD patients, even when in stable clinical condition, express four critical markers of endothelial activation, intercellular adhesion molecule 1, vascular-cell adhesion molecule 1, E-selectin, and P-selectin.[178] Additionally, SCD patients often experience abnormal rates of infection.[76] This seems counterintuitive given that SCD patients typically have abnormally higher immune cell counts.[55,163,164] There is considerable clinical and theoretical evidence that show the critical role of RBC adhesion to inflamed vascular wall in inducing vaso-occlusive crisis.[16,170,177] Interestingly, high absolute neutrophil count in SCD has been correlated as a predictive marker for clinical complications.[163] The most accepted model for vaso-occlusive crisis suggests RBCs, leukocytes, platelets, and plasma proteins are all factors in inducing endothelial dysfunction and ultimately occlusion.[163] However, the biophysical interplay between leukocyte adhesion to inflammation upon administration of infusion therapy is not fully understood. Specifically, the standard clinical target is the reduction of %HbS for obvious reasons. However, there is no consideration to how such changes may impact the adhesion of leukocytes to the vascular wall. Previous studies suggest the relationship between the fraction of rigid RBCs present in the blood, i.e., %HbS, and leukocyte adhesion to inflammation seems to be non-linear.[10] Thus, it is critical to investigate how leukocyte adhesion to inflammation is altered upon administration of infusion therapy. Uncovering this information could prove valuable in understanding how to minimize or optimize leukocyte adhesion for clinical purposes using better-prescribed infusion therapy.

This chapter presents a blood infusion mimic where we add healthy non-SCD RBCs to pre-infusion SCD blood samples. We chose to closely mimic the simple blood transfusion process,

which entails the addition of healthy non-SCD donor RBCs to treated SCD patients. We then perfuse these infused samples through an inflamed vascular wall microfluidic model and quantify WBC adhesion. We find that WBC adhesion density is variable upon administration of blood infusion. Each SCD patient blood sample that underwent the mimic infusion process registered a unique response in WBC adhesion patterns. The findings presented in this chapter shows there is an evident alteration in the biophysical interactions between infused RBCs, rigid RBCs, and leukocytes in the infusion process. These findings suggest there is a potential for optimizing infusion therapy based on the desired WBC adhesion pattern to inflammation.

7.4. Results

We begin this study by collecting blood samples from SCD patients who are regularly treated with blood infusions. We collect blood samples before the blood transfusion. For this study, we were able to collect eight unique SCD patient samples. Information including SCD donor genotype, age, gender, and pre-infusion blood conditions can be seen in Table 7.1. We aimed to collect another sample from the SCD donor's post-infusion therapy specifically for electrophoresis and hematocrit analysis. Unfortunately, logistical issues with the patient's inability to stay in the clinic post-infusion deterred us from collecting a complete set of post-infusion samples. The post-infusion sample information collected can be seen in Table 7.1., missing information is denoted with a dash in Table 7.1. In addition, to general patient information, we performed a complete blood count (CBC) analysis on all the eight SCD patient pre-infusion samples. Information including total WBC count, platelet count, mean corpuscular volume (MCV), neutrophil fraction, lymphocyte fraction, monocyte fraction, eosinophil fraction, and basophil fraction can be seen in

Table 7.2. In addition to the eight SCD patients, Table 7.2. also shows the average CBC values for non-SCD blood donors.

We analyze a subset of both pre-infusion and actual post-infusion blood samples via ektacytometry deformability analysis. The deformability elongation curves for our patients can be shown in Figure 7.1. We see the deformability curves for all eight pre-infusion samples analyzed in Figure 7.1.A. More notably, Patient 6 registers the least deformable pre-infusion blood sample with a maximum elongation index value of 0.266, Figure 7.1.A. Conversely, the most deformable pre-infusion blood samples came from Patients 4 and 6, both registering an elongation index of ~0.51, Figure 7.1.A. We were able to obtain the actual post-infusion samples from SCD Patients 2, 4, and 8. We compare the ektacytometry deformability curves of the pre-infusion and post-

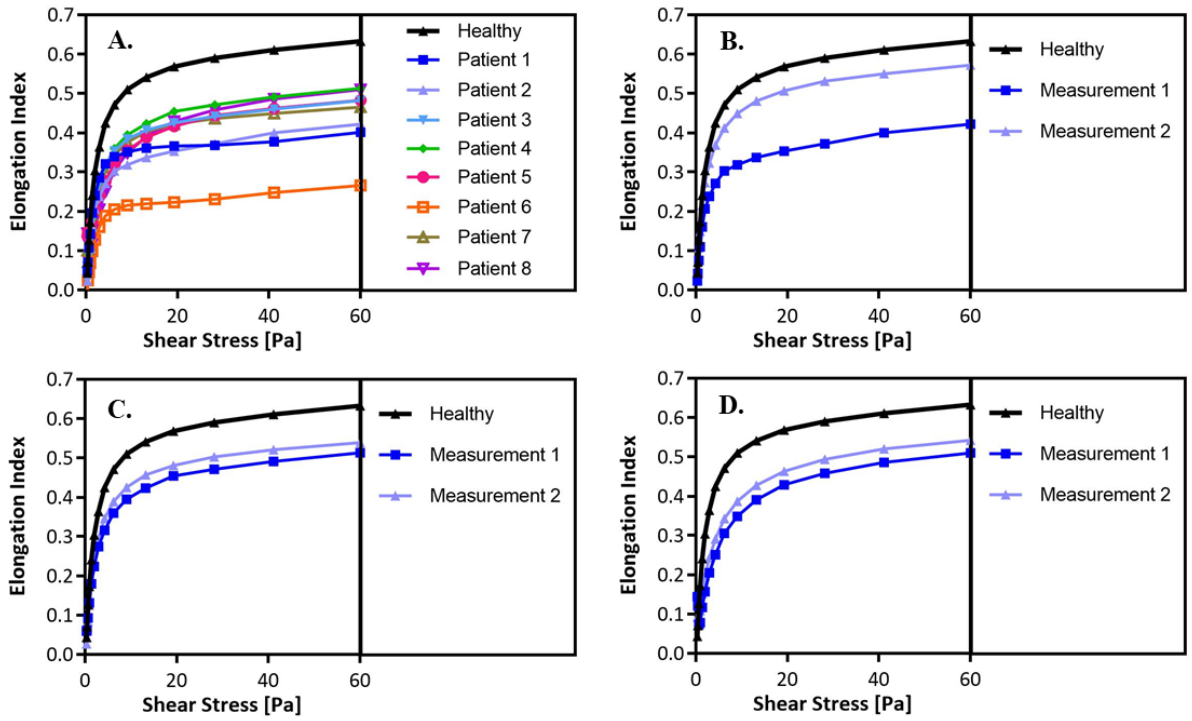

Figure 7.1. Deformability Analysis Via Ektacytometry of Infusion Patients.

Standard ektacytometry deformability analysis at constant osmolality (~290 mOsmol/kg) and variable shear stress. (A) Ektacytometry analysis of all eight infusion patients of PRE-infusion samples. Ektacytometry measurements of PRE-infusion sample denoted as Measurement 1, and POST-infusion sample denoted as Measurement 2 for (B) Patient 2, (C) Patient 4, and (D) Patient 8. All figures include a healthy non-SCD deformability curve for reference.

infusion samples for SCD Patients 2, 4, and 8 shown in Figure 7.1.B., Figure 7.1.C., and Figure 7.1.D. respectively. The pre-infusion measurement is denoted as *Measurement 1*, and the post-infusion analysis is denoted as *Measurement 2*. In all of Figure 7.1. we implement a deformability curve of non-SCD blood samples denoted as *Healthy*. Interestingly, Patient 2 experienced the greatest increase in maximum elongation index value post-infusion climbing from a value of 0.422 to 0.572, Figure 7.1.B. We do not observe a drastic change in post-infusion maximum elongation indices for both Patient 4 and Patient 8, Figure 7.1.C. and Figure 7.1.D. respectively.

Table 7.1. Sickle Cell Disease Infusion Patient Demographics and Blood Profile Information.

Patient	SCD Genotype	Age	Gender	PRE-infusion Hematocrit	POST-infusion Hematocrit	PRE-infusion %S Fraction	POST-infusion %S Fraction	PRE-infusion EIMax	POST-infusion EIMax
#	-	years	(M/F)	%	%	%	%	-	-
1	SS	16	M	31.1	34.2	31.3	24.6	0.401	-
2	SS	21	M	24.2	-	86.6	-	0.422	0.572
3	SS	16	M	24.6	-	34.1	-	0.482	-
4	SS	19	F	23.9	30.5	39.8	29.2	0.513	0.539
5	SS	22	F	32.0	-	44.7	-	0.483	-
6	SS	9	M	24.5	-	17.6	-	0.266	-
7	SS	13	M	33.5	-	21.3	-	0.465	-
8	SC	11	F	29.3	-	33.8	-	0.51	0.542

Table with SCD infusion patient information including SCD genotype, age in years, gender (male or female), pre-infusion hematocrit, post-infusion hematocrit, pre-infusion %HbS fraction, post-infusion %HbS fraction, pre-infusion and post-infusion maximum elongation indices as registered with ektacytometry deformability analysis. Missing therapies indicate the patient was not processed post-infusion therapy administration.

We collect a surplus of pre-infusion SCD blood samples and partition them into multiple 1 mL whole blood pre-infusion aliquots. Leveraging the PPFC model, we perfuse the raw pre-infusion SCD blood samples at a shear rate of 500 s^{-1} and aim to quantify the WBC adhesion density of the pre-infusion condition, Figure 7.2. The endothelial layer is inflamed via exposure to iL-1β approximately four hours before blood perfusion, as described in Chapter 2. We organize

our SCD patients from highest WBC adhesion density to lowest, with Patient 1 registering a ~1,000 WBCs adhered/mm^2 and Patient 8 with ~ 300 WBCs adhered/mm^2. We average all the pre-infusion adhesion densities, ~600 WBCs adhered/mm^2, shown as the AVG bar in Figure 7.2.

We take surplus pre-infusion SCD blood sample aliquots and begin adding RBCs at controlled volumes to increase the hematocrit to the desired percentage. We take fresh, healthy non-SCD donor blood and isolate RBCs. We determine the volume of RBCs to add to the SCD pre-infusion samples using Equation 3 from Chapter 2. Once the aliquot has its hematocrit altered, we perfuse individual samples through the PPFC model at a shear rate of 500 s^{-1} and again quantify the WBC adhesion density onto the inflamed endothelial monolayer. We adjust the hematocrit of SCD blood samples up to a hematocrit of 50%. We are able to collect post-infusion samples from

Table 7.2. Sickle Cell Disease Infusion Patient Complete Blood Count.

Patient	Total WBC	PLT	MCV	Neutrophil	Lymphocyte	Monocyte	Eosinophil	Basophil
#	K/uL	K/uL	fl	%	%	%	%	%
1	15.9	370	90.1	54.9	30.6	10.9	1.8	0.5
2	20.1	228	90.3	41.9	36.5	15.5	4.7	0.8
3	15.8	430	89.2	41.0	12.3	4.0	3.5	0.6
4	19.4	293	93	50.7	28.7	10.1	9.0	0.6
5	11.7	352	89	76.7	11.6	8.8	2.1	0.4
6	17.5	529	90.7	51.7	35.1	10.6	1.5	0.4
7	12.80	427	91.8	51.6	22	13.6	11.5	0.7
8	5.2	262	91.3	47.7	42	8.0	1.3	0.3
Non-SCD	6.5	253	90	50	30	5	2.5	0.75

Table with SCD infusion patient complete blood count information. Complete blood count average for healthy Non-SCD blood sample is shown in the last row.

all eight SCD patients for perfusion studies. Following the individual perfusion of all the hematocrit-adjusted infusion samples, we perfuse the actual post-infusion blood sample from SCD patients. We quantify the WBC adhesion onto the inflamed monolayer as an adhesion density for

all individual patients. From here, we choose to normalize all WBC adhesion densities both in the actual post-infusion sample and in hematocrit adjusted infusion mimicked samples to the actual pre-infusion WBC adhesion density that is shown in Figure 7.2. These results are then represented as a percent change in WBC adhesion compared to the pre-infusion WBC adhesion for each unique SCD patient, Figure 7.3.

For Patient 1, we see a positive percent change in WBC adhesion when the hematocrit was adjusted to ~37%, Figure 7.3.A. Interestingly, when the hematocrit was adjusted further, a negative percent change in WBC adhesion is observed. This pattern is also the case for the patient actual post-infusion sample. For Patient 2, we see a negative percent change in WBC adhesion in the hematocrit adjusted samples, however, the post-infusion sample registered a WBC adhesion density very close to the pre-infusion sample, Figure 7.3.B. This trend was also observed for Patient 5 and Patient 8, Figure 7.3.E. and Figure 7.3.H., respectively. A variable pattern in WBC adhesion is observed for both Patients 3 and 4, Figure 7.3.C. and Figure 7.3.D. respectively. There

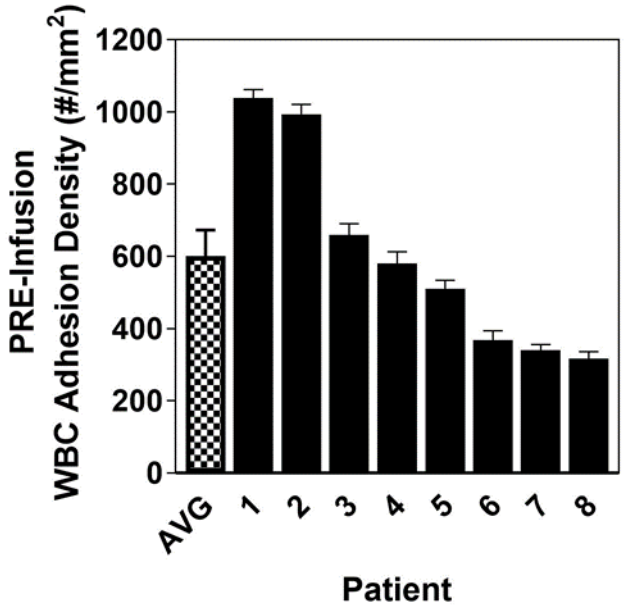

Figure 7.2. White Blood Cell Adhesion Density for Sickle Cell Disease Patients.

Quantified WBC binding to inflamed endothelial layer after 5 min of laminar whole blood flow at a wall shear rate of 500 s^{-1}. The AVG bar denotes the average adhesion density of all patients. Error bars represent standard error for each donor.

was an oscillating-type trend in percent change of WBC adhesion in the hematocrit-adjusted samples in both these cases. Additionally, in both these patients, the actual post-infusion sample had a negative percent change in WBC adhesion than the pre-infusion sample. For Patient 6, we observe a positive percent change in WBC adhesion in both the hematocrit adjusted samples and the post-infusion sample, Figure 7.3.F. More specifically, we see a ~80% increase in WBC a dhesion when the hematocrit is adjusted to ~35%. For Patient 7, we observe a negative percent change in WBC adhesion when the hematocrit is initially adjusted to ~39%. There is a positive percent change in WBC adhesion observed at higher hematocrits and the post-infusion sample, Figure 7.3.G. Overall, Figure 7.3. shows the WBC adhesion density trends upon the artificial hematocrit adjustments. The artificially adjusted hematocrits aim to mimic the infusion process.

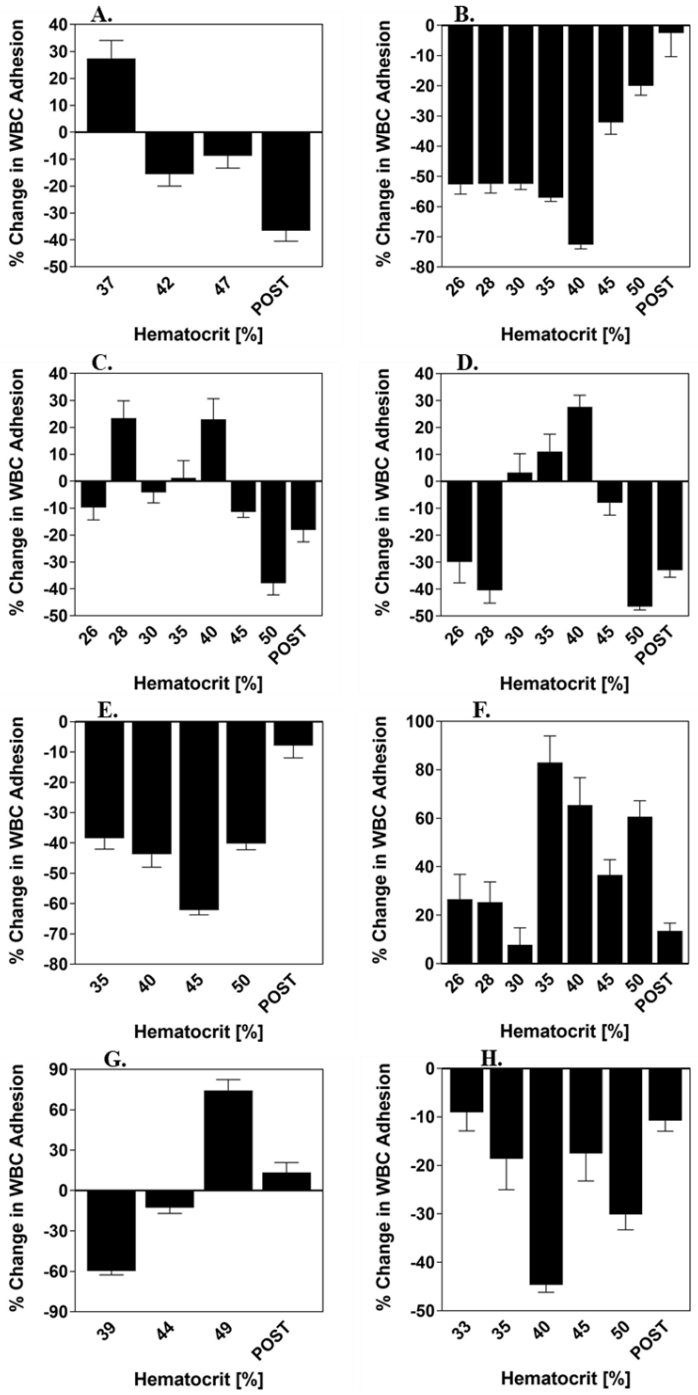

Figure 7.3. Quantified White Blood Cell Binding to an IL-1β Inflamed Endothelial Layer *in vitro* as a Function of Increasing Hematocrit.

Blood samples from SCD patients is adjusted by hematocrit with the controlled addition of healthy non-SCD donor RBCs. Trials are plotted as a change in WBC adhesion compared to the WBC adhesion density in the PRE-infusion condition of each independent donor. Inflammation of the endothelium is induced by exposure to inflammatory cytokine IL-1β for four hours prior to blood perfusion. Quantified WBC binding to an inflamed endothelial layer at a wall shear rate of 500 s^{-1} for SCD Patients (A) 1, (B) 2, (C) 3, (D) 4, (E) 5, (F) 6, (G) 7, (H) 8. Statistical analysis of adherent density was performed using two-way ANOVA to test all WBC adhesion against each individual Patient PRE-infusion condition. No asterisks represent no significant difference found. Error bars represent standard error.

7.5. Discussion

Throughout this dissertation, we have focused on the loss of RBC membrane deformability and any downstream effects of this change as it relates to disease, specifically SCD. One of the most notable characteristics of SCD is the loss of RBC membrane deformability which ultimately leads to systemic issues and overall reduced quality of life in SCD patients.[42,55] One notable impact of increased rigidity in RBCs is increased cell fragility and likelihood to lyse releasing heme into the bloodstream.[177] As a result of increased hemolysis in SCD, higher rates of vascular inflammation are well documented in this disease.[163,170,178,179] This ultimately results in chronic inflammation and increased risk for vaso-occlusion and infection.[55,76,177,180] To combat this ailment, blood transfusions have become standard practice when treating SCD without or combined with a pharmaceutical treatment approach.[62,174–176,181] Standard transfusion practice aims to increase the oxygen transport capacity of patients and reduce the risk for vaso-occlusive crisis, which is done by typically targeting to lower the %HbS to less than 30%.[175] As the %HbS is lowered in the whole blood, reasonably, the fraction of RBCs with a high propensity to be highly rigid is reduced. Standard blood transfusion practices do not take into consideration how these mentioned changes happening upon infusion therapy administration can alter the immune cell adhesion capability to inflammation. Despite the known role of leukocyte adhesion to vascular wall inflammation,[163,182] there is little work that explores the mechanisms of blood flow dynamics and leukocyte adhesion to inflammation as it relates to blood transfusion therapy.

This work presents a microfluidic blood flow model paired with a hematocrit adjustment process that mimics simple blood infusion therapy to examine how blood transfusions impact leukocyte adhesion in SCD. Moreover, we aim to draw attention to immune cell adhesion patterns upon administration of infusion therapy. Ultimately, we aim to uncover any predictive marker that

may help optimize blood transfusion practices to either minimize or maximize leukocyte adhesion to inflammation based on the desired clinical outcome. One of the primary goals of this study is to identify any potential blood characteristic that may determine leukocyte adhesion to inflammation tendencies. Specifically, we take a close look at SCD transfusion patient %HbS or %S fraction, ektacytometry deformability analysis, and CBC for the pre-infusion condition. Due to logistical issues, we could make these same analyses for the actual post-infusion samples for only a subset of the eight SCD patients examined in this study. We analyze the WBC adhesion density onto an inflamed endothelial layer in a microfluidic model for all eight patients.

We take a look back at the WBC adhesion density to an inflamed vascular wall of healthy non-SCD donor blood presented in Chapter 3, Figure 3.3.B. Although, the data from Figure 3.3. was obtained via blood perfusion in a ~254 μm channel; Chapter 3 also concludes that there was no significant difference in WBC adhesion to inflammation between ~127 μm and ~254 μm channel heights.[10] The endothelial monolayers were prepared and inflamed using the identical methodology to the one presented in this chapter. The approximate average WBC adhesion density to inflammation at a WSR of ~500 s^{-1} is ~1,300 WBCs/mm^2. Although the absolute WBC counts for the whole blood utilized in these experiments were not quantified, we make the deduction that they are likely to be close to the average CBC counts for healthy non-SCD blood donors, shown in Table 7.2., the value of the total WBC count is ~6.5 K/μL. With these assumptions made, we can approximate the WBC adhesion binding efficiency by dividing the WBC adhesion density by the total number of WBCs present in the blood sample perfused; this ratio is then multiplied by a scaling factor of 10^6. We opted to make this comparison so we can normalize across variable total WBC concentrations across blood samples. Using the parameters stated above, blood perfusion for ~5 minutes at a WSR of 500 s^{-1} in a channel height of 254 μm requires ~4 mL of whole blood

with a total WBC concentration of ~ 6.5 K/μL, if the WBC adhesion density is ~1,300 WBC/mm^2, then the WBC binding efficiency for healthy non-SCD donors is ~50 WBCs bound/mm^2/WBCs fed x 10^6. We perform a similar calculation across the eight SCD pre-infusion samples and result in an average WBC binding efficiency of ~40 WBCs bound/mm^2/WBCs fed x 10^6. This comparison again highlights the fact that having a greater WBC concentration does not necessarily translate to a greater adhesion density. On average, our eight SCD donors have a total WBC count about 2.3x fold times larger than a healthy non-SCD blood donor.

One major shortcoming of this investigation was forgoing leukocyte adhesion ligand profile characterization of our SCD donors. As shown in Chapter 6, the WBC adhesion ligand profiles of SCD patients differ greatly from healthy non-SCD donor WBCs, resembling a pre-activated state with overexpression of ligand MAC-1 and under-expression of L-Selectin, Figure 6.1. Total WBC composition did not differ greatly in our SCD infusion patients and average healthy non-SCD donors, Table 7.2. Roughly 50% of leukocytes present are neutrophils, 30% are lymphocytes, and 10% are monocytes. The remainder is made up of smaller fractions of eosinophils and basophils. Given these similarities in leukocyte fractional compositions, it is likely that the differences in WBCs density between healthy non-SCD donors and the eight pre-infusion SCD patients, Figure 7.2., is a result of differences in the WBC adhesion ligand profiles.

Patient 2 is notably a compelling case, given that they registered the highest %S fraction in our patient pool, ~86.6%. The pre-infusion RBC deformability analysis of Patient 2 was not abnormal for a HbSS genotype SCD patient, registering a maximum elongation index of 0.422. Patient 2 was one of the patients for whom we could analyze their post-infusion blood sample with ektacytometry. Notably, Patient 2 recorded a maximum elongation index of 0.572, which is a notable improvement in whole blood deformability, Figure 7.1.B. Upon examining WBC adhesion

with the hematocrit adjustment, we found a negative percent change in WBC adhesion for all hematocrits examined. However, the actual post-infusion sample did not exhibit a WBC adhesion density that was notably different from the WBC adhesion density of the pre-infusion sample. We observe similar trends for Patient 5 and Patient 8 but cannot identify any correlation in pre-infusion blood characteristics that could predict these outcomes in WBC adhesion density.

Another notable case is that of Patient 6, who registered the lowest %S fraction, ~17.6%. However, Patient 6 also registered the lowest whole blood deformability amongst all SCD infusion patients, with a maximum elongation index of 0.266. Based on the work presented in Chapter 4, we can deduce that the rigid RBC population or %S fraction, in this patient has a relatively high degree of stiffness, given that there is a small %S fraction, but also a considerably low deformability elongation index. When examining the effects of hematocrit adjustment with Patient 6, we find increasing the hematocrit using the infusion mimicking methodology that there was always a positive percent change in WBC adhesion density, Figure 7.3.F. This result suggests that for this patient, infusion therapy will likely increase WBC adhesion density.

Patients 1, 3, 4, and 7 all are notable cases because they exhibit an oscillating-type trend in percent change in WBC adhesion density upon hematocrit adjustment. Both Patient 3 and Patient 4 recorded a typical %S fraction of 34.1% and 39.8%, respectively. Patient 1 and Patient 7 recorded a %S fraction of 31.1% and 33.5%, respectively. The ektacytometry whole blood elongation analysis did not reveal an abnormally low RBC deformability, both Patient 3 and Patient 4 registering maximum elongation indices ~0.50, Table 7.1., and Patient 1 and Patient 7 registering maximum elongation indices ~0.43.

Variation across samples is a confounding factor that makes it challenging to identify a clear cause for the observations made in this infusion therapy mimicking study. There is

undeniable evidence that hematocrit is a major factor in determining leukocyte adhesion. This thesis also shows that leukocyte adhesion patterns to the vascular wall are affected by the fraction of rigid RBCs, or %S fraction, present in the whole blood. Unfortunately, for logistical reasons, we could not collect a complete detailed data set for all SCD infusion patients that include both pre-infusion and post-infusion hematocrit, %S fraction, and ektacytometry elongation index analyses. Drawing definitive conclusions from the WBC adhesion assays performed in this study is difficult without statistical power. Due to SCD blood donor availability and, in general, the nature of sample variation, we performed only one experiment per patient and hematocrit point, n=1. Although a difference in WBC adhesion magnitude change is observed, there is no statistical difference in WBC adhesion detected. This problem is a limitation of the results presented in this chapter.

7.6. Conclusions

To our knowledge, this is the first study that directly investigates how WBC adhesion to inflammation is altered upon administration of blood transfusion therapy in SCD. It may be difficult to draw definitive conclusions from these preliminary results. However, it is evident that leukocyte adhesion is changed notably upon the administration of infusion therapy. Moreover, we observed a unique change in WBC adhesion trends for each individual SCD infusion patient examined in this study. This observation serves as evidence of a very patient-specific leukocyte adhesion response to infusion therapy. These preliminary findings highlight the need to probe further the biophysical interplay between rigid RBCs, leukocyte adhesion to vascular inflammation, and infusion therapy. Such insights could prove invaluable in providing guidelines for optimizing blood transfusion practices and increasing the efficacy of this prevalent therapy in

relation to immune cell functionality and SCD pathogenesis. Additionally, insights could aid in the development of novel tools for SCD management.

Chapter 8 : Vascular-Targeted Particle Efficacy in the Presence of Rigid Red Blood Cells: Implications for Performance in Diseased Blood

8.1. Publication Information

The work presented in this chapter is published as: Mario Gutierrez, Lauro Sebastian Ojeda, and Omolola Eniola-Adefeso. "Vascular-targeted particle efficacy in the presence of rigid red blood cells: Implications for performance in diseased blood." Biomicrofluidics 12.4 (2018): 042217. [12]

Modifications have been made to the published document to adapt the content to this text. The goal of this chapter is to probe how model drug particle adhesion to inflammation is impacted in the presence of rigid red blood cells in an *in vitro* model of blood flow.

8.2. Abstract

The field of drug delivery has taken an interest in combating numerous blood and heart diseases via the use of injectable vascular-targeted carriers. However, vascular-targeted carrier technology has encountered limited efficacy due to a variety of challenges associated with the immense complexity of *in vivo* blood flow environment, including the hemodynamic interactions of blood cells that impact their margination and adhesion to the vascular wall. RBC physiology, i.e., size, shape, and deformability, drive cellular distribution in blood flow and has been shown to

impact VTC margination to the vessel wall significantly. RBC shape and deformability are altered in certain human diseases, yet little experimental work has been conducted to understand the effect of these alterations, specifically RBC rigidity, on VTC dynamics in physiological blood flow. In this work, we investigate the impact of RBCs of varying stiffness on the adhesion efficacy of particles of various size, modulus, and shape onto an inflamed endothelial layer in a human vasculature-inspired, *in vitro* blood flow model. The rigid RBC compositions and degrees of RBC stiffness evaluated are analogous to conditions in diseases such as sickle cell disease. We find that particles of different size, modulus, and shape yield drastically different adhesion patterns in blood flow in the presence of rigid RBCs when compared to 100% healthy RBCs. Specifically, up to 50% reduction in the localization and adhesion of non-deformable 2 μm particles to the vessel wall was observed in the presence of rigid RBCs. Interestingly, deformable 2 μm particles showed enhanced vessel wall localization and adhesion, by up to 85%, depending on the rigidity of RBCs evaluated. Ultimately, this work experimentally clarifies the importance of considering RBC rigidity in the intelligent design of particle therapeutics and highlights possible implications for a wide range of diseases relating to RBC deformability.

8.3. Introduction

As discussed in previous chapters, blood is a highly concentrated non-Newtonian suspension of RBCs, WBCs, platelets, and plasma. [13] The high deformability of RBCs is a unique characteristic that significantly influences particle margination in blood flow. [92–95] In particular, the deformable RBCs are vastly susceptible to experiencing a lift force, which causes them to migrate away from the vessel wall and localize in the radial center of the vessel as blood flows. [28,38,93,96] Particle-RBC collisions in the core of the vessel then promote the migration of particles

towards the vessel wall. [38,92] It is known that particle size is a critical factor that determines the margination efficacy of particle therapeutics. [109,112,183–186] In particular, work done by Charoenphol *et al*. indicates that spherical microparticles (MPs) best marginate to the vascular wall, and nanometer-sized VTCs exhibit less efficient margination. [108,113] Namdee *et al*. attribute this reduced margination to spherical nanoparticles (NPs) getting trapped in the RBC core. [112] Once out of the RBC core, the near-absolute absence of RBCs near the vessel wall, i.e., CFL, allows the proper binding of particles to the vessel wall. [38,92] Given the importance of RBC deformability in the margination of particles and hence their adhesion to the vascular, any alteration in RBC flexibility, as found in certain human diseases, [3,97] would undoubtedly affect particle margination and adhesion.

To date, despite a vast number of computational and experimental studies that have examined RBC and particle margination in blood flow, there is no investigation into how changes in RBC deformability impact particle margination and, hence, binding efficacy. Thus, the work presented in this chapter experimentally probes the direct impact of rigidified RBCs on the adhesion dynamics of particles in blood flows via *in vitro* assays in a PPFC. We report that particle adhesion in human blood flow can be significantly reduced or improved depending on the particle modulus, shape, and size, where being deformable can lead to a positive impact of rigid RBCs on particle adhesion. We believe this proposed work is the first comprehensive, experimental investigation into how rigidified RBCs affect the ability of VTCs to marginate and adhere to the vascular wall. The knowledge presented is of importance as it can provide opportunities for developing new therapeutics with high efficacy in human diseases.

8.4. Results

8.4.1. Effect of Rigid RBCs on 2 µm Stiff Polystyrene Particles as a function of RBC Rigidity

We began by examining how the presence of rigidified RBCs affects the adhesion of 2 µm "rigid" polystyrene MPs to an activated HUVEC layer in whole blood flow. We tested a range of RBC rigidities (9x, 4x, and 2x times more rigid than healthy RBCs) and at different concentrations (20%, 30%, 50%, 70%, 90%, and 100%) of rigid RBCs in the blood. Polystyrene spheres were used as a proxy for biodegradable polymeric particle carriers. As previously described, the 2 µm PS spheres were functionalized with biotinylated sLe^a at ~1,000 sLe^a site/μm^2 and introduced into whole blood samples at a concentration of ~10^6 particles/mL of blood.[106,113] RBCs 9x more rigid than healthy RBCs are presented as the *highly rigid* condition, ones that were 4x more rigid presented as *moderately rigid*, and RBCs 2x more rigid are labeled as *slightly rigid*. The EIs produced by the 0.75 mM and 0.5 mM TBHP treatments are of particular interest due to their pathological relevancy; the rigidities of RBCs in SCD patients in stable condition and SCD patients in crisis closely resembles the RBC rigidities generated with 0.5 mM and 0.75 mM TBHP, respectively.[10,121] Also, it is known that patients can have different fractions (percentages) of rigidified RBCs present in their whole blood.[10,121]

Figure 8.1. shows the impact of RBC rigidity on particle adhesion to the vessel wall as a function of RBC stiffness in a 127 µm height channel. The data is represented as the fraction reduction in particle adhesion in rigid RBC conditions relative to the adhesion of the same particles in a healthy condition, i.e., no rigid RBC present, to eliminate donor-to-donor variations. The raw adhesion density for the healthy condition represented in Figure 8.1. is shown in Figure 8.2. We show in Figure 8.1. that the presence of rigid RBCs in the blood flow produces a reduction in the adhesion of 2 µm PS MPs relative to the binding found in the healthy control regardless of the

RBC stiffness and percentage of rigid RBCs present. For assays with *highly rigid* RBCs, a maximum reduction (~50%, $p<0.01$) in the adhesion of the PS MPs occurred when 20% of the total RBCs present were rigidified (Figure 8.1.A.). As we increased the percentage of the rigid RBCs in the blood sample, there was a slight decrease in the adhesion reduction to ~25% lower than adhesion in the healthy control. However, the reduction in MP adhesion beyond the 30% rigid RBC in flow mark was not significant; i.e., PS MP adhesion in blood with *highly rigid* RBCs was not statistically different from adhesion in healthy conditions. Figure 8.1.B. shows a plot of the trend in 2 µm PS particle adhesion reduction for the case *where moderately* rigid RBCs were present in the blood flow. Here, we show a non-linear relationship between adhesion reduction and the percent of rigid RBCs present in the blood. Initially, the decrease in MP adhesion increased as the percentage of rigid RBCs in the blood increased up to the 50% mark, corresponding to the highest adhesion reduction (~52%, $p<0.01$). As the percentage of rigid RBCs in the blood increased beyond the 50%, the decrease in MP adhesion was reduced. At 100% *moderately rigid*

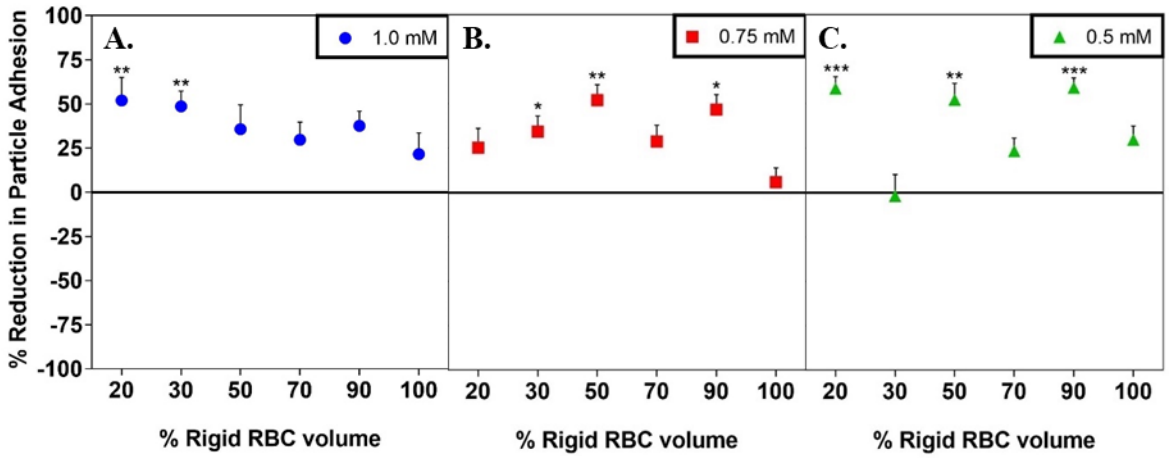

Figure 8.1. The Adhesion of 2 µm Polystyrene Particle to Inflamed Endothelium *in vitro* by Red Blood Cell Rigidity.

Quantified 2 µm polystyrene particle binding to an IL-1β inflamed endothelial layer at 10^6 particles/mL of whole blood as a function of rigid RBCs present, i.e., % volume rigid RBC, each figure utilized rigid RBCs with different degrees of rigidity (A) 1.0 mM treated RBCs (highly rigid), (B) 0.75 mM treated RBCs (moderately rigid), and (C) 0.5 mM treated RBCs (slightly rigid). A WSR of 1,000 s^{-1} was used for all the shown conditions. Polystyrene particles are conjugated with NeutrAvidin and functionalized with sLe^a binding ligand, ~1,000 sites/μm^2. All trials plotted as reduction compared to respective healthy controls, i.e., no rigid RBCs present, thus eliminating donor variation. Error bars represent standard error. Statistical analysis of adherent density was performed using two-way ANOVA to test all particle adhesion versus healthy particle adhesion control. (*) indicates $p<0.05$, (**) indicates $p<0.01$, and (***) indicates $p<0.001$.

RBCs present in the flow, no difference in particle adhesion was observed relative to the binding in the healthy condition. Interestingly, there was no particular trend in the impact of the *slightly rigid* RBCs on the adhesion of the *2* µm PS MP as the percentage of rigid RBCs is increased (Figure 8.1.C.). Instead, we observed the highest reduction in adhesion (~58%, $p<0.001$) when

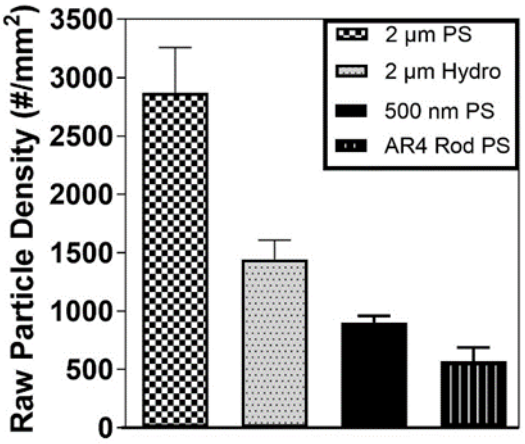

Figure 8.2. Raw Particle Binding to Inflamed Endothelium *in vitro*.

Quantified particle binding to an IL-1β inflamed endothelial layer at 10^6 particles/mL of whole blood at healthy conditions, i.e., no rigid RBCs are present. Blood is at 40% hematocrit and is perfused at a WSR of 1,000 s^{-1} for all the shown conditions. All particle types are conjugated with NeutrAvidin and functionalized with sLe^a binding ligand, ~1,000 sites/µm^2. Error bars represent standard error.

20%, 50%, and 90% of total RBCs present were slightly rigid. Conversely, there was a negligible reduction in MP adhesion when 30% of RBCs present are rigidified. At 70% and 100% of the *slightly rigid* RBCs present, the adhesion of the 2 µm PS MPs was reduced by ~25%, which was not significant from the healthy condition.

8.4.2. Effect of Rigid RBCs on 2 µm Deformable Hydrogel Particles as a function of RBC Rigidity

To evaluate the impact of particle deformability on the dynamics of adhesion in the presence of rigid RBCs, we fabricated 2 µm hydrogel (PEG-based) particles (PEG-MP) and

modulated the cross-linking density to achieve particle deformability similar to the deformability reported for WBCs(~113 kPa, Young's Modulus).[114] The PEG-MPs were conjugated with sLe^a at ~1,000 sLe^a site/μm^2, similar to polystyrene MPs. Figure 8.3.A. shows the percent difference in the adhesion of the 2 µm PEG-MP in the presence of the *highly rigid* RBCs relative to the healthy

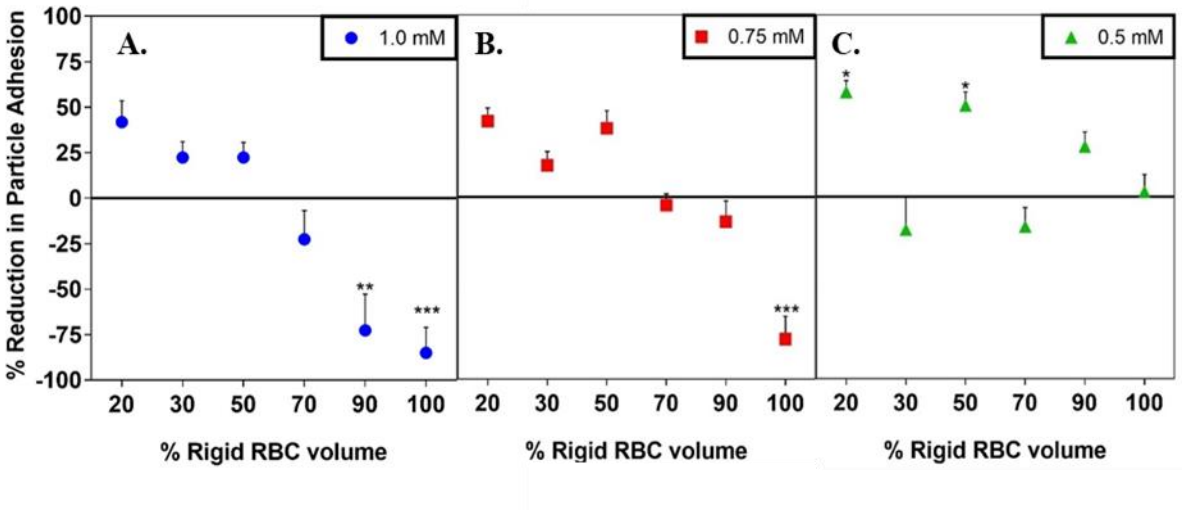

Figure 8.3. The Adhesion of 2 µm Hydrogel Particle to Inflamed Endothelium *in vitro* by Red Blood Cell Rigidity.

Quantified 2 µm hydrogel particle binding to an IL-1β inflamed endothelial layer at 10^6 particles/mL of whole blood as a function of rigid RBCs present, i.e., % volume rigid RBC, each figure utilized rigid RBCs with different degrees of rigidity (A) 1.0 mM treated RBCs (highly rigid), (B) 0.75 mM treated RBCs (moderately rigid), and (C) 0.5 mM treated RBCs (slightly rigid). A WSR of 1,000 s^{-1} was used for all the shown conditions. Hydrogel particles are conjugated with NeutrAvidin and functionalized with sLe^a binding ligand, ~1,000 sites/μm^2. All trials plotted as reduction compared to respective healthy controls, i.e., no rigid RBCs present, thus eliminating donor variation. Error bars represent standard error. Statistical analysis of adherent density was performed using two-way ANOVA to test all particle adhesion versus healthy particle adhesion control. (*) indicates $p<0.05$, (**) indicates $p<0.01$, and (***) indicates $p<0.001$.

condition. At the lowest concentration of *highly rigid* RBCs, e.g., 20%, we observed a slight reduction in the adhesion of 2 µm PEG-MP, which represents the maximum adhesion reduction seen for this particle type across all rigid RBCs concentrations similar to the observation with the non-deformable polystyrene MPs. Interestingly, when the level of rigid RBCs present is increased, the reduction in hydrogel particle adhesion relative to healthy condition decreased linearly. A negative percent reduction in PEG-MP adhesion is present beyond 50% *highly rigid* RBCs in the blood, which translates to a raw particle adhesion that is higher than the level achieved in a healthy blood flow condition. Surprisingly, when 100% of the RBCs present are rigidified, we observe an

adhesion reduction of -85% ($p<0.001$), i.e., nearly twice the adhesion density of PEG-MPs that was found as compared to the healthy condition. A visual representation of the enhanced 2 µm PEG-MP adhesion to the endothelial layer is presented in Figure 8.4. When examining the impact of the *moderately rigid* RBCs, we observe a similar trend to the one seen for the *highly rigid ones*. At low percentages of the *moderately rigid* RBCs present in blood flow, a slight reduction in adhesion was observed for the PEG MPs relative to the healthy condition. As the percentage of rigid RBCs present increased, the particle adhesion improved towards similar values as obtained for the healthy condition. However, unlike the *highly rigid* RBCs case, an enhanced PEG-MP adhesion relative to the healthy condition was only observed at 100% *moderately rigid* RBCs present in flow, ~-78% ($p<0.001$). Finally, when we examine the adhesion of the PEG-MP in the presence of the *slightly rigid* RBCs, we saw a similar oscillate-trend as was observed for polystyrene MPs in Figure 8.1.C. A reduction in particle adhesion occurred when 20%, 50%, and

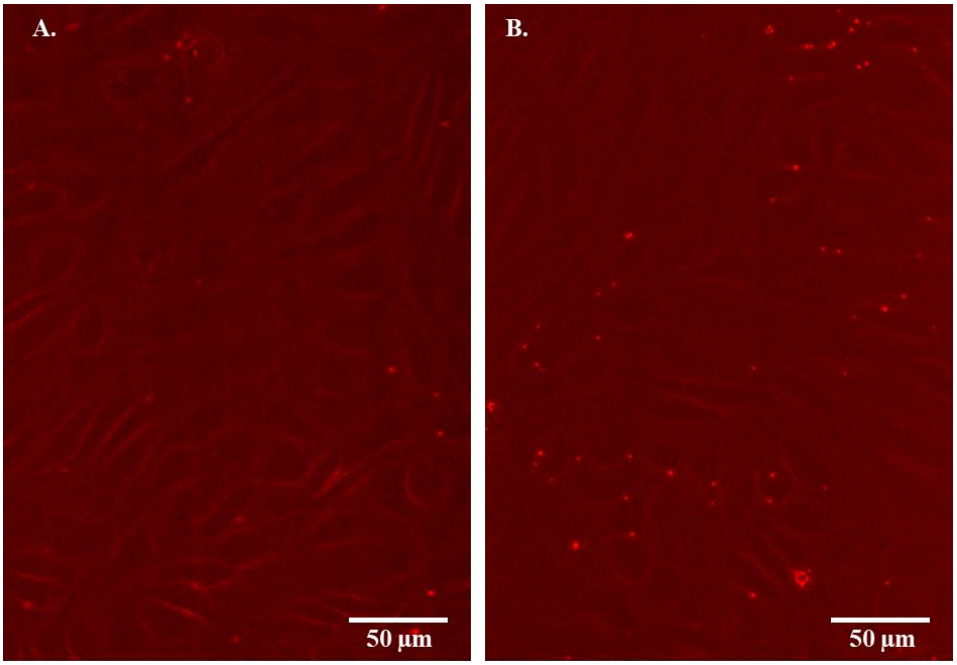

Figure 8.4. Hydrogel 2 µm Particle Binding on Confluent Monolayer of HUVEC.

Fluorescent rhodamine images of hydrogel particles adhered to HUVEC while blood is perfused at a WSR of 1,000 s^{-1}. (A) shows condition with healthy blood, i.e., no rigid RBCs present. (B) shows condition with 100% rigid RBCs treated with 1.0 mM TBHP present.

90% of the RBCs present were rigid. When 30%, 70%, and 100% of the RBCs present were rigid, no difference in 2 µm hydrogel particle adhesion was observed compared to particle adhesion in the healthy condition.

8.4.3. Effect of Rigid RBCs on rigid 500 nm Polystyrene Particles as a function of RBC Rigidity

Given the significant impact of rigid RBCs on adhesion patterns observed for MPs, we investigated the adhesion performance of rigid polystyrene NPs, which are typically proposed for drug delivery applications. Here, we used 500 nm-sized polystyrene particles and functionalized them with sLe^a as described with MPs. We have previously demonstrated that spherical nanoparticles between 100 – 500 nm show the same margination and adhesion patterns in human blood flow. [108,113] Again, the adhesion of the 500 nm polystyrene NPs in blood flow with rigidified RBCs is presented relative to adhesion in a healthy condition. Figure 8.2. shows the raw particle adhesion density for 500 nm polystyrene particles at a WSR of 1,000 s^{-1} (~900 #/mm^2), which was lower than the adhesion observed for polystyrene MPs in line with previous works.[113] As shown in Figure 8.5., rigidified RBCs in blood did not have any significant impact on the adhesion of PS NPs regardless of the level of RBC rigidity. Also, no specific particle adhesion reduction trend was visible when the percentage of rigid RBCs was varied.

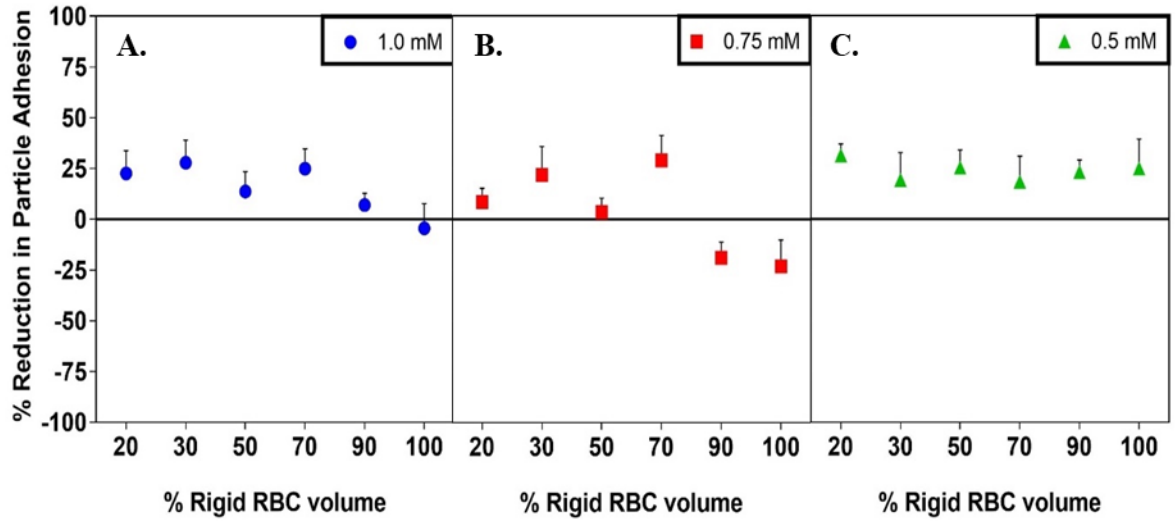

Figure 8.5. The Adhesion of 500 nm Polystyrene Particles to Inflamed Endothelium *in vitro* by Red Blood Cell Rigidity.

Quantified 500 nm polystyrene particle binding to an IL-1β inflamed endothelial layer at 10^6 particles/mL of whole blood as a function of rigid RBCs present, i.e., % volume rigid RBC, each figure utilized rigid RBCs with different degrees of rigidity (A) 1.0 mM treated RBCs (highly rigid), (B) 0.75 mM treated RBCs (moderately rigid), and (C) 0.5 mM treated RBCs (slightly rigid. A WSR of 1,000 s^{-1} was used for all the shown conditions. Polystyrene particles are conjugated with NeutrAvidin and functionalized with sLe^a binding ligand, ~1,000 sites/μm^2. All trials plotted as reduction compared to respective healthy controls, i.e., no rigid RBCs present, thus eliminating donor variation. Error bars represent standard error. Statistical analysis of adherent density was performed using two-way ANOVA to test all particle adhesion versus healthy particle adhesion control. (*) indicates $p<0.05$, (**) indicates $p<0.01$, and (***) indicates $p<0.001$.

8.4.4. Effect of Rigid RBCs on rigid Ellipsoidal Polystyrene Particles as a function of RBC Rigidity

We also investigated the adhesion performance of non-spherical particles in whole blood containing rigidified RBCs due to prior interest in the use of such particles in cellular targeting and drug delivery. Previous reports show that non-spherical, specifically rods, particles can exhibit better adhesion capabilities when compared to spherical counterparts. [183,184,186–188] Here, we use polystyrene rod particles that were generated from heat-stretching of 2 µm spherical particles to an aspect ratio of 4 (AR4). Figure 8.6. shows the adhesion reduction trends for sLe^a-coated rods in the presence of rigid RBCs across the different levels of rigidity evaluated. The raw rod particle adhesion density in normal blood at a WSR of 1,000 s^{-1} is shown in Fig S1. Interestingly, negligible

differences in adhesion were observed for most blood flow conditions, with the exception being rods in blood with 100% *highly rigid* RBCs (Figure 8.6.A.). Here, the level of rod particle adhesion reduction was ~-50% ($p<0.05$), which translates to a 50% greater rod adhesion density compared to their adhesion when no rigid RBCs were present. While the rod particle exhibited negative reductions for other conditions with the *highly rigid* RBCs, these were not significant relative to the healthy condition.

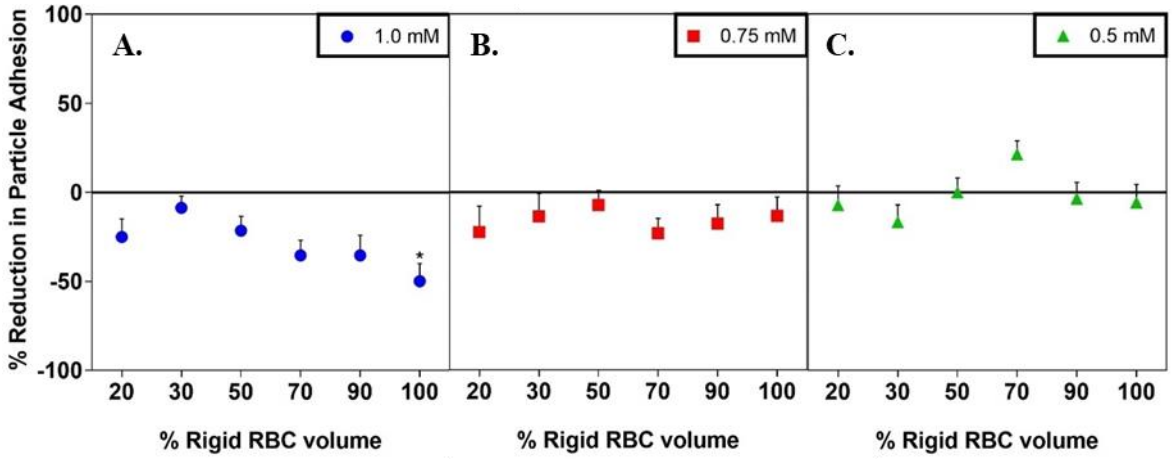

Figure 8.6. The Adhesion of 2 µm Volume Polystyrene Rod (AR4) Particles to an Inflamed Endothelium *in vitro* by Red Blood Cell Rigidity.

Quantified AR4 rod polystyrene particle binding to an IL-1β inflamed endothelial layer at 10^6 particles/mL of whole blood as a function of rigid RBCs present, i.e., % volume rigid RBC, each figure utilized rigid RBCs with different degrees of rigidity (A) 1.0 mM treated RBCs (highly rigid), (B) 0.75 mM treated RBCs (moderately rigid), and (C) 0.5 mM treated RBCs (slightly rigid). A WSR of 1,000 s^{-1} was used for all the shown conditions. AR4 polystyrene rod particles are conjugated with NeutrAvidin and functionalized with sLe^a binding ligand, ~1,000 sites/µm^2. All trials plotted as reduction compared to respective healthy controls, i.e., no rigid RBCs present, thus eliminating donor variation. Error bars represent standard error. Statistical analysis of adherent density was performed using two-way ANOVA to test all particle adhesion versus healthy particle adhesion control. (*) indicates $p<0.05$.

8.4.5. Effect of Targeting Ligand Density on Particle Adhesion Trends

With the understanding that particle adhesion in flow is a function of the receptor-ligand kinetics, which can vary with the targeting ligand density, we evaluated the particle adhesion at a higher targeting ligand density and whether this increase would significantly alter the trend for the impact of rigid RBCs observed at the lower site density. The experimental conditions in Figure

8.1.A. and Figure 8.3.A. were repeated but with MPs at three times the sLe^a density using the most rigid RBCs (1.0 mM TBHP).

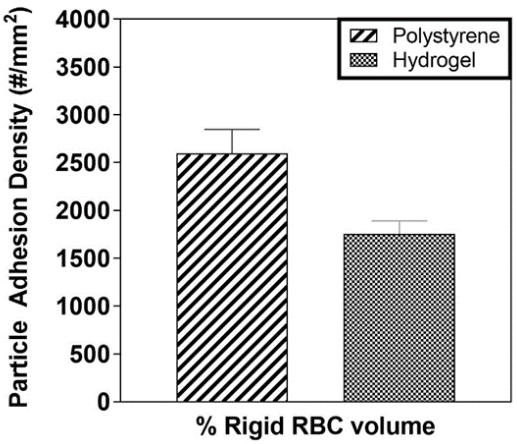

Figure 8.7. Raw Particle Binding to Inflamed Endothelium *in vitro* at Higher Adhesion Ligand Density.

Quantified particle binding to an IL-1β inflamed endothelial layer at 10^6 particles/mL of whole blood at healthy conditions, i.e., no rigid RBCs are present. Blood is at 40% hematocrit and is perfused at a WSR of 1,000 s^{-1} for all the shown conditions. All particle types are conjugated with NeutrAvidin and functionalized with sLe^a binding ligand, ~3,000 sites/μm^2. Error bars represent standard error.

We focus on only the 2 μm spheres for these assays, given that minimal differences in adhesion were observed across all rigid RBCs for the smaller spheres and rods. The raw adhesion data for particles in healthy blood (0% rigid RBCs) is shown in Figure 8.7. Our results show that the particle adhesion reduction trends for both polystyrene and hydrogel 2 μm MPs at the higher density of 3,000 sites/μm^2 are similar to the adhesion trends observed with particles at the lower site density of 1,000 sites/μm^2 for all, but one of the tested conditions (Figure 8.8.). The higher site density only significantly alters the particle adhesion difference for the hydrogel MPs at the 70% rigid RBCs composition, where the adhesion level at the 3,000 sites/μm^2 density did not change with or without rigid RBCs present, contrary to the positive response observed with rigid RBCs at the 1000 sites/μm^2. Also, the particle adhesion levels are only slightly higher with the 3,000 sites/μm^2 sLe^a density for the hydrogel, and not the polystyrene, MPs (Figure 8.7.),

suggesting the adhesion kinetics is in a transport-limited regime for both ligand site densities evaluated. [113]

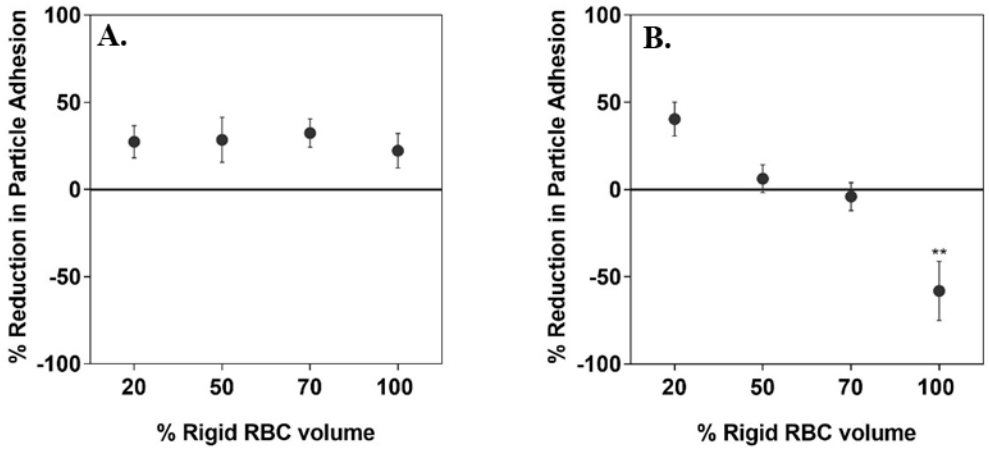

Figure 8.8. The Adhesion of 2 µm Particles with Different Binding Ligand Densities to Inflamed Endothelium *in vitro* by Red Blood Cell Rigidity.

Quantified 2 µm (A) polystyrene and (B) hydrogel particle binding to an IL-1β inflamed endothelial layer at 10^6 particles/mL of whole blood as a function of rigid RBCs present, i.e., % volume rigid RBC, each figure utilized rigid RBCs 9x more rigid than healthy RBCs, i.e., treated with 1.0 mM TBHP. A WSR of 1,000 s^{-1} was used for all the shown conditions. Polystyrene and hydrogel particles are conjugated with NeutrAvidin and functionalized with sLe^a binding ligand with either ~3,000 or ~1,000 sites/µm^2. All trials plotted as reduction compared to respective healthy controls, i.e., no rigid RBCs present, thus eliminating donor variation. Error bars represent standard error. Statistical analysis of adherent density was performed using two-way ANOVA to test all particle adhesion between both sLe^a ligand densities, ~3,000 and ~1,000 sites/µm2. (*) indicates $p<0.05$, (**) indicates $p<0.01$.

8.4.6. Effect of Rigid RBCs on Particle Localization

To better understand how the particle adhesion trends presented above develop in the presence of rigid RBCs, we investigated particle localization to the cell-free layer in whole blood flow. We examined the localization of 2 µm PS, 2 µm PEG-MP, and 500 nm PS particles by first mixing non-functionalized particles into reconstituted (~40% Hct) whole blood with varying rigid RBC conditions at a concentration of ~10^6 particles/mL of whole blood. The blood sample was perfused through a ~100 µm channel (no HUVEC present) at a WSR of ~1,000 s^{-1}, and a confocal microscope was used to image particle density in the CFL at about 2 µm from the vessel wall. The CFL has been reported to range from 2-7 µm in humans depending on variables such as hematocrit,

vessel geometry, and flow rates. [47,189–191] Given the particle sizes examined in this study, 500 nm – 2 µm diameter, focusing on the plane 2 µm from the vessel wall can provide a good indicator of whether the particles of interest were able to exit the bulk flow and localize near the wall, i.e., a good indicator of successful margination.

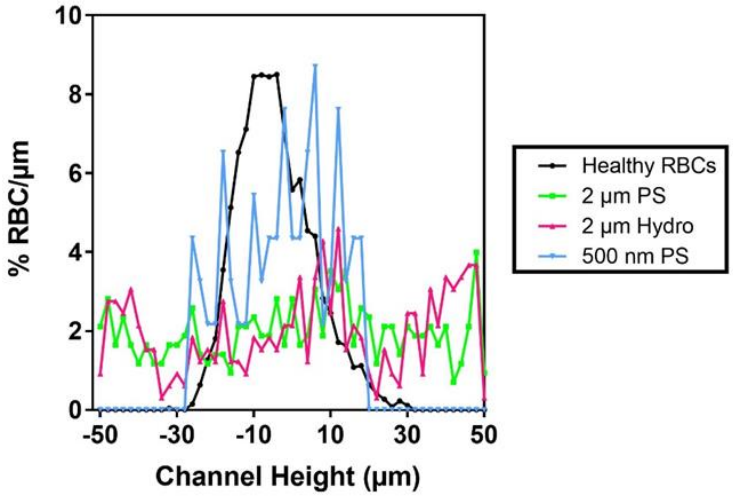

Figure 8.9. Confocal Particle Distributions.

Particle density distributions in a channel of height 100 µm at 1,000 s^{-1}. Condition applicable for all particle types is 40% hematocrit with 100% rigid RBC volume present. Rigid RBCs used for all conditions are 9x more rigid than regular RBCs, i.e., treated with 1.0 mM TBHP. Density distribution of fluorescently tagged (wheat germ agglutinin 488) healthy RBCs is overlaid (black curve) to compare with particle density distributions.

A full scan of the channel height is represented as a distribution in Figure 8.9. We normalized the particle localization density in all conditions where rigid RBCs were present to the particle localization density for the healthy condition. Figure 8.10.A. shows the raw particle localization density for all particles in healthy conditions. Figure 8.10.B. shows the percent change in localization density of 2 µm polystyrene in the presence of rigid RBCs. For most conditions where rigid RBCs were present, we observed a significant decrease in the localization of 2 µm PS particles to the CFL in the presence of the *highly* and *moderately* rigid RBCs. Conversely, Figure 8.10.C. shows that the percent change in the localization of 2 µm PEG MPs dramatically increased

compared to localization in a healthy blood condition when a high amount of the *highly* and *moderately* rigid RBCs were present (70% and 100%).

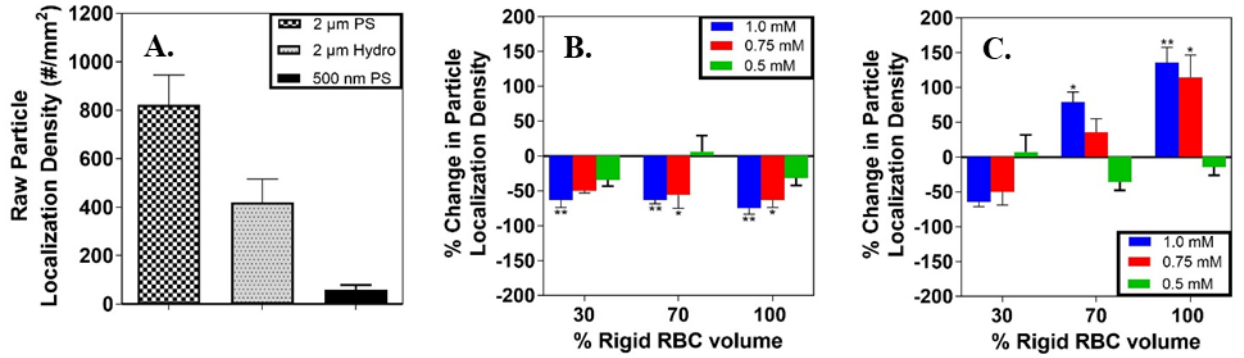

Figure 8.10. Particle Localization to Cell Free Layer in the Presence of Rigid Red Blood Cells.

Quantified particle localization densities 2 µm away from vessel wall in a channel of height ~100 µm at ~1,000 s^{-1} and ~10^6 particles/mL of whole blood as a function of rigid RBCs present, i.e., % volume rigid RBC, and rigid RBCs with different degrees of rigidity, 1.0 mM (highly rigid), 0.75 mM (moderately rigid), and 0.5 mM treated RBCs (slightly rigid). (A) The raw particle localization density in a healthy control, i.e., with no rigid RBCs present. The normalized percent change in particle localization for varying rigid RBC conditions for the (B) 2 µm stiff polystyrene spheres and (C) 2 µm deformable hydrogel spheres. All particles are not functionalized with a targeting ligand. Error bars represent standard error. Statistical analysis of localization density was performed using two-way ANOVA to test particle localization density in rigid RBC conditions compared to healthy control, i.e., no rigid RBCs present. (*) indicates $p<0.05$ and (**) indicates $p<0.01$.

For the 500 nm PS particles, particle localization density significantly decreased relative to the healthy condition for all rigid RBC conditions (Figure 8.11.). Previous work has shown that nano-sized particles do not marginate to the vessel wall as efficiently as MPs, and the results shown in Figure 8.10.A. are in agreement. [109,112,183–186] The presence of RBC rigidity in blood seems to exacerbate this poor NP margination effect.

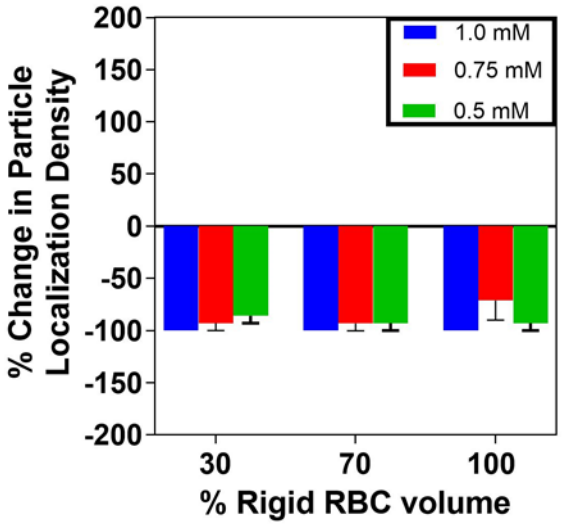

Figure 8.11. Polystyrene 500 nm Particle Localization to Cell Free Layer in the Presence of Rigid Red Blood Cells.

Quantified 500 nm polystyrene particle localization densities 2 μm away from vessel wall in a channel of height 100 μm at 1,000 s^{-1} and 106 particles/mL of whole blood as a function of rigid RBCs present, i.e., % volume rigid RBC, and rigid RBCs with different degrees of rigidity, 1.0 mM treated RBCs (most rigid), 0.75 mM treated RBCs, and 0.5 mM treated RBCs (least rigid). Particles are not functionalized with a targeting ligand. Error bars represent standard error. Statistical analysis of localization density was performed using two-way ANOVA to test particle localization density in rigid RBC conditions compared to healthy control, i.e., no rigid RBCs present. (*) indicates $p<0.05$ and (**) indicates $p<0.01$.

8.5. Discussion

Several human conditions can be characterized by the loss of RBC deformability, [3,7,97–102] with SCD being the most described, [3] but also includes HIV, T2D, and natural aging. [7,98–102] This presence of altered RBC membrane deformability in the blood is not without consequences; increased RBC membrane rigidity has been linked to pulmonary vascular resistance, crisis pain in SCD, and lowered cardiovascular health. [192] Gutierrez *et al*. recently reported that less deformable RBCs in blood severely reduced the adhesion of WBCs to an inflamed vessel wall in blood flow. [10] However, to date, no experimental evidence has been put forth in the literature that evaluates VTC adhesion performance in a diseased (rigid RBC) blood model. The margination and adhesion efficacy of a polymeric drug carrier highly depend on their interaction with cellular components of blood; thus, it is likely that the simultaneous presence of VTCs and rigid RBCs in the bloodstream could significantly alter the margination and adhesion dynamics of VTCs to the

vascular wall. In this work, we evaluated the impact of artificially rigidified RBCs on the margination and adhesion of rigid polystyrene (PS) and deformable hydrogel particles, as models for polymeric VTCs, *in vitro* via human blood flow assays. We examined microparticles (MPs) along with nanoparticles (NPs) precisely because, under normal conditions, MPs exhibit a higher margination capability over NPs, as shown by previous investigators. [108,113,193] Our findings demonstrate that many different levels of rigidified RBCs mixed in with healthy RBCs result in a decrease in the margination and adhesion of these PS particles to the wall, but, in some cases, a dramatic increase in the margination and adhesion of deformable MPs. Overall, this work highlights the significance of factoring the impact of RBC rigidity into designing translatable particle technology into practical therapeutics. The previously noted shift towards stiffer RBCs with natural aging further highlights the relevance of the presented work as the bulk of the proposed use of VTCs are focused on the elderly, including cardiovascular diseases that continue to be the primary cause of mortality globally.[194]

In line with the prior work with WBCs, our results show that the presence of rigid RBCs of varying rigidity reduces the blood flow adhesion of polystyrene microspheres by up to ~50%, depending on the level of RBC rigidity and the fraction composition of the rigid RBCs in the blood. Notably, the maximum impact of these altered RBCs is seen when they co-exist in the blood flow with healthy RBCs. Gutierrez *et al*. previously attributed the rigid RBC-induced reduction in WBC adhesion to heterogeneous collisions in blood flow, [10] which Graham and coworkers describe as the physical interaction between rigid (*stiff*) and deformable (*soft*) cells. [30,31] First, the heterogeneous collisions between stiff and soft RBCs lead to an expanded RBC core, i.e., rigid RBCs are found closer to the vessel wall (in the CFL), which occurs because the rigid RBCs experience a substantial displacement upon collision with the deformable RBCs. Second, the

increased presence of RBCs in the CFL causes an increase in heterogeneous collisions between RBCs and WBCs. [10] We suspect the same two-step effect of heterogeneous collisions is responsible for the reduced adhesion of the PS microspheres in blood flow with rigidified RBCs. Although a direct comparison between WBC and PS particle behavior in rigid RBC blood flow conditions may not be entirely relevant due to size and modulus differences, the general similarity of the observed trend between the two suggests a likely scenario of rigid RBCs present in the CFL preventing MPs from entering the CFL in large numbers. Essentially, rigid RBCs displaced to the wall by collisions with their softer counterparts take up spots in the CFL that otherwise would be occupied by MPs. Indeed, we observed a decrease in the localization of polystyrene MPs at a 2 μm distance from the vessel wall (Figure 8.10.B.) as compared to the localization of the same particles in healthy blood flow. While it is possible that collisions between rigid RBCs and polystyrene MPs could also disrupt adhesion, the results are presented in Figure 8.8. showing similar levels of adhesion reduction with the presence of rigid RBCs for MP with 3x more ligand density suggest that altered adhesion kinetics is not a major factor in dictating the observed particle adhesion trends. Thus, this leads us to speculate that particle margination, or alteration in particle motion in the cell-free layer, plays a bigger role in influencing how particles adhere in the presence of rigid RBCs.

We also probed how particle size can affect the particle adhesion trends in blood flow with the presence of rigid RBCs; we compared the adhesion of polystyrene MPs and NPs (2 μm and 500 nm). We find that the adhesion reductions observed for NPs are not as significant as the reductions seen for MPs despite a similar adhesion trend for both particle sizes in the case where *highly* and *moderately* rigid RBCs were present. We speculate that the primary source of this different response to rigid RBCs between micro-and nanospheres is the higher propensity that MPs

have to marginate towards the vessel wall than NPs. With more microspheres at the cell-free layer, there is a greater opportunity for heterogeneous collisions with rigid RBCs and hence a more significant adverse effect on the final particle adhesion at the wall. Of note, even upon experiencing a greater magnitude of reduction, the microsphere adhesion density is still higher than that for nanospheres, Figure 8.2. However, it possible that the physical size of particles itself also contributes to the difference in magnitude of the negative impact of rigid RBCs on microspheres versus nanospheres. Other things being equal, microspheres will experience a more significant displacement upon collision due to having a more substantial momentum, which then likely translates to the larger spheres needing to overcome a higher force to adhere firmly. [195] Along this line, we find that the levels of the adhesion reductions experienced by the 2 μm PS microspheres evaluated here, while significantly higher than for PS NPs. Additionally, 2 μm PS MP adhesion reductions are generally lower than previously reported for WBCs, with an average diameter of 7 - 12 μm, under the same rigid RBC flow conditions. [10]

The case where RBCs were *slightly rigid* is interesting because an oscillate-type trend is observed for the adhesion of PS microspheres, but not for nanospheres. Here, RBCs are not as stiff as in previous conditions. However, specific percentages (20%, 50%, and 90%) of the *slightly rigid* RBCs present produced a reduction in microsphere adhesion while others had no effect (30%, 70%, and 100%), Figure 8.1.C. This oscillate-type behavior in microsphere adhesion at different percentages of rigid RBCs present is also observed in the adhesion of hydrogel microspheres, Figure 8.3.C. Thus, this behavior seems to be particle-size-dependent. Possible variations in localization of *slightly* rigid RBCs are likely responsible for these adhesion trends, in which the motion of individual RBCs is not readily visualized in high shear blood flow with a physiological hematocrit level as evaluated here. A theoretical simulation could potentially help clarify this

oscillate-type trend. Theoretical models have been utilized to investigate how cellular shape and deformability impacts how objects behave in flow. [27,30,34,196] Some computational models have also examined how MPs and NPs marginate and affect drug delivery. [193] Work by Müller *et al*. simulates the margination of MPs and NPs, concluding, like many others, that MPs have a higher probability of localizing closer to the vessel wall compared to NPs. [193] Other interesting theoretical investigations have been able to modulate cellular rigidity in their simulations to investigate heterogeneous collisions' effect on margination. [30] Such models have served as adequate approximations that highlight some of the governing physics, such as lift force and heterogeneous collisions, that aid in giving rise to the observed blood flow phenomena. However, such simulations cannot fully recapitulate the complex behavior of blood flow due to limitations in computing power, which is often overcome by oversimplifications. To date, no theoretical approach has been established that investigates how increases in RBC membrane rigidity impact the ability of MPs and NPs to localize and ultimately bind to the vessel wall. Thus, future work, experimental and computational, is still needed to understand this phenomenon further.

Perhaps the most intriguing result from this study is the adhesion trend of the 2 μm deformable PEG-based hydrogel particles. Recent works in particle drug delivery have looked into modulating particle elasticity as a method to increase therapeutic efficacy. [114,197–201] Deformable particle drug carriers have become of high interest due to their capability for reduced cellular internalization and increased circulation time *in vivo*. [201,202] Previous investigations have developed deformable particle carriers with a wide range of sizes (22 nm - 9 μm) and modulus (200 Pa – 3 MPa), [114,197,203–205] with modulus tuned to resemble RBCs and even platelets in some cases closely. [198,199] Here, we examined deformable PEG-based MPs with a modulus similar to what is observed for WBCs. [114] When small percentages of *highly* and *moderately rigid* (1.0 mM

and 0.75 mM TBHP treated) RBCs are present, a slight reduction in hydrogel particle binding is observed. However, as the percentage of rigid RBCs is increased, particle adhesion to the vessel wall began to improve. For example, at a 100% of the *highly rigid* RBCs, the 2 μm hydrogel particle binding is enhanced by ~85%, Figure 8.3.A. We hypothesize that a combination of distinct phenomena, including increased heterogeneous collisions with rigid RBCs, are affecting the localization capability of hydrogel particles in the presence of rigid RBCs. Previous theoretical works suggest deformable particles do not marginate towards the vessel wall as compared to rigid particles. [31,206] Here, we see a substantial increase, up to 136%, in particle localization in the CFL for the 2 μm hydrogels with the presence of rigid RBCs, Figure 8.10.C. These results are counterintuitive since it would be expected that rigid particles experience greater displacement and thus would experience enhanced localization in the presence of rigid RBCs. Previous work has shown that the presence of WBCs in whole blood enhanced hydrogel MP adhesion to the vascular wall. [114] The presence of WBCs improves deformable MP (modulus similar to WBC modulus) adhesion as compared to adhesion in an RBC-plasma solution, showing that the WBCs in the CFL enhanced deformable MP adhesion. [114] We suspect that mismatched, i.e., heterogeneous collisions with rigid RBCs in addition to WBCs in the CFL promote deformable particle margination to the vessel wall. Still, this does not offer a complete explanation as to why having a small percentage of rigid RBCs in the blood produces a slight reduction in hydrogel MP adhesion. Additionally, although these PEG-MPs had a modulus closely resembling the modulus of WBCs, they do not behave like WBCs in the presence of rigid RBCs, as was reported by Gutierrez *et al*., suggesting that size is a key factor in predicting particle/cell behavior in the presence of rigid RBCs. [10] Another possible explanation for the differences in adhesion patterns between stiff and deformable MPs is the ability of deformable particles to spread onto the surface once they have adherent to the wall.

Unlike WBCs and deformable particles, stiff polystyrene particles do not spread on the surface and thus would experience a higher disruptive force from flow and potentially colliding rigid RBCs localized near the vessel wall. Also, although the same equivalent diameter, stiff particles would have a smaller contact area with the wall, which impacts adhesion strength. However, the fact that the impact of rigid RBCs on polystyrene microspheres did not change significantly with the significant increase in particle ligand density (Figure 8.8.A.) would suggest particle spreading; hence improved adhesion kinetics is not a significant contributor to the differences in the adhesion pattern between polystyrene and hydrogel microspheres.

Particle shape has been proposed as a major factor influencing particle localization and binding efficacy. Previous results have shown that ellipsoidal-shaped particles exhibit enhanced adhesion compared to spherical counterparts. [184,186,188] In this study, we probe how particle shape alters adhesion in the presence of rigid RBCs. Our obtained results show that the adhesion of rigid, rod-shaped particles is not reduced in the presence of rigid RBCs, unlike the spherical PS particle types tested; thus, hinting that particle shape is a major factor in particle-RBC interactions. The relatively unaffected, or in some cases enhanced, adhesion of rod particles in the presence of rigid RBCs is likely due to rod particles having (1) a larger contact area with endothelial layer and (2) a streamlined shape with a small surface area exposed to shear flow. Localization of rigid RBCs near the vessel wall results in increased collisions with particles in the CFL, preventing them from firmly adhering or even knock them off the vascular wall completely. Having a streamlined shape while bound to the endothelial layer would then explain why rod particle adhesion is not as drastically affected by the presence of rigid RBCs. In addition to this, the typical tumbling, rolling dynamics, and lateral drifting velocity observed in rod particles in the flow could be enhanced by

heterogeneous collisions with rigid RBCs. [207] Future experimental and computational analysis is needed to verify particle adhesion in the presence of rigid RBCs data.

8.6. Conclusions

This work shows that the presence of rigid RBCs in whole blood can have a significant impact on the localization and adhesion capabilities of vascular-targeted carriers. We utilize an artificial rigidification method to rigidify healthy RBCs aiming to mimic various hematologic diseases that directly affect RBC membrane deformability. Then we reconstitute rigid RBCs, with varying degrees of rigidity, into whole blood at distinct fractions and perfuse through a microfluidic model at physiologically relevant conditions. We aim to probe how changing particle deformability, size, and shape in the presence of rigid RBCs could affect particle adhesion capabilities. Firstly, we find that the adhesion capability of micro-sized, rigid polymeric spheres is highly reduced in the presence of rigid RBCs regardless of RBC degree of rigidity or rigid RBC concentration. Interestingly, deformable micro-sized sphere adhesion is reduced in the presence of small amounts of rigid RBCs. However, when a high percentage of rigid RBCs are present, the adhesion of deformable micro-sized particles is enhanced by up to 85%. We observe that nano-sized particles' adhesion capability is only slightly reduced in the presence of rigid RBCs. Moreover, we find that ellipsoidal particle adhesion is either enhanced or not affected by the presence of rigid RBCs. Overall, this work offers compelling evidence that the presence of rigid RBCs in whole blood can either significantly impact the localization and adhesion functionality of targeted drug carriers in whole blood, which can hold critical implications for a wide range of diseases affecting RBC deformability. The variable adhesion performance of particles observed

under distinct percentages of rigid RBCs and RBC stiffness suggests particle therapeutics efficacy can vastly vary between patients and disease severity. This unique information presented in this work can be highly valuable for the future development of personalized particle therapeutics with high adhesion efficacy in diseased blood.

Chapter 9 **: Conclusions and Future Directions**

9.1. Overall Dissertation Conclusions and Summary

In this dissertation, I have elucidated some of the biophysical contributions rigid RBCs have on the distribution and adhesion functionality of other cells in blood flow. I investigated and characterized RBC rigidity as it relates to SCD. The work presented in this thesis is important because the findings can potentially clarify biophysical characteristics of blood disorders with altered RBCs deformability and aid in the design of novel treatment protocols for the clinical management of such diseases. Blood disorders affect about 5% of the population worldwide, with an estimated ~100,000 Americans affected by SCD alone. Patients diagnosed with SCD will have a significantly shortened lifespan with compromised quality of life beginning in childhood. Current treatments for SCD, including the use of powerful narcotics (e.g., opiate), bone marrow transplant, and chronic blood transfusions.[42,52,117] Bone marrow transplant can be entirely curative but is also a highly invasive and costly procedure. Thus, pharmaceutical use for pain management and chronic transfusions remains the standard of care protocols. Unfortunately, typically patients become opiate-dependent as young adults. Thus, there is a dire need to develop novel therapeutic strategies to reduce the severe symptoms and heavy opiate use for SCD patients. The insights gained from this presented work can potentially have a profound impact on understanding the pathophysiology of SCD.[171,172] This understanding can lead to novel approaches to disease management, ultimately reducing infections, hospitalizations, and opiate use in the large

patient population unable to receive marrow transplant – the only curative procedure in SCD to date.[173] Overall, the research product from this dissertation provides a wealth of new data on cellular distribution and dynamics under different blood flow conditions that can be used to refine existing computational models for better prediction of cell dynamics in blood flows. For example, the stiffened RBC model presented in Chapter 3 was incorporated into a 3-Dimensional blood flow model to examine the margination of rigid RBCs and platelets.[40] Availability of robust and optimal numerical methods will allow for prediction of interactions in blood flow not currently achievable via *in vitro* and *in vivo* assays, which would impact the understanding and treatment of all ailments characterized by significant rigidity in RBC membranes not only SCD, but also including hyperglycemia, malaria, and natural aging.[171,172] Additionally, a better understanding of blood dynamics can be utilized to intelligently design personalized particle therapeutics for vascular use.

In Chapter 3, we investigate the impact artificially rigidified RBCs have on WBC adhesion capability under physiological blood flow conditions. Our results showed that the presence of rigid RBCs in blood flow led to a significant reduction in WBC adhesion to an inflamed vascular wall model in blood flow. Importantly, we uncovered a non-linear relationship in the WBC adhesion reduction and the fraction of rigid RBCs present in the whole blood. We also find that rigidified RBCs tend to localize closer to the vessel wall than deformable healthy counterparts. These results and methodologies open an opportunity for improving *in vitro* models of blood flow, specifically ones that can control proportion and degree of stiffness in RBCs.

In Chapter 4, we developed a predictive model that builds upon the ektacytometry technique. To build this predictive model, we rely on artificially rigidifying healthy RBCs to precisely control degree stiffness in RBCs, the proportion of stiff RBCs in the bulk blood sample, and uniformity of stiffness in the stiff RBC population. We parameterize these results and

extrapolate to interpret better the rigid, or HbS concentrated, RBC population in an SCD blood sample. We find that ektacytometry deformability measurements often underestimate the stiffness of rigid RBC population in a blood sample. The results presented here not only offer the opportunity for improvement of the ektacytometry technique but also offer a tool for building more precise *in vitro* models of rigid blood. Specifically, we can artificially construct a blood sample from healthy donor blood that resembles the stiffness and other key blood characteristics of an SCD blood sample.

In Chapter 5, we make an interesting clinical observation when working with pediatric SCD patients. We observe that an SCD patient of SC genotype registered an abnormal high bulk blood rigidity. This observation was of interest given the patient's genotype since SC is clinically accepted as a milder genotype of SCD. In addition, the patient has an abnormally high rate of hospital admissions and was thought to be faking painful episodes. Overall, these observations hint at the potentially larger role RBC rigidity can have on patient outcomes.

In Chapter 6, we build upon the *in vitro* blood flow model presented in Chapter 3 and the predictive model developed in Chapter 4 to probe further the impact of RBC rigidity in influencing WBC adhesion functionality in SCD. We analyze the blood profiles and general blood characteristics of a pool of pediatric SCD patients. Firstly, we examine the WBC adhesion to inflammation in a PPFC model using the SCD donor blood. Using the characterization of the SCD donor blood, we reconstruct separate blood models using non-SCD donor blood and match hematocrit, WBC count, RBC population rigidity, and rigid RBC fraction. Using the artificial blood models, we isolate the RBC rigidity factor and examine WBC adhesion to inflammation with and without RBC rigidity. We find that in most cases, the presence of rigid RBCs in blood flow led to a reduced capability for WBCs to adhere to inflammation. These results serve as

surmounting evidence of the detrimental impact rigid RBCs in blood flow have on the adhesion functionality of WBCs to inflammation on the vascular wall.

In Chapter 7, we examine how WBC adhesion is altered upon administration of infusion therapy in SCD. We leverage an artificial model of blood infusion therapy to probe this issue. We take blood samples from SCD patients pre-infusion treatment and add controlled volumes of non-SCD healthy RBCs to increase the hematocrit of the SCD blood sample. Subsequently, we perfuse RBC spiked blood samples through the PPFC model and examine WBC adhesion. We find that alterations in WBC adhesion upon infusion therapy are highly variable and unique for each individual SCD patient. In some cases, infusion of RBCs increases the WBC adhesion density to inflammation, and in other cases, the opposite is observed. Ultimately, this preliminary work suggests an opportunity to improve infusion therapy in SCD and potentially prescribe more controlled infusions based on the desired immune outcome.

In Chapter 8, we examine how vascular-targeted carriers perform in the presence of rigid RBCs in blood flow. Specifically, we test a variety of particle conditions, including particle size, deformability, and shape. We find that the adhesion efficacy of particle carriers is highly variable in the presence of rigid RBCs inf blood flow in combination with particle characteristics. The results from this investigation offer insight into the intricate influence RBCs, specifically rigid RBCs, have on particle drug carriers in blood flow and open novel avenues for the intelligent design of vascular-targeted carriers.

In conclusion, we demonstrate that RBC membrane rigidity is a highly influential factor in influencing cellular dynamics in general blood flow. Overall, the work presented in this dissertation characterizes RBC rigidity and elucidates the biophysical contribution of the rigid RBCs on the distribution and adhesion functionality of other blood cells as it relates to SCD. The

insights gained from this preliminary work would have a profound impact on understanding the pathophysiology of SCD.[171,172] This understanding can lead to novel approaches to disease management, ultimately reducing infections, hospitalizations, and opiate use in the large patient population unable to receive a hematopoietic stem cell transplant.[173]

9.2. Future Directions

This dissertation has further elucidated the role of RBC membrane deformability on cellular dynamics in blood flow and the resulting impact on the functionality of other blood cell types. The presented work lays the foundation for many potential future projects both of both experimental and computational nature. Considering the general status and need for more information in the research field, we highlight the impact and areas of improvement of the work presented in this dissertation. We feature the following major areas for improvement.

Primarily, we focused on examining the impact rigid RBCs in blood flow had on the functionality of WBCs, specifically on the adhesion to inflammation capability. However, this was the only other major blood cell type that was examined in terms of adhesion to the vascular wall. Previous work by Walton *et al*. suggests interactions between the RBC core lead to enhanced platelet accumulation in vascular injury.[208,209] There is considerable interest in examining the behavior of platelets in the presence of rigid RBCs in blood flow. Additionally, most of the work presented in this dissertation leveraged the robust *in vitro* PPFC model, which served as a paradigm for inflammation in a vascular wall. Although a robust model for microvasculature, there is a limitation in size and geometry simplification. It is inconclusive if the patterns observed in a microfluidic setting can be extrapolated to larger blood vessels and intricate vessel geometry. Work by Khoury *et al*. shows that the deposition of particles in a real-sized 3D carotid artery model

is highly influenced by vessel geometry and size.[210] Further probing the impact of rigidified RBCs in blood flow in complex vessel geometry is a logical next step. Overall, the work presented in this thesis can open new opportunities for further developing *in vitro* models of blood flow and opening new avenues for better understanding SCD. Better understanding the impact a seemingly simple change in cellular characteristics such as increased RBC membrane rigidity can have on cellular functionality and ultimately downstream patient outcome in blood flow can help in the development of novel therapeutics or improvement of existing treatment practices.

Some of the specific potential areas of interest for future research are listed below.

1) Impact of RBC shape alteration on flow dynamics. This thesis focused almost entirely on isolating the impact of RBC membrane deformability alteration, as it is a common characteristic in many diseases. However, shape alteration is also a common cellular change in many blood disorders. It is known that RBC shape is a contributing factor in the enhanced lift force experienced in flow.[28] Work in the field has shown that spherical RBCs exhibit altered flow patterns in an artificial microvascular network.[211] Preliminary work from the Eniola lab explored the alteration of RBC shape with the added factor of membrane stiffening. The shape of RBCs is easily altered by changing the osmolality of the solution in which they are suspended. However, the shape change is reversed when osmolality is returned to a neutral level. By coupling the osmolality change with a TBHP treatment, the RBCs membranes were stiffened and were less likely to return to their regular discocyte shape when osmolality was returned to physiological conditions. These results proved helpful in making interesting whole blood reconstitutions using rigid spherical RBCs and regular deformable or rigid discocyte RBCs, Figure 9.1. This

capability can lead to the development of *in vitro* models, like the one presented in Chapter 3, that can explore the extent RBC shape alteration can have on cellular behavior related to hereditary diseases spherocytosis and malaria.[155,212]

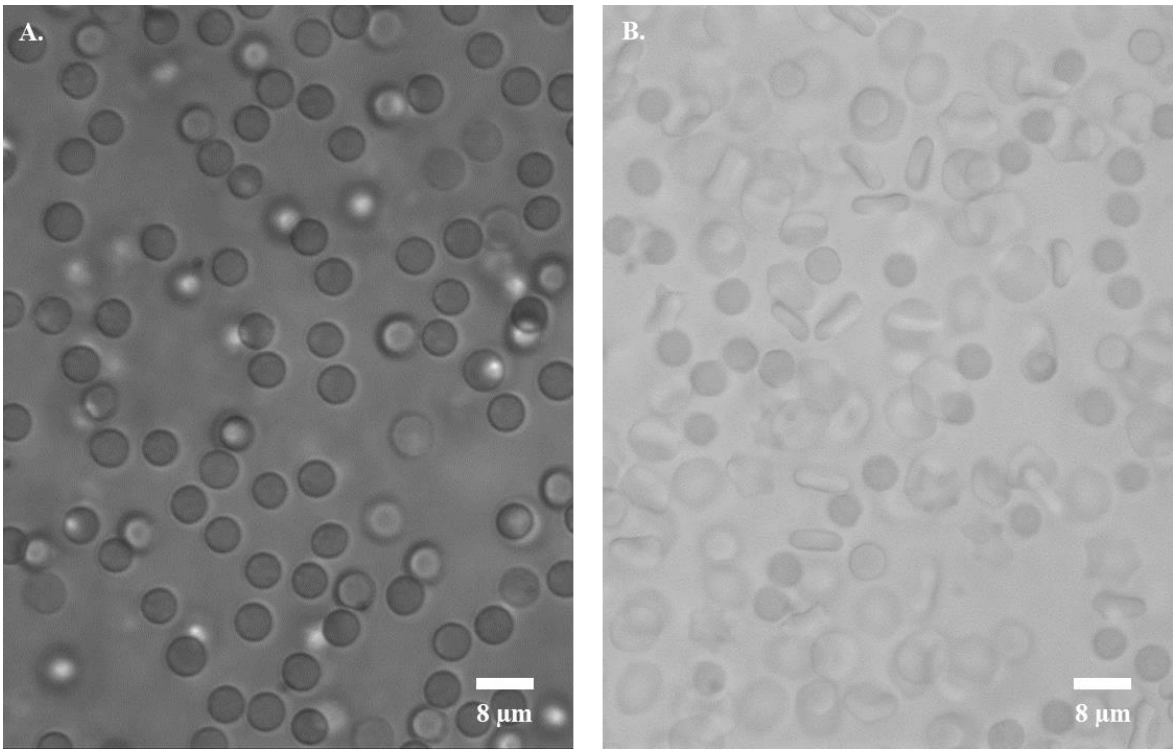

Figure 9.1. Brightfield Images of Spherical Red Blood Cells.

RBCs are suspended in phosphate buffer solution with 200 mM sodium salicylate to alter osmolality of solution. 1.0 mM TBHP solution is then added to RBC suspension to induce membrane stiffening. (A) shows rigid spherical RBCs. Stiffened spherical RBCs are then removed from solution and reconstituted in a neutral osmolality solution with other non-treated RBCs. (B) shows stiffened spherical RBCs in same solution as regular discocyte shape RBCs.

2) Computational modeling of RBC shape alteration on cellular dynamics. Similar to the previous suggestion, any conclusions drawn from the experimental exploration of RBC shape alteration are likely to be more robust when supplemented with a computational investigation. The groundwork for building 3D blood flow models exists already; the future work would entail making shape alterations to RBC geometry.

3) Impact of rigid RBCs in blood flow in larger complex vessel geometry. As previously stated in section 9.1. of this chapter, most of the work presented in this dissertation was accomplished in a microfluidic setting, using sub ~250 μm vessel sizes. It would be interesting to explore the effects of rigid RBCs in blood flow in a large geometry with more complex vessel geometry and flow patterns.
4) Investigate vascular-targeted carrier performance in large vessel geometry with rigid RBCs present. Like the previous suggestion, it would be interesting to explore how particle drug carriers perform in large complex geometry. Specifically, many of the target diseases for particle drug carrier therapeutics are of a vascular nature, e.g., atherosclerosis, and complications arise in large blood vessels, e.g., carotid artery. Additionally, such diseases may also involve some alteration to healthy whole blood characteristics. Thus, it is an attractive avenue to explore particle carrier adhesion efficacy in large vessel geometry in the presence of disease altered blood.
5) Further characterization of rigid RBC and whole blood model as SCD mimic. As shown in Chapter 4, we were able better to estimate the average population rigidity of SCD blood samples. With this capability, we paired the artificial stiffening model from Chapter 3 to develop an artificial blood model in Chapter 6 that mimicked the characteristics of SCD blood samples. This blood model focused almost entirely on matching the stiffness of the rigid RBC population. There is interest in further refining the artificial blood model for many reasons. For example, in a scenario where there is no accessibility to diseased blood, such as a restriction to SCD blood samples, normal non-diseased blood can be altered to match the

characteristics of diseased blood. Additionally, non-diseased blood can be altered to match the characteristics of other blood disorders such as hereditary spherocytosis and malaria.

6) Further investigate how rigid RBCs localized in CFL impact WBC adhesion. One of the significant conclusions from this thesis was that indeed the presence of rigid RBCs in blood flow leads to the reduced capability for WBCs to adhere to inflammation. We deduced that one of the factors contributing to this observation was the reduced ability for WBCs to escape the bulk blood flow and enter the CFL. However, one of the shortcomings of our studies was that we analyzed our microscopy data in static images, i.e., we quantified our adhesion data in still images after a specific time of blood flow in the PPFC model. It would be interesting to examine the adhesion process live and quantify firm WBC adhesion to the inflamed endothelial layer and WBC rolling on the endothelial layer.
7) We hypothesize that rigid RBCs localized in the CFL increase collision frequency with loosely adhered WBCs on the vascular wall. We hypothesize that this increased collision frequency leads to a reduced rate of firm WBC adhesion to inflammation. Future work should further characterize adhesion ligands profiles on WBCs used in these types of investigations. Subsequently, we would like to quantify firm WBC adhesion versus rolling in the presence of rigid RBCs.
8) Building upon the previous suggestion, future work should analyze WBC adhesion ligand profiles of SCD donor blood and further probe WBC adhesion tendencies, i.e., firm adhesion versus rolling, compares to the artificial rigid RBC blood model.

9) Investigate the effect of SCD blood plasma on WBC adhesion patterns. The work presented in this dissertation primarily focused on investigating the biophysical effects of RBC rigidity in blood flow. However, we did not explore any biochemistry in the blood plasma of SCD patients as a means of explaining the results we observed. It is a reasonable next step to explore the plasma profile of SCD donor blood and test its effect on potentially inducing endothelial dysfunction and inflammation. Additionally, it would be of interest to see if the blood plasma conditions affect the adhesion ligand profile of the WBCs in the SCD patient blood sample.

10) Further exploration of infusion therapy in SCD. The work presented in Chapter 7 is very preliminary results, as we show there is a unique pattern in WBC adhesion density upon administration of infusion therapy for each distinctive patient sample we examined. It would be interesting to do a more detailed study probing the addition of RBCs to pre-infusion SCD blood samples. Ideally, we would like to see if we can target a specific WBC adhesion density. Furthermore, further characterizing pre-infusion SCD patient samples can translate to predict the outcome of infusion better as well as understand what other factors in the blood influence that outcome. Additionally, it would be interesting to explore the infusion mimicking process on SCD blood samples that do not undergo infusion therapy but are treated with a pharmaceutical approach to see if similar patterns in WBC adhesion density are observed. Overall, future work on this project should aim to characterize the benefit of transfusion, offering a quantitative approach, i.e.,

standardized criteria for how patients get transfused, which can be formulated for the future use of this modality for treatment in SCD.

References

(1) Go, A. S.; Mozaffarian, D.; Roger, V. L.; Benjamin, E. J.; Berry, J. D.; Borden, W. B.; Bravata, D. M.; Dai, S.; Ford, E. S.; Fox, C. S.; Franco, S.; Fullerton, H. J.; Gillespie, C.; Hailpern, S. M.; Heit, J. A.; Howard, V. J.; Huffman, M. D.; Kissela, B. M.; Kittner, S. J.; Lackland, D. T.; Lichtman, J. H.; Lisabeth, L. D.; Magid, D.; Marcus, G. M.; Marelli, A.; Matchar, D. B.; McGuire, D. K.; Mohler, E. R.; Moy, C. S.; Mussolino, M. E.; Nichol, G.; Paynter, N. P.; Schreiner, P. J.; Sorlie, P. D.; Stein, J.; Turan, T. N.; Virani, S. S.; Wong, N. D.; Woo, D.; Turner, M. B. Heart Disease and Stroke Statistics-2013 Update: A Report from the American Heart Association. *Circulation*. 2013.

(2) Mohandas, N.; Chasis, J. A. Red Blood Cell Deformability, Membrane Material Properties and Shape: Regulation by Transmembrane, Skeletal and Cytosolic Proteins and Lipids. *Semin. Hematol.* **1993**, *30* (3), 171–192.

(3) Rees, D. C.; Williams, T. N.; Gladwin, M. T. Sickle-Cell Disease. *Lancet* **2010**, *376* (9757), 2018–2031.

(4) Gladwin, M. T.; Sachdev, V.; Jison, M. L.; Shizukuda, Y.; Plehn, J. F.; Minter, K.; Brown, B.; Coles, W. A.; Nichols, J. S.; Ernst, I.; Hunter, L. A.; Blackwelder, W. C.; Schechter, A. N.; Rodgers, G. P.; Castro, O.; Ognibene, F. P. Pulmonary Hypertension as a Risk Factor for Death in Patients with Sickle Cell Disease. *N. Engl. J. Med.* **2004**, *350* (9), 886–895.

(5) Sachdev, V.; Machado, R. F.; Shizukuda, Y.; Rao, Y. N.; Sidenko, S.; Ernst, I.; St. Peter, M.; Coles, W. A.; Rosing, D. R.; Blackwelder, W. C.; Castro, O.; Kato, G. J.; Gladwin, M. T. Diastolic Dysfunction Is an Independent Risk Factor for Death in Patients With Sickle Cell Disease. *J. Am. Coll. Cardiol.* **2007**, *49* (4), 472–479.

(6) Baskurt, O. K.; Gelmont, D.; Meiselman, H. J. Red Blood Cell Deformability in Sepsis. *Am. J. Respir. Crit. Care Med.* **1998**, *157* (2), 421–427.

(7) Athanassiou, G. A.; Moutzouri, A. G.; Gogos, C. A.; Skoutelis, A. T. Red Blood Cell Deformability in Patients with Human Immunodeficiency Virus Infection. *Eur. J. Clin. Microbiol. Infect. Dis.* **2010**, *29* (7), 845–849.

(8) Barabino, G. A.; Mclntire, L. V; Eskin, S. G.; Sears, D. A.; Udden, M. Endothelial Cell Interactions With Sickle Cell, Sickle Trait, Mechanically Injured, and Normal Erythrocytes Under Controlled Flow. *Blood* **1987**, *70* (1), 152–157.

(9) Alapan, Y.; Kim, C.; Adhikari, A.; Gray, K. E.; Gurkan-Cavusoglu, E.; Little, J. A.; Gurkan, U. A. Sickle Cell Disease Biochip: A Functional Red Blood Cell Adhesion Assay for Monitoring Sickle Cell Disease. *Transl. Res.* **2016**, *173*, 74-91.e8.

(10) Gutierrez, M.; Fish, M. B.; Golinski, A. W.; Eniola-Adefeso, O. Presence of Rigid Red Blood Cells in Blood Flow Interfere with the Vascular Wall Adhesion of Leukocytes. *Langmuir* **2018**, acs.langmuir.7b03890.

(11) Gutierrez, M.; Shamoun, M.; Seu, K. G.; Tanski, T.; Kalfa, T. A.; Eniola-Adefeso, O. Characterizing Bulk Rigidity of Rigid Red Blood Cell Populations in Sickle-Cell Disease Patients. *Sci. Rep.* **2021**, *11* (1), 7909.

(12) Gutierrez, M.; Ojeda, L. S.; Eniola-Adefeso, O. Vascular-Targeted Particle Binding Efficacy in the Presence of Rigid Red Blood Cells: Implications for Performance in Diseased Blood. *Biomicrofluidics* **2018**, *12* (4), 042217.
(13) Rhoades, R. A.; Bell, D. R. *Medical Phisiology: Principles for Clinical Medicine*; Lippincott Williams & Wilkins, 2012.
(14) Pearson, M. J.; Lipowsky, H. H. Influence of Erythrocyte Aggregation on Leukocyte Margination in Postcapillary Venules of Rat Mesentery. *Am. J. Physiol. Circ. Physiol.* **2000**, *279* (4), H1460–H1471.
(15) Pappu, V.; Bagchi, P. Hydrodynamic Interaction between Erythrocytes and Leukocytes Affects Rheology of Blood in Microvessels. *Biorheology*. IOS Press January 1, 2007, pp 191–215.
(16) Munn, L. L.; Melder, R. J.; Jain, R. K. Role of Erythrocytes in Leukocyte-Endothelial Interactions: Mathematical Model and Experimental Validation. *Biophys. J.* **1996**, *71* (1), 466–478.
(17) Sobczynski, D. J.; Charoenphol, P.; Heslinga, M. J.; Onyskiw, P. J.; Namdee, K.; Thompson, A. J.; Eniola-Adefeso, O. Plasma Protein Corona Modulates the Vascular Wall Interaction of Drug Carriers in a Material and Donor Specific Manner. *PLoS One* **2014**, *9* (9), e107408.
(18) Kim, S.; Ong, P. K.; Yalcin, O.; Intaglietta, M.; Johnson, P. C. The Cell-Free Layer in Microvascular Blood Flow. *Biorheology* **2009**, *46* (3), 181–189.
(19) Firrell, J. C.; Lipowsky, H. H. Leukocyte Margination and Deformation in Mesenteric Venules of Rat. *Am J Physiol Hear. Circ Physiol* **1989**, *256* (6), H1667-1674.
(20) Tangelder, G. J.; Teirlinck, H. C.; Slaaf, D. W.; Reneman, R. S. Distribution of Blood Platelets Flowing in Arterioles. *Am. J. Physiol.* **1985**, *248* (3 Pt 2), H318-23.
(21) Walcheck, B.; Moore, K. L.; McEver, R. P.; Kishimoto, T. K. Neutrophil-Neutrophil Interactions under Hydrodynamic Shear Stress Involve L-Selectin and PSGL-1. A Mechanism That Amplifies Initial Leukocyte Accumulation of P-Selectin in Vitro. *J. Clin. Invest.* **1996**, *98* (5), 1081–1087.
(22) Kim, S.; Kong, R. L.; Popel, A. S.; Intaglietta, M.; Johnson, P. C. Temporal and Spatial Variations of Cell-Free Layer Width in Arterioles. *Am. J. Physiol. Circ. Physiol.* **2007**, *293* (3), H1526–H1535.
(23) Maeda, N.; Suzuki, Y.; Tanaka, J.; Tateishi, N. Erythrocyte Flow and Elasticity of Microvessels Evaluated by Marginal Cell-Free Layer and Flow Resistance. *Am. J. Physiol.* **1996**, *271* (6 Pt 2), H2454-61.
(24) Abbitt, K. B.; Nash, G. B. Characteristics of Leucocyte Adhesion Directly Observed in Flowing Whole Blood in Vitro. *Br. J. Haematol.* **2001**, *112* (1), 55–63.
(25) Fedosov, D. A.; Fornleitner, J.; Gompper, G. Margination of White Blood Cells in Microcapillary Flow. *Phys. Rev. Lett.* **2012**, *108* (2), 028104.
(26) Marth, W.; Aland, S.; Voigt, A. Margination of White Blood Cells: A Computational Approach by a Hydrodynamic Phase Field Model. *J. Fluid Mech.* **2016**, *790*, 389–406.
(27) Fedosov, D. A.; Gompper, G. White Blood Cell Margination in Microcirculation. *Soft Matter* **2014**, *10* (17), 2961–2970.
(28) Cantat, I.; Misbah, C. Lift Force and Dynamical Unbinding of Adhering Vesicles under Shear Flow. *Phys. Rev. Lett.* **1999**, *83* (4), 880–883.
(29) Crowl, L. M.; Fogelson, A. L. Computational Model of Whole Blood Exhibiting Lateral Platelet Motion Induced by Red Blood Cells. *Int. j. numer. method. biomed. eng.* **2010**, *26*,

471–487.
(30) Kumar, A.; Graham, M. D. Mechanism of Margination in Confined Flows of Blood and Other Multicomponent Suspensions. *Phys. Rev. Lett.* **2012**, *109* (10), 10536–10548.
(31) Kumar, A.; Henríquez Rivera, R. G.; Graham, M. D. Flow-Induced Segregation in Confined Multicomponent Suspensions: Effects of Particle Size and Rigidity. *J. Fluid Mech.* **2013**, *738*, 423–462.
(32) Clemetson, K. J.; Clemetson, J. M. Platelet Collagen Receptors. In *Thrombosis and Haemostasis*; 2001; Vol. 86, pp 189–197.
(33) Passos, A.; Sherwood, J. M.; Kaliviotis, E.; Agrawal, R.; Pavesio, C.; Balabani, S. The Effect of Deformability on the Microscale Flow Behavior of Red Blood Cell Suspensions. *Phys. Fluids* **2019**, *31* (9), 091903.
(34) Kumar, A.; Graham, M. D. Margination and Segregation in Confined Flows of Blood and Other Multicomponent Suspensions. *Soft Matter* **2012**, *8* (41), 10536.
(35) Crowl, L. M.; Fogelson, A. L. Computational Model of Whole Blood Exhibiting Lateral Platelet Motion Induced by Red Blood Cells. *Int. j. numer. method. biomed. eng.* **2010**, *26* (3–4), 471–487.
(36) Yazdani, A.; Li, X.; Em Karniadakis, G. Dynamic and Rheological Properties of Soft Biological Cell Suspensions. *Rheol. acta* **2016**, *55* (6), 433–449.
(37) Liu, Y.; Liu, W. K. Rheology of Red Blood Cell Aggregation by Computer Simulation. *J. Comput. Phys.* **2006**, *220* (1), 139–154.
(38) Zhao, H.; Shaqfeh, E. S. G.; Narsimhan, V. Shear-Induced Particle Migration and Margination in a Cellular Suspension. *Phys. Fluids* **2012**, *24* (1), 011902.
(39) Li, X.; Dao, M.; Lykotrafitis, G.; Karniadakis, G. E. Biomechanics and Biorheology of Red Blood Cells in Sickle Cell Anemia. *J. Biomech.* **2017**, *50*, 34–41.
(40) Czaja, B.; Gutierrez, M.; Závodszky, G.; de Kanter, D.; Hoekstra, A.; Eniola-Adefeso, O. The Influence of Red Blood Cell Deformability on Hematocrit Profiles and Platelet Margination. *PLOS Comput. Biol.* **2020**, *16* (3), e1007716.
(41) Piel, F. B.; Hay, S. I.; Gupta, S.; Weatherall, D. J.; Williams, T. N. Global Burden of Sickle Cell Anaemia in Children under Five, 2010-2050: Modelling Based on Demographics, Excess Mortality, and Interventions. *PLoS Med.* **2013**, *10* (7).
(42) Piel, F. B.; Steinberg, M. H.; Rees, D. C. Sickle Cell Disease. *N. Engl. J. Med.* **2017**, *376* (16), 1561–1573.
(43) Basak, S.; Ferrone, F. A.; Wang, J. T. Kinetics of Domain Formation by Sickle Hemoglobin Polymers. *Biophys. J.* **1988**, *54* (5), 829–843.
(44) Booth, C.; Inusa, B.; Obaro, S. K. Infection in Sickle Cell Disease: A Review. *Int. J. Infect. Dis.* **2010**, *14* (1), e2–e12.
(45) Brousse, V.; Buffet, P.; Rees, D. The Spleen and Sickle Cell Disease: The Sick(Led) Spleen. *Br. J. Haematol.* **2014**, *166* (2), 165–176.
(46) Zhang, D.; Xu, C.; Manwani, D.; Frenette, P. S. Neutrophils, Platelets, and Inflammatory Pathways at the Nexus of Sickle Cell Disease Pathophysiology. *Blood* **2016**, *127* (7), 801–809.
(47) Yamaguchi, S.; Yamakawa, T.; Niimi, H. Cell-Free Plasma Layer in Cerebral Microvessels. *Biorheology* **1992**, *29* (2–3), 251–260.
(48) Schreier, D. A.; Forouzan, O.; Hacker, T. A.; Sheehan, J.; Chesler, N. Increased Red Blood Cell Stiffness Increases Pulmonary Vascular Resistance and Pulmonary Arterial Pressure. *J. Biomech. Eng.* **2016**, *138* (2), 021012.

(49) Ohene-Frempong, K.; Weiner, S. J.; Sleeper, L. A.; Miller, S. T.; Embury, S.; Moohr, J. W.; Wethers, D. L.; Pegelow, C. H.; Gill, F. M. Cerebrovascular Accidents in Sickle Cell Disease: Rates and Risk Factors. *Blood* **1998**, *91* (1), 288–294.
(50) Saiki, R.; Scharf, S.; Faloona, F.; Mullis, K.; Horn, G.; Erlich, H.; Arnheim, N. Enzymatic Amplification of Beta-Globin Genomic Sequences and Restriction Site Analysis for Diagnosis of Sickle Cell Anemia. *Science (80-.).* **1985**, *230* (4732), 1350–1354.
(51) Bunn, H. F.; Noguchi, C. T.; Hofrichter, J.; Schechter, G. P.; Schechter, A. N.; Eaton, W. A. Molecular and Cellular Pathogenesis of Hemoglobin SC Disease. *Proc. Natl. Acad. Sci. U. S. A.* **1982**, *79* (23 I), 7527–7531.
(52) McCavit, T. L. Sickle Cell Disease. *Pediatr. Rev.* **2012**, *33* (5), 195–204; quiz 205–206.
(53) Villagra, J.; Shiva, S.; Hunter, L. A.; Machado, R. F.; Gladwin, M. T.; Kato, G. J. Platelet Activation in Patients with Sickle Disease, Hemolysis-Associated Pulmonary Hypertension, and Nitric Oxide Scavenging by Cell-Free Hemoglobin. *Blood* **2007**, *110* (6), 2166–2172.
(54) Aarts, P.; Heethaar, R.; Sixma, J. Red Blood Cell Deformability Influences Platelets--Vessel Wall Interaction in Flowing Blood. *Blood* **1984**, *64* (6), 1228–1233.
(55) Kato, G. J.; Piel, F. B.; Reid, C. D.; Gaston, M. H.; Ohene-Frempong, K.; Krishnamurti, L.; Smith, W. R.; Panepinto, J. A.; Weatherall, D. J.; Costa, F. F.; Vichinsky, E. P. Sickle Cell Disease. *Nature Reviews Disease Primers*. Nature Publishing Group March 15, 2018, pp 1–22.
(56) Platt, O. S.; Brambilla, D. J.; Rosse, W. F.; Milner, P. F.; Castro, O.; Steinberg, M. H.; Klug, P. P. Mortality In Sickle Cell Disease -- Life Expectancy and Risk Factors for Early Death. *N. Engl. J. Med.* **1994**, *330* (23), 1639–1644.
(57) Gluckman, E.; Cappelli, B.; Bernaudin, F.; Labopin, M.; Volt, F.; Carreras, J.; Simões, B. P.; Ferster, A.; Dupont, S.; De La Fuente, J.; Dalle, J. H.; Zecca, M.; Walters, M. C.; Krishnamurti, L.; Bhatia, M.; Leung, K.; Yanik, G.; Kurtzberg, J.; Dhedin, N.; Kuentz, M.; Michel, G.; Apperley, J.; Lutz, P.; Neven, B.; Bertrand, Y.; Vannier, J. P.; Ayas, M.; Cavazzana, M.; Matthes-Martin, S.; Rocha, V.; Elayoubi, H.; Kenzey, C.; Bader, P.; Locatelli, F.; Ruggeri, A.; Eapen, M.; Bordon, V.; Labarque, V.; Pereira, M.; Bittencourt, H.; Petersen, H.; Deconninck, E.; Jubert, C.; Perrin, J.; Cahn, J. Y.; Bruno, B.; Bordigoni, P.; Mechinaud, F.; Vernant, J. P.; Stephan, J. L.; Suttorp, M.; Strahm, B.; Da Cunha, C. B.; Garwer, B.; Rothmayer, M.; Wendelin, K.; Graphakos, S.; Tbakhi, A.; Naeimi, N.; Zuckerman, T.; Sharon, P. B.; Yaniv, I.; Amos, T.; Prete, A.; Lo Nigro, L.; Lanino, E.; Faraci, M.; Ciceri, F.; Marktel, S.; De Simone, G.; Messina, C.; Bartolomeo, P. D. I.; Santarone, S.; Vallisa, D.; Bertaina, A.; Arcese, W.; Foa, R.; Berger, M.; Maximova, N.; Wallet, S.; Bazuaye, G. N.; Maschan, A.; De Heredia, C. D.; Bieler, C. B.; Pato, J. R.; Heras, I.; Trevor, R.; Abayomi, K.; Thomson, J.; Fasth, A.; Frödin, U.; Ljugman, P.; Ansari, M.; Güngör, T.; Unal, E.; Pehlivan, M.; Anak, S.; Ozturk, G.; Unal, A.; Lawson, S.; Keshani, J.; Drake, A.; Wynn, R.; Williams, J.; Jagsia, M.; Leung, W.; Abraham, A.; Sahdey, I.; Margolis, D.; Eames, G.; Horwitz, E.; Cowan, M.; Kapoor, N.; Rowley, S.; Megason, G.; Rogers, Z.; Bolaños-Meade, J.; Hudspeth, M.; Rosenthal, J.; Olson, T.; Kassow, K.; Selby, G.; Haines, H.; Chaudhury, S. Sickle Cell Disease: An International Survey of Results of HLA-Identical Sibling Hematopoietic Stem Cell Transplantation. *Blood* **2017**, *129* (11), 1548–1556.
(58) Lu, M.; Rab, M. A. E.; Shevkoplyas, S. S.; Sheehan, V. A. Blood Rheology Biomarkers in Sickle Cell Disease. *Experimental Biology and Medicine*. SAGE Publications Inc. January

1, 2020, pp 155–165.
(59) Niihara, Y.; Miller, S. T.; Kanter, J.; Lanzkron, S.; Smith, W. R.; Hsu, L. L.; Gordeuk, V. R.; Viswanathan, K.; Sarnaik, S.; Osunkwo, I.; Guillaume, E.; Sadanandan, S.; Sieger, L.; Lasky, J. L.; Panosyan, E. H.; Blake, O. A.; New, T. N.; Bellevue, R.; Tran, L. T.; Razon, R. L.; Stark, C. W.; Neumayr, L. D.; Vichinsky, E. P. A Phase 3 Trial of <scp>l</Scp> -Glutamine in Sickle Cell Disease. *N. Engl. J. Med.* **2018**, *379* (3), 226–235.
(60) Thornburg, C. D.; Files, B. A.; Luo, Z.; Miller, S. T.; Kalpatthi, R.; Iyer, R.; Seaman, P.; Lebensburger, J.; Alvarez, O.; Thompson, B.; Ware, R. E.; Wang, W. C. Impact of Hydroxyurea on Clinical Events in the BABY HUG Trial. *Blood* **2012**, *120* (22), 4304–4310.
(61) Ware, R. E.; Davis, B. R.; Schultz, W. H.; Brown, R. C.; Aygun, B.; Sarnaik, S.; Odame, I.; Fuh, B.; George, A.; Owen, W.; Luchtman-Jones, L.; Rogers, Z. R.; Hilliard, L.; Gauger, C.; Piccone, C.; Lee, M. T.; Kwiatkowski, J. L.; Jackson, S.; Miller, S. T.; Roberts, C.; Heeney, M. M.; Kalfa, T. A.; Nelson, S.; Imran, H.; Nottage, K.; Alvarez, O.; Rhodes, M.; Thompson, A. A.; Rothman, J. A.; Helton, K. J.; Roberts, D.; Coleman, J.; Bonner, M. J.; Kutlar, A.; Patel, N.; Wood, J.; Piller, L.; Wei, P.; Luden, J.; Mortier, N. A.; Stuber, S. E.; Luban, N. L. C.; Cohen, A. R.; Pressel, S.; Adams, R. J. Hydroxycarbamide versus Chronic Transfusion for Maintenance of Transcranial Doppler Flow Velocities in Children with Sickle Cell Anaemia - TCD with Transfusions Changing to Hydroxyurea (TWiTCH): A Multicentre, Open-Label, Phase 3, Non-Inferiority Trial. *Lancet* **2016**, *387* (10019), 661–670.
(62) Hilliard, L. M.; Kulkarni, V.; Sen, B.; Caldwell, C.; Bemrich-Stolz, C.; Howard, T. H.; Brandow, A.; Waite, E.; Lebensburger, J. D. Red Blood Cell Transfusion Therapy for Sickle Cell Patients with Frequent Painful Events. *Pediatr. Blood Cancer* **2018**, *65* (12), e27423.
(63) DeBaun, M. R.; Gordon, M.; McKinstry, R. C.; Noetzel, M. J.; White, D. A.; Sarnaik, S. A.; Meier, E. R.; Howard, T. H.; Majumdar, S.; Inusa, B. P. D.; Telfer, P. T.; Kirby-Allen, M.; McCavit, T. L.; Kamdem, A.; Airewele, G.; Woods, G. M.; Berman, B.; Panepinto, J. A.; Fuh, B. R.; Kwiatkowski, J. L.; King, A. A.; Fixler, J. M.; Rhodes, M. M.; Thompson, A. A.; Heiny, M. E.; Redding-Lallinger, R. C.; Kirkham, F. J.; Dixon, N.; Gonzalez, C. E.; Kalinyak, K. A.; Quinn, C. T.; Strouse, J. J.; Miller, J. P.; Lehmann, H.; Kraut, M. A.; Ball, W. S.; Hirtz, D.; Casella, J. F. Controlled Trial of Transfusions for Silent Cerebral Infarcts in Sickle Cell Anemia. *N. Engl. J. Med.* **2014**, *371* (8), 699–710.
(64) Lakkakula, B. V. K. S.; Sahoo, R.; Verma, H.; Lakkakula, S. Pain Management Issues as Part of the Comprehensive Care of Patients with Sickle Cell Disease. *Pain Management Nursing*. W.B. Saunders December 1, 2018, pp 558–572.
(65) Brown, S. E.; Weisberg, D. F.; Balf-Soran, G.; Sledge, W. H. Sickle Cell Disease Patients with and without Extremely High Hospital Use: Pain, Opioids, and Coping. *J. Pain Symptom Manage.* **2015**, *49* (3), 539–547.
(66) Carden, M. A.; Fay, M. E.; Lu, X.; Mannino, R. G.; Sakurai, Y.; Ciciliano, J. C.; Hansen, C. E.; Chonat, S.; Joiner, C. H.; Wood, D. K.; Lam, W. A. Extracellular Fluid Tonicity Impacts Sickle Red Blood Cell Deformability and Adhesion. *Blood* **2017**, *130* (24), 2654–2663.
(67) Ballas, S.; Smith, E. Red Blood Cell Changes during the Evolution of the Sickle Cell Painful Crisis. *Blood* **1992**, *79* (8).
(68) Ballas, S.; Larner, J.; Smith, E.; Surrey, S.; Schwartz, E.; Rappaport, E. Rheologic

Predictors of the Severity of the Painful Sickle Cell Crisis. *Blood* **1988**, *72* (4).
(69) Connes, P.; Lamarre, Y.; Waltz, X.; Ballas, S. K.; Lemonne, N.; Etienne-Julan, M.; Hue, O.; Hardy-Dessources, M.-D.; Romana, M. Haemolysis and Abnormal Haemorheology in Sickle Cell Anaemia. *Br. J. Haematol.* **2014**, *165* (4), 564–572.
(70) Parrow, N. L.; Violet, P.-C.; Tu, H.; Nichols, J.; Pittman, C. A.; Fitzhugh, C.; Fleming, R. E.; Mohandas, N.; Tisdale, J. F.; Levine, M. Measuring Deformability and Red Cell Heterogeneity in Blood by Ektacytometry. *J. Vis. Exp.* **2018**, No. 131, e56910.
(71) Bento, D.; Rodrigues, R.; Faustino, V.; Pinho, D.; Fernandes, C.; Pereira, A.; Garcia, V.; Miranda, J.; Lima, R.; Bento, D.; Rodrigues, R. O.; Faustino, V.; Pinho, D.; Fernandes, C. S.; Pereira, A. I.; Garcia, V.; Miranda, J. M.; Lima, R. Deformation of Red Blood Cells, Air Bubbles, and Droplets in Microfluidic Devices: Flow Visualizations and Measurements. *Micromachines* **2018**, *9* (4), 151.
(72) Tomaiuolo, G. Biomechanical Properties of Red Blood Cells in Health and Disease towards Microfluidics. *Biomicrofluidics* **2014**, *8* (5), 051501.
(73) Kim, J.; Lee, H.; Shin, S. Advances in the Measurement of Red Blood Cell Deformability: A Brief Review. *J. Cell. Biotechnol.* **2015**, *1* (1), 63–79.
(74) Islamzada, E.; Matthews, K.; Guo, Q.; Santoso, A. T.; Duffy, S. P.; Scott, M. D.; Ma, H. Deformability Based Sorting of Stored Red Blood Cells Reveals Donor-Dependent Aging Curves. *Lab Chip* **2020**, *20* (2), 226–235.
(75) Turhan, A.; Weiss, L. A.; Mohandas, N.; Coller, B. S.; Frenette, P. S. Primary Role for Adherent Leukocytes in Sickle Cell Vascular Occlusion: A New Paradigm. *Proc. Natl. Acad. Sci. U. S. A.* **2002**, *99* (5), 3047–3051.
(76) Johnston, R. B.; Newman, S. L.; Struth, A. G. Increased Susceptibility to Infection in Sickle Cell Disease: Defects of Opsonization and of Splenic Function. *Birth Defects Orig. Artic. Ser.* **1975**, *11* (1), 322–327.
(77) RAAB, S. O.; ATHENS, J. W.; HAAB, O. P.; BOGGS, D. R.; ASHENBRUCKER, H.; CARTWRIGHT, G. E.; WINTROBE, M. M. GRANULOKINETICS IN NORMAL DOGS. *Am. J. Physiol.* **1964**, *206*, 83–88.
(78) Boggs, D. R.; Hyde, F.; Srodes, C. An Unusual Pattern of Neutrophil Kinetics in Sickle Cell Anemia. *Blood* **1973**, *41* (1), 59–65.
(79) Canalli, A. A.; Franco-Penteado, C. F.; Saad, S. T. O.; Conran, N.; Costa, F. F. Increased Adhesive Properties of Neutrophils in Sickle Cell Disease May Be Reversed by Pharmacological Nitric Oxide Donation. *Haematologica* **2008**, *93* (4), 605–609.
(80) Benkerrou, M.; Delarche, C.; Brahimi, L.; Fay, M.; Vilmer, E.; Elion, J.; Gougerot-Pocidalo, M. A.; Elbim, C. Hydroxyurea Corrects the Dysregulated L-Selectin Expression and Increased H2O2 Production of Polymorphonuclear Neutrophils from Patients with Sickle Cell Anemia. *Blood* **2002**, *99* (7), 2297–2303.
(81) Lawrence, M. B.; Springer, T. A. Leukocytes Roll on a Selectin at Physiologic Flow Rates: Distinction from and Prerequisite for Adhesion through Integrins. *Cell* **1991**, *65* (5), 859–873.
(82) Man, Y.; Goreke, U.; Kucukal, E.; Hill, A.; An, R.; Liu, S.; Bode, A.; Solis-Fuentes, A.; Nayak, L. V.; Little, J. A.; Gurkan, U. A. Leukocyte Adhesion to P-Selectin and the Inhibitory Role of Crizanlizumab in Sickle Cell Disease: A Standardized Microfluidic Assessment. *Blood Cells, Mol. Dis.* **2020**, *83*, 102424.
(83) Jimenez, M. A.; Tutuncuoglu, E.; Barge, S.; Novelli, E. M.; Sundd, P. Quantitative Microfluidic Fluorescence Microscopy to Study Vaso-Occlusion in Sickle Cell Disease.

Haematologica. Ferrata Storti Foundation October 2, 2015, pp e390–e393.
(84) Koehl, B.; Nivoit, P.; El Nemer, W. E.; Lenoir, O.; Hermand, P.; Pereira, C.; Brousse, V.; Guyonnet, L.; Ghinatti, G.; Benkerrou, M.; Colin, Y.; Le van Kim, C.; Tharaux, P. L. The Endothelin B Receptor Plays a Crucial Role in the Adhesion of Neutrophils to the Endothelium in Sickle Cell Disease. *Haematologica* **2017**, *102* (7), 1161–1172.
(85) Aarts, P.; Bolhuis, P.; Sakariassen, K.; Heethaar, R.; Sixma, J. Red Blood Cell Size Is Important for Adherence of Blood Platelets to Artery Subendothelium. *Blood* **1983**, *62* (1), 214–217.
(86) Namdee, K.; Carrasco-Teja, M.; Fish, M. B.; Charoenphol, P.; Eniola-Adefeso, O. Effect of Variation in Hemorheology between Human and Animal Blood on the Binding Efficacy of Vascular-Targeted Carriers. *Sci. Rep.* **2015**, *5* (1), 11631.
(87) Petros, R. A.; DeSimone, J. M. Strategies in the Design of Nanoparticles for Therapeutic Applications. *Nat. Rev. Drug Discov.* **2010**, *9* (8), 615–627.
(88) Lusis, A. J. Atherosclerosis. *Nature* **2000**, *407* (6801), 233–241.
(89) Klingenberg, R.; Hansson, G. K. Treating Inflammation in Atherosclerotic Cardiovascular Disease: Emerging Therapies. *Eur. Heart J.* **2009**, *30* (23), 2838–2844.
(90) Gentile, F.; Curcio, A.; Indolfi, C.; Ferrari, M.; Decuzzi, P. The Margination Propensity of Spherical Particles for Vascular Targeting in the Microcirculation. *J. Nanobiotechnology* **2008**, *6* (1), 9.
(91) Godin, B.; Serda, R. E.; Sakamoto, J.; Decuzzi, P.; Ferrari, M.; Godin, B.; Serda, R. E.; Sakamoto, J.; Decuzzi, P.; Ferrari, M. Nanoparticles for Cancer Detection and Therapy. In *Nanotechnology*; Wiley-VCH Verlag GmbH & Co. KGaA: Weinheim, Germany, 2010.
(92) D'Apolito, R.; Tomaiuolo, G.; Taraballi, F.; Minardi, S.; Kirui, D.; Liu, X.; Cevenini, A.; Palomba, R.; Ferrari, M.; Salvatore, F.; Tasciotti, E.; Guido, S. Red Blood Cells Affect the Margination of Microparticles in Synthetic Microcapillaries and Intravital Microcirculation as a Function of Their Size and Shape. *J. Control. Release* **2015**, *217*, 263–272.
(93) Tan, J.; Thomas, A.; Liu, Y. Influence of Red Blood Cells on Nanoparticle Targeted Delivery in Microcirculation. *Soft Matter* **2012**, *8* (6), 1934–1946.
(94) Lanotte, L.; Tomaiuolo, G.; Misbah, C.; Bureau, L.; Guido, S. Red Blood Cell Dynamics in Polymer Brush-Coated Microcapillaries: A Model of Endothelial Glycocalyx *in Vitro*. *Biomicrofluidics* **2014**, *8* (1), 014104.
(95) Tomaiuolo, G.; Preziosi, V.; Simeone, M.; Guido, S.; Ciancia, R.; Martinelli, V.; Rinaldi, C.; Rotoli, B. A Methodology to Study the Deformability of Red Blood Cells Flowing in Microcapillaries in Vitro. *Ann. Ist. Super. Sanita* **2007**, *43* (2), 186–192.
(96) Geislinger, T. M.; Franke, T. Hydrodynamic Lift of Vesicles and Red Blood Cells in Flow — from Fåhræus & Lindqvist to Microfluidic Cell Sorting. *Adv. Colloid Interface Sci.* **2014**, *208*, 161–176.
(97) Mohandas, N.; Gallagher, P. G. Red Cell Membrane: Past, Present, and Future. *Blood* **2008**, *112* (10), 3939–3948.
(98) Agrawal, R.; Smart, T.; Nobre-Cardoso, J.; Richards, C.; Bhatnagar, R.; Tufail, A.; Shima, D.; Jones, P. H.; Pavesio, C. Assessment of Red Blood Cell Deformability in Type 2 Diabetes Mellitus and Diabetic Retinopathy by Dual Optical Tweezers Stretching Technique. *Sci. Rep.* **2016**, *6*, 15873.
(99) Solerte, S.; Fioravanti, M.; Pezza, N.; Locatelli, M.; Schifino, N.; Cerutti, N.; Severgnini, S.; Rondanelli, M.; Ferrari, E. Hyperviscosity and Microproteinuria in Central Obesity:

Relevance to Cardiovascular Risk. *Int. J. Obes.* **1997**, *21* (6), 417–423.
(100) Wysocki, M.; Krotkiewski, M.; Braide, M.; Bagge, U. Hemorheological Disturbances, Metabolic Parameters and Blood Pressure in Different Types of Obesity. *Atherosclerosis* **1991**, *88* (1), 21–28.
(101) Ward, K. A.; Baker, C.; Roebuck, L.; Wickline, K.; Schwartz, R. W. Red Blood Cell Deformability: Effect of Age and Smoking. *Age (Omaha).* **1991**, *14* (3), 73–77.
(102) Khecuriani, R.; Lomsadze, G.; Arabuli, M.; Sanikidze, T. Deformability of Red Blood Cells and Human Aging. *Georgian Med. News* **2010**, No. 182, 42–46.
(103) Hajitou, A.; Pasqualini, R.; Arap, W. Vascular Targeting: Recent Advances and Therapeutic Perspectives. *Trends Cardiovasc. Med.* **2006**, *16* (3), 80–88.
(104) Psarros, C.; Lee, R.; Margaritis, M.; Antoniades, C. Nanomedicine for the Prevention, Treatment and Imaging of Atherosclerosis. *Nanomedicine* **2012**, *8 Suppl 1*, S59-68.
(105) Namdee, K.; Thompson, A. J.; Golinski, A.; Mocherla, S.; Bouis, D.; Eniola-Adefeso, O. In Vivo Evaluation of Vascular-Targeted Spheroidal Microparticles for Imaging and Drug Delivery Application in Atherosclerosis. *Atherosclerosis* **2014**, *237* (1), 279–286.
(106) Onyskiw, P. J.; Eniola-Adefeso, O. Effect of PEGylation on Ligand-Based Targeting of Drug Carriers to the Vascular Wall in Blood Flow. *Langmuir* **2013**, *29* (35), 11127–11134.
(107) Huang, A. D. A. J.; Furie, M. B.; Nicholson, S. C.; Fischbarg, J.; Liebovitch, L. S.; Silverstein, S. C. Effects of Human Neutrophil Chemotaxis Across Human Endothelial Cell Monolayers on the Permeability of These Monolayers to Ions and Macromolecules. *J. Cell. Physiol.* **1988**, *135*, 355–366.
(108) Charoenphol, P.; Mocherla, S.; Bouis, D.; Namdee, K.; Pinsky, D. J.; Eniola-Adefeso, O. Targeting Therapeutics to the Vascular Wall in Atherosclerosis–Carrier Size Matters. *Atherosclerosis* **2011**, *217* (2), 364–370.
(109) Charoenphol, P.; Onyskiw, P. J.; Carrasco-Teja, M.; Eniola-Adefeso, O. Particle-Cell Dynamics in Human Blood Flow: Implications for Vascular-Targeted Drug Delivery. *J. Biomech.* **2012**, *45* (16), 2822–2828.
(110) Huang, R. B.; Eniola-Adefeso, O. Shear Stress Modulation of IL-1-Induced E-Selectin Expression in Human Endothelial Cells. *PLoS One* **2012**, *7* (2), 1–11.
(111) Fromen, C. A.; Fish, M. B.; Zimmerman, A.; Adili, R.; Holinstat, M.; Eniola-Adefeso, O. Evaluation of Receptor-Ligand Mechanisms of Dual-Targeted Particles to an Inflamed Endothelium. *Bioeng. Transl. Med.* **2016**, *1* (1), 103–115.
(112) Namdee, K.; Thompson, A. J.; Charoenphol, P.; Eniola-Adefeso, O. Margination Propensity of Vascular-Targeted Spheres from Blood Flow in a Microfluidic Model of Human Microvessels. *Langmuir* **2013**, *29* (8), 2530–2535.
(113) Charoenphol, P.; Huang, R. B.; Eniola-Adefeso, O. Potential Role of Size and Hemodynamics in the Efficacy of Vascular-Targeted Spherical Drug Carriers. *Biomaterials* **2010**, *31* (6), 1392–1402.
(114) Fish, M. B.; Fromen, C. A.; Lopez-Cazares, G.; Golinski, A. W.; Scott, T. F.; Adili, R.; Holinstat, M.; Eniola-Adefeso, O. Exploring Deformable Particles in Vascular-Targeted Drug Delivery: Softer Is Only Sometimes Better. *Biomaterials* **2017**, *124*, 169–179.
(115) Fairbanks, B. D.; Schwartz, M. P.; Bowman, C. N.; Anseth, K. S. Photoinitiated Polymerization of PEG-Diacrylate with Lithium Phenyl-2,4,6-Trimethylbenzoylphosphinate: Polymerization Rate and Cytocompatibility. *Biomaterials* **2009**, *30* (35), 6702–6707.

(116) Majima, T.; Schnabel, W.; Weber, W. Phenyl-2,4,6-trimethylbenzoylphosphinates as Water-soluble Photoinitiators. Generation and Reactivity of O□Ṗ(C6H5)(O−) Radical Anions. *Die Makromol. Chemie* **1991**, *192* (10), 2307–2315.
(117) Stuart, M. J.; Nagel, R. L. Sickle-Cell Disease. *Lancet (London, England)* **2004**, *364* (9442), 1343–1360.
(118) Alapan, Y.; Little, J. A.; Gurkan, U. A. Heterogeneous Red Blood Cell Adhesion and Deformability in Sickle Cell Disease. *Sci. Rep.* **2014**, *4*, 1–8.
(119) Papaioannou, T.; Stefanadis, C. Vascular Wall Shear Stress: Basic Principles and Methods. *Hell. J Cardiol* **2005**.
(120) Sakariassen, K. S.; Orning, L.; Turitto, V. T. The Impact of Blood Shear Rate on Arterial Thrombus Formation. *Futur. Sci. OA* **2015**, *1* (4), fso.15.28.
(121) Dobbe, J. G. G.; Hardeman, M. R.; Streekstra, G. J.; Strackee, J.; Ince, C.; Grimbergen, C. A. Analyzing Red Blood Cell-Deformability Distributions. *Blood Cells, Mol. Dis.* **2002**, *28* (3), 373–384.
(122) Caprari, P.; Bozzi, A.; Malorni, W.; Bottini, A.; Iosi, F.; Santini, M. T.; Salvati, A. M. Junctional Sites of Erythrocyte Skeletal Proteins Are Specific Targets of Tert-Butylhydroperoxide Oxidative Damage. *Chem. Biol. Interact.* **1995**, *94* (3), 243–258.
(123) Goldsmith, H. L.; Spain, S. Margination of Leukocytes in Blood Flow through Small Tubes. *Microvasc. Res.* **1984**, *27* (2), 204–222.
(124) Nobis, U.; Pries, A. R.; Cokelet, G. R.; Gaehtgens, P. Radial Distribution of White Cells during Blood Flow in Small Tubes. *Microvasc. Res.* **1985**, *29* (3), 295–304.
(125) Iigo, Y.; Suematsu, M.; Higashida, T.; Oheda, J.; Matsumoto, K.; Wakabayashi, Y.; Ishimura, Y.; Miyasaka, M.; Takashi, T. Constitutive Expression of ICAM-1 in Rat Microvascular Systems Analyzed by Laser Confocal Microscopy. *Am. J. Physiol. - Hear. Circ. Physiol.* **1997**, *273* (1).
(126) Granger, D. N.; Kubes, P. The Microcirculation and Inflammation: Modulation of Leukocyte-Endothelial Cell Adhesion. *J. Leukoc. Biol.* **1994**, *55* (5), 662–675.
(127) Ley, K.; Gaehtgens, P. Endothelial, Not Hemodynamic, Differences Are Responsible for Preferential Leukocyte Rolling in Rat Mesenteric Vanules. *Circ. Res.* **1991**, *69* (4), 1034–1041.
(128) Dremza, I. K.; Lapshina, E. A.; Kujawa, J.; Zavodnik, I. B. Oxygen-Related Processes in Red Blood Cells Exposed to *Tert* -Butyl Hydroperoxide. *Redox Rep.* **2006**, *11* (4), 185–192.
(129) Awogu, A. U. Leucocyte Counts in Children with Sickle Cell Anaemia Usefulness of Stable State Values during Infections. *West Afr. J. Med.* **2000**, *19* (1), 55–58.
(130) Adam, M.; Ardinger, H.; Pagon, R.; Al, E. *Sickle Cell Disease - GeneReviews® - NCBI Bookshelf*; 2017.
(131) Lim, H.; Back, S. M.; Nam, J.; Choi, H. Determination of Red Blood Cell Deformability Using Centrifugal Force in a Three-Dimensional-Printed Mini-Disk (3D-PMD). *PLoS One* **2018**, *13* (5).
(132) Llaudet-Planas, E.; Vives-Corrons, J. L.; Rizzuto, V.; Gómez-Ramírez, P.; Sevilla Navarro, J.; Coll Sibina, M. T.; García-Bernal, M.; Ruiz Llobet, A.; Badell, I.; Velasco-Puyó, P.; Dapena, J. L.; Mañú-Pereira, M. M. Osmotic Gradient Ektacytometry: A Valuable Screening Test for Hereditary Spherocytosis and Other Red Blood Cell Membrane Disorders. *Int. J. Lab. Hematol.* **2018**, *40* (1), 94–102.
(133) Groner, W.; Mohandas, N.; Bessis, M. New Optical Technique for Measuring Erythrocyte

Deformability with the Ektacytometer. *Clin. Chem.* **1980**, *26* (10).
(134) Bessis, M.; Mohandas, N.; Feo, C. Automated Ektacytometry: A New Method of Measuring Red Cell Deformability and Red Cell Indices. *Blood Cells* **1980**, *6* (3), 315–327.
(135) Rab, M. A. E.; van Oirschot, B. A.; Bos, J.; Merkx, T. H.; van Wesel, A. C. W.; Abdulmalik, O.; Safo, M. K.; Versluijs, B. A.; Houwing, M. E.; Cnossen, M. H.; Riedl, J.; Schutgens, R. E. G.; Pasterkamp, G.; Bartels, M.; van Beers, E. J.; van Wijk, R. Rapid and Reproducible Characterization of Sickling during Automated Deoxygenation in Sickle Cell Disease Patients. *Am. J. Hematol.* **2019**, *94* (5), 575–584.
(136) Nikitin, S. Y.; Ustinov, V. D.; Yurchuk, Y. S.; Lugovtsov, A. E.; Lin, M. D.; Priezzhev, A. V. New Diffractometric Equations and Data Processing Algorithm for Laser Ektacytometry of Red Blood Cells. *J. Quant. Spectrosc. Radiat. Transf.* **2016**, *178*, 315–324.
(137) Baskurt, O. K.; Meiselman, H. J. Data Reduction Methods for Ektacytometry in Clinical Hemorheology. *Clin. Hemorheol. Microcirc.* **2013**, *54* (1), 99–107.
(138) Caprari, P.; Bozzi, A.; Malorni, W.; Bottini, A.; Iosi, F.; Santini, M. T.; Salvati, A. M. Junctional Sites of Erythrocyte Skeletal Proteins Are Specific Targets of Tert-Butylhydroperoxide Oxidative Damage. *Chem. Biol. Interact.* **1995**, *94* (3), 243–258.
(139) Baskurt, O. K.; Hardeman, M. R.; Uyuklu, M.; Ulker, P.; Cengiz, M.; Nemeth, N.; Shin, S.; Alexy, T.; Meiselman, H. J. Parameterization of Red Blood Cell Elongation Index – Shear Stress Curves Obtained by Ektacytometry. *Scand. J. Clin. Lab. Invest.* **2009**, *69* (7), 777–788.
(140) Qiu, Y.; Ahn, B.; Sakurai, Y.; Hansen, C. E.; Tran, R.; Mimche, P. N.; Mannino, R. G.; Ciciliano, J. C.; Lamb, T. J.; Joiner, C. H.; Ofori-Acquah, S. F.; Lam, W. A. Microvasculature-on-a-Chip for the Long-Term Study of Endothelial Barrier Dysfunction and Microvascular Obstruction in Disease. *Nat. Biomed. Eng.* **2018**, *2* (6), 453–463.
(141) Mannino, R.; Myers, D. R.; Sakurai, Y.; Ware, R. E.; Barabino, G.; Lam, W. Increased Erythrocyte Rigidity Is Sufficient to Cause Endothelial Dysfunction in Sickle Cell Disease. *Blood* **2012**, *120* (21), 818–818.
(142) Segal, J. B.; Strouse, J. J.; Beach, M. C.; Haywood, C.; Witkop, C.; Park, H.; Wilson, R. F.; Bass, E. B.; Lanzkron, S. Hydroxyurea for the Treatment of Sickle Cell Disease. *Evidence report/technology assessment*. March 2008, pp 1–95.
(143) Lemonne, N.; Charlot, K.; Waltz, X.; Ballas, S. K.; Lamarre, Y.; Lee, K.; Hierso, R.; Connes, C.; Etienne-Julan, M.; Romana, M.; Connes, P. Hydroxyurea Treatment Does Not Increase Blood Viscosity and Improves Red Blood Cell Rheology in Sickle Cell Anemia. *Haematologica*. Ferrata Storti Foundation October 2, 2015, pp e383–e386.
(144) Buchanan, G. R. "Packaging" of Fetal Hemoglobin in Sickle Cell Anemia. *Blood*. American Society of Hematology January 23, 2014, pp 464–465.
(145) Saraf, S. L.; Molokie, R. E.; Nouraie, M.; Sable, C. A.; Luchtman-Jones, L.; Ensing, G. J.; Campbell, A. D.; Rana, S. R.; Niu, X. M.; Machado, R. F.; Gladwin, M. T.; Gordeuk, V. R. Differences in the Clinical and Genotypic Presentation of Sickle Cell Disease around the World. *Paediatric Respiratory Reviews*. NIH Public Access March 2014, pp 4–12.
(146) McCurdy, P. R.; Sherman, A. S. Irreversibly Sickled Cells and Red Cell Survival in Sickle Cell Anemia. A Study with Both DF32P and 51CR. *Am. J. Med.* **1978**, *64* (2), 253–258.
(147) Bertles, J. F.; Milner, P. F. Irreversibly Sickled Erythrocytes: A Consequence of the Heterogeneous Distribution of Hemoglobin Types in Sickle-Cell Anemia. *J. Clin. Invest.*

1968, *47* (8), 1731–1741.
(148) Rabai, M.; Detterich, J. A.; Wenby, R. B.; Hernandez, T. M.; Toth, K.; Meiselman, H. J.; Wood, J. C. Deformability Analysis of Sickle Blood Using Ektacytometry. In *Biorheology*; IOS Press, 2014; Vol. 51, pp 159–170.
(149) Fabry, M. E.; Kaul, D. K.; Raventos-Suarez, C.; Chang, H.; Nagel, R. L. SC Erythrocytes Have an Abnormally High Intracellular Hemoglobin Concentration. Pathophysiological Consequences. *J. Clin. Invest.* **1982**, *70* (6), 1315–1319.
(150) Embury, S. H. The Clinical Pathophysiology of Sickle Cell Disease. *Annu. Rev. Med.* **1986**, *37* (1), 361–376.
(151) Ballas, S.; Larner, J.; Smith, E.; Surrey, S.; Schwartz, E.; Rappaport, E. The Xerocytosis of Hb SC Disease. *Blood* **1987**, *69* (1), 124–130.
(152) Sachdev, V.; Machado, R. F.; Shizukuda, Y.; Rao, Y. N.; Sidenko, S.; Ernst, I.; St Peter, M.; Coles, W. A.; Rosing, D. R.; Blackwelder, W. C.; Castro, O.; Kato, G. J.; Gladwin, M. T. Diastolic Dysfunction Diastolic Dysfunction Is an Independent Risk Factor for Death in Patients With Sickle Cell Disease. **2007**.
(153) Ferrone, F. A.; Hofrichter, J.; Eaton, W. A. Kinetics of Sickle Hemoglobin Polymerization. I. Studies Using Temperature-Jump and Laser Photolysis Techniques. *J. Mol. Biol.* **1985**, *183* (4), 591–610.
(154) Aprelev, A.; Stephenson, W.; Noh, H.; Meier, M.; Ferrone, F. A. The Physical Foundation of Vasoocclusion in Sickle Cell Disease. *Biophys. J.* **2012**, *103* (8), L38–L40.
(155) Wiley, J. S.; Wiley, J. S. Red Cell Survival Studies in Hereditary Spherocytosis Find the Latest Version : Red Cell Survival Studies in Hereditary Spherocytosis. **1970**, *49* (4), 666–672.
(156) Franco, R. S.; Yasin, Z.; Palascak, M. B.; Ciraolo, P.; Joiner, C. H.; Rucknagel, D. L. The Effect of Fetal Hemoglobin on the Survival Characteristics of Sickle Cells. **2006**, *108* (3), 1073–1076.
(157) Ballas, S. K.; Connes, P. Rheological Properties of Sickle Erythrocytes in Patients with Sickle-Cell Anemia: The Effect of Hydroxyurea, Fetal Hemoglobin, and α-Thalassemia. *Eur. J. Haematol.* **2018**, *101* (6), 798–803.
(158) Treiber, F.; Mabe, P. A.; Wilson, G. Psychological Adjustment of Sickle Cell Children and Their Siblings. *Child. Heal. Care* **1987**, *16* (2), 82–88.
(159) Fanos, J. H.; Fahrner, K.; Jelveh, M.; King, R.; Tejeda, D. The Sibling Center: A Pilot Program for Siblings of Children and Adolescents with a Serious Medical Condition. *Journal of Pediatrics*. Elsevier June 1, 2005, pp 831–835.
(160) Deavin, A.; Greasley, P.; Dixon, C. Children's Perspectives on Living with a Sibling with a Chronic Illness. *Pediatrics*. American Academy of Pediatrics August 1, 2018.
(161) Gualandro, S. F. M.; Fonseca, G. H. H.; Yokomizo, I. K.; Gualandro, D. M.; Suganuma, L. M. Cohort Study of Adult Patients with Haemoglobin SC Disease: Clinical Characteristics and Predictors of Mortality. *Br. J. Haematol.* **2015**, *171* (4), 631–637.
(162) Abbitt, K. B.; Nash, G. B. Rheological Properties of the Blood Influencing Selectin-Mediated Adhesion of Flowing Leukocytes. *Am. J. Physiol. Heart Circ. Physiol.* **2003**, *285* (1), H229-40.
(163) Okpala, I. The Intriguing Contribution of White Blood Cells to Sickle Cell Disease - A Red Cell Disorder. *Blood Reviews*. Churchill Livingstone March 1, 2004, pp 65–73.
(164) Okpala, I. The Management of Crisis in Sickle Cell Disease. *Eur. J. Haematol.* **2009**, *60* (1), 1–6.

(165) Jr, J. R.; SL, N.; AG, S. Increased Susceptibility to Infection in Sickle Cell Disease: Defects of Opsonization and of Splenic Function. *Birth Defects Orig. Artic. Ser.* **1975**, *11* (1), 322–327.
(166) Ley, K.; Tedder, T. F. Leukocyte Interactions with Vascular Endothelium. New Insights into Selectin-Mediated Attachment and Rolling. *J. Immunol.* **1995**, *155* (2), 525–528.
(167) Ley, K.; Allietta, M.; Bullard, D. C.; Morgan, S. Importance of E-Selectin for Firm Leukocyte Adhesion in Vivo. *Circ. Res.* **1998**, *83* (3), 287–294.
(168) Tan, P.; Luscinskas, F. W.; Homer-Vanniasinkam, S. Cellular and Molecular Mechanisms of Inflammation and Thrombosis. *Eur. J. Vasc. Endovasc. Surg.* **1999**, *17* (5), 373–389.
(169) Kaul, D. K.; Fabry, M. E.; Nagel, R. L. Microvascular Sites and Characteristics of Sickle Cell Adhesion to Vascular Endothelium in Shear Flow Conditions: Pathophysiological Implications. *Proc. Natl. Acad. Sci. U. S. A.* **1989**, *86* (9), 3356–3360.
(170) Kucukal, E.; Ilich, A.; Key, N. S.; Little, J. A.; Gurkan, U. A. Red Blood Cell Adhesion to Heme-Activated Endothelial Cells Reflects Clinical Phenotype in Sickle Cell Disease. *Am. J. Hematol.* **2018**, *93* (8), 1050–1060.
(171) Park, Y.; Best, C. A.; Badizadegan, K.; Dasari, R. R.; Feld, M. S.; Kuriabova, T.; Henle, M. L.; Levine, A. J.; Popescu, G. Measurement of Red Blood Cell Mechanics during Morphological Changes. *Proc. Natl. Acad. Sci. U. S. A.* **2010**, *107* (15), 6731–6736.
(172) Kameneva, M. V.; Garrett, K. O.; Watach, M. J.; Borovetz, H. S. Red Blood Cell Aging and Risk of Cardiovascular Diseases. *Clinical Hemorheology and Microcirculation*. IOS Press January 1, 1998, pp 67–74.
(173) Aslam, H. M.; Yousuf, S.; Kassim, A.; Iqbal, S. M.; Hashmi, S. K. Hematopoietic Stem Cell Transplantation for Adult Sickle Cell Disease in the Era of Universal Donor Availibility. *Bone Marrow Transplantation*. Nature Publishing Group November 1, 2018, pp 1390–1400.
(174) Drasar, E.; Igbineweka, N.; Vasavda, N.; Free, M.; Awogbade, M.; Allman, M.; Mijovic, A.; Thein, S. L. Blood Transfusion Usage among Adults with Sickle Cell Disease - a Single Institution Experience over Ten Years. *Br. J. Haematol.* **2011**, *152* (6), 766–770.
(175) Howard, J. Sickle Cell Disease: When and How to Transfuse. *Hematol. (United States)* **2016**, *2016* (1), 625–631.
(176) Raphael, J. L.; Oyeku, S. O.; Kowalkowski, M. A.; Mueller, B. U.; Ellison, A. M. Trends in Blood Transfusion among Hospitalized Children with Sickle Cell Disease. *Pediatr. Blood Cancer* **2013**, *60* (11), 1753–1758.
(177) Kato, G. J.; Steinberg, M. H.; Gladwin, M. T. Intravascular Hemolysis and the Pathophysiology of Sickle Cell Disease. *Journal of Clinical Investigation*. American Society for Clinical Investigation March 1, 2017, pp 750–760.
(178) Solovey, A.; Lin, Y.; Browne, P.; Choong, S.; Wayner, E.; Hebbel, R. P. Circulating Activated Endothelial Cells in Sickle Cell Anemia. *N. Engl. J. Med.* **1997**, *337* (22), 1584–1590.
(179) Connes, P.; Coates, T. D. Autonomic Nervous System Dysfunction: Implication in Sickle Cell Disease. *C. R. Biol.* **2013**, *336* (3), 142–147.
(180) Du, E.; Diez-Silva, M.; Kato, G. J.; Dao, M.; Suresh, S. Kinetics of Sickle Cell Biorheology and Implications for Painful Vasoocclusive Crisis. *Proc. Natl. Acad. Sci. U. S. A.* **2015**, *112* (5), 1422–1427.
(181) DeBaun, M. R.; Gordon, M.; McKinstry, R. C.; Noetzel, M. J.; White, D. A.; Sarnaik, S. A.; Meier, E. R.; Howard, T. H.; Majumdar, S.; Inusa, B. P. D.; Telfer, P. T.; Kirby-Allen,

M.; McCavit, T. L.; Kamdem, A.; Airewele, G.; Woods, G. M.; Berman, B.; Panepinto, J. A.; Fuh, B. R.; Kwiatkowski, J. L.; King, A. A.; Fixler, J. M.; Rhodes, M. M.; Thompson, A. A.; Heiny, M. E.; Redding-Lallinger, R. C.; Kirkham, F. J.; Dixon, N.; Gonzalez, C. E.; Kalinyak, K. A.; Quinn, C. T.; Strouse, J. J.; Miller, J. P.; Lehmann, H.; Kraut, M. A.; Ball, W. S.; Hirtz, D.; Casella, J. F. Controlled Trial of Transfusions for Silent Cerebral Infarcts in Sickle Cell Anemia. *N. Engl. J. Med.* **2014**, *371* (8), 699–710.

(182) Zhang, D.; Xu, C.; Manwani, D.; Frenette, P. S. Neutrophils, Platelets, and Inflammatory Pathways at the Nexus of Sickle Cell Disease Pathophysiology. *Blood*. American Society of Hematology February 18, 2016, pp 801–809.

(183) Gentile, F.; Chiappini, C.; Fine, D.; Bhavane, R. C.; Peluccio, M. S.; Cheng, M. M.-C.; Liu, X.; Ferrari, M.; Decuzzi, P. The Effect of Shape on the Margination Dynamics of Non-Neutrally Buoyant Particles in Two-Dimensional Shear Flows. *J. Biomech.* **2008**, *41* (10), 2312–2318.

(184) Toy, R.; Hayden, E.; Shoup, C.; Baskaran, H.; Karathanasis, E. The Effects of Particle Size, Density and Shape on Margination of Nanoparticles in Microcirculation. *Nanotechnology* **2011**, *22* (11), 115101.

(185) Tan, J.; Shah, S.; Thomas, A.; Ou-Yang, H. D.; Liu, Y. The Influence of Size, Shape and Vessel Geometry on Nanoparticle Distribution. *Microfluid. Nanofluidics* **2013**, *14* (1–2), 77–87.

(186) Thompson, A. J.; Mastria, E. M.; Eniola-Adefeso, O. The Margination Propensity of Ellipsoidal Micro/Nanoparticles to the Endothelium in Human Blood Flow. *Biomaterials* **2013**, *34* (23), 5863–5871.

(187) Toy, R.; Peiris, P. M.; Ghaghada, K. B.; Karathanasis, E. Shaping Cancer Nanomedicine: The Effect of Particle Shape on the *in Vivo* Journey of Nanoparticles. *Nanomedicine* **2014**, *9* (1), 121–134.

(188) Lee, S.-Y.; Ferrari, M.; Decuzzi, P. Shaping Nano-/Micro-Particles for Enhanced Vascular Interaction in Laminar Flows. *Nanotechnology* **2009**, *20* (49), 495101.

(189) Tateishi, N.; Suzuki, Y.; Soutani, M.; Maeda, N. Flow Dynamics of Erythrocytes in Microvessels of Isolated Rabbit Mesentery: Cell-Free Layer and Flow Resistance. *J. Biomech.* **1994**, *27* (9), 1119–1125.

(190) Bagchi, P. Mesoscale Simulation of Blood Flow in Small Vessels. *Biophys. J.* **2007**, *92* (6), 1858–1877.

(191) International Society of Biorheology., M.; Popel, A. S. *Biorheology.*; Pergamon Press, 2001; Vol. 38.

(192) Schreier, D. A.; Forouzan, O.; Hacker, T. A.; Sheehan, J.; Chesler, N. Increased Red Blood Cell Stiffness Increases Pulmonary Vascular Resistance and Pulmonary Arterial Pressure. *J. Biomech. Eng.* **2016**, *138* (2), 021012.

(193) Müller, K.; Fedosov, D. A.; Gompper, G. Margination of Micro- and Nano-Particles in Blood Flow and Its Effect on Drug Delivery. *Sci. Rep.* **2015**, *4* (1), 4871.

(194) Benjamin, E. J.; Blaha, M. J.; Chiuve, S. E.; Cushman, M.; Das, S. R.; Deo, R.; de Ferranti, S. D.; Floyd, J.; Fornage, M.; Gillespie, C.; Isasi, C. R.; Jiménez, M. C.; Jordan, L. C.; Judd, S. E.; Lackland, D.; Lichtman, J. H.; Lisabeth, L.; Liu, S.; Longenecker, C. T.; Mackey, R. H.; Matsushita, K.; Mozaffarian, D.; Mussolino, M. E.; Nasir, K.; Neumar, R. W.; Palaniappan, L.; Pandey, D. K.; Thiagarajan, R. R.; Reeves, M. J.; Ritchey, M.; Rodriguez, C. J.; Roth, G. A.; Rosamond, W. D.; Sasson, C.; Towfighi, A.; Tsao, C. W.; Turner, M. B.; Virani, S. S.; Voeks, J. H.; Willey, J. Z.; Wilkins, J. T.; Wu, J. H.; Alger,

H. M.; Wong, S. S.; Muntner, P.; American Heart Association Statistics Committee and Stroke Statistics Subcommittee. Heart Disease and Stroke Statistics-2017 Update: A Report From the American Heart Association. *Circulation* **2017**, *135* (10), e146–e603.
(195) Thompson, A. J.; Eniola-Adefeso, O. Dense Nanoparticles Exhibit Enhanced Vascular Wall Targeting over Neutrally Buoyant Nanoparticles in Human Blood Flow. *Acta Biomater.* **2015**, *21*, 99–108.
(196) Fedosov, D. A.; Fornleitner, J.; Gompper, G. Margination of White Blood Cells in Microcapillary Flow. *Phys. Rev. Lett.* **2012**, *108* (2), 028104.
(197) Anselmo, A. C.; Zhang, M.; Kumar, S.; Vogus, D. R.; Menegatti, S.; Helgeson, M. E.; Mitragotri, S. Elasticity of Nanoparticles Influences Their Blood Circulation, Phagocytosis, Endocytosis, and Targeting. *ACS Nano* **2015**, *9* (3), 3169–3177.
(198) Doshi, N.; Zahr, A. S.; Bhaskar, S.; Lahann, J.; Mitragotri, S. Red Blood Cell-Mimicking Synthetic Biomaterial Particles. *Proc. Natl. Acad. Sci. U. S. A.* **2009**, *106* (51), 21495–21499.
(199) Doshi, N.; Orje, J. N.; Molins, B.; Smith, J. W.; Mitragotri, S.; Ruggeri, Z. M. Platelet Mimetic Particles for Targeting Thrombi in Flowing Blood. *Adv. Mater.* **2012**, *24* (28), 3864–3869.
(200) Anselmo, A. C.; Modery-Pawlowski, C. L.; Menegatti, S.; Kumar, S.; Vogus, D. R.; Tian, L. L.; Chen, M.; Squires, T. M.; Sen Gupta, A.; Mitragotri, S. Platelet-like Nanoparticles: Mimicking Shape, Flexibility, and Surface Biology of Platelets To Target Vascular Injuries. *ACS Nano* **2014**, *8* (11), 11243–11253.
(201) Anselmo, A. C.; Mitragotri, S. Impact of Particle Elasticity on Particle-Based Drug Delivery Systems. *Adv. Drug Deliv. Rev.* **2017**, *108*, 51–67.
(202) Mitragotri, S.; Lahann, J. Physical Approaches to Biomaterial Design. *Nat. Mater.* **2009**, *8* (1), 15–23.
(203) Merkel, T. J.; Jones, S. W.; Herlihy, K. P.; Kersey, F. R.; Shields, A. R.; Napier, M.; Luft, J. C.; Wu, H.; Zamboni, W. C.; Wang, A. Z.; Bear, J. E.; DeSimone, J. M. Using Mechanobiological Mimicry of Red Blood Cells to Extend Circulation Times of Hydrogel Microparticles. *Proc. Natl. Acad. Sci. U. S. A.* **2011**, *108* (2), 586–591.
(204) Hu, Y.; Xie, J.; Tong, Y. W.; Wang, C.-H. Effect of PEG Conformation and Particle Size on the Cellular Uptake Efficiency of Nanoparticles with the HepG2 Cells. *J. Control. Release* **2007**, *118* (1), 7–17.
(205) Cui, J.; Björnmalm, M.; Liang, K.; Xu, C.; Best, J. P.; Zhang, X.; Caruso, F. Super-Soft Hydrogel Particles with Tunable Elasticity in a Microfluidic Blood Capillary Model. *Adv. Mater.* **2014**, *26* (43), 7295–7299.
(206) Müller, K.; Fedosov, D. A.; Gompper, G. Understanding Particle Margination in Blood Flow – A Step toward Optimized Drug Delivery Systems. *Med. Eng. Phys.* **2016**, *38* (1), 2–10.
(207) Decuzzi, P.; Pasqualini, R.; Arap, W.; Ferrari, M. Intravascular Delivery of Particulate Systems: Does Geometry Really Matter? *Pharm. Res.* **2009**, *26* (1), 235–243.
(208) Walton, B. L.; Lehmann, M.; Skorczewski, T.; Holle, L. A.; Beckman, J. D.; Cribb, J. A.; Mooberry, M. J.; Wufsus, A. R.; Cooley, B. C.; Homeister, J. W.; Pawlinski, R.; Falvo, M. R.; Key, N. S.; Fogelson, A. L.; Neeves, K. B.; Wolberg, A. S. Elevated Hematocrit Enhances Platelet Accumulation Following Vascular Injury. *Blood* **2017**, *129* (18), 2537–2546.
(209) Lehmann, M.; Schoeman, R. M.; Krohl, P. J.; Wallbank, A. M.; Samaniuk, J. R.; Jandrot-

Perrus, M.; Neeves, K. B. Platelets Drive Thrombus Propagation in a Hematocrit and Glycoprotein VI-Dependent Manner in an in Vitro Venous Thrombosis Model. *Arterioscler. Thromb. Vasc. Biol.* **2018**, *38* (5), 1052–1062.

(210) Khoury, M.; Epshtein, M.; Zidan, H.; Zukerman, H.; Korin, N. Mapping Deposition of Particles in Reconstructed Models of Human Arteries. *J. Control. Release* **2020**, *318*, 78–85.

(211) Reinhart, W. H.; Piety, N. Z.; Goede, J. S.; Shevkoplyas, S. S. Effect of Osmolality on Erythrocyte Rheology and Perfusion of an Artificial Microvascular Network. *Microvasc. Res.* **2015**, *98*, 102–107.

(212) Hou, H. W.; Bhagat, A. A. S.; Chong, A. G. L.; Mao, P.; Tan, K. S. W.; Han, J.; Lim, C. T. Deformability Based Cell Margination--a Simple Microfluidic Design for Malaria-Infected Erythrocyte Separation. *Lab Chip* **2010**, *10* (19), 2605–2613.